Universitetet i Stavanger

Faculty of Science and Technology

Bachelor Thesis

Study Program/Specialization:	Spring Semester 2023
Mechanical Engineering	Open/Restricted Access

Authors: Martin Kvilhaug, Kevin Velde Njaa

Martin Kvilhaug: .....

Kevin Velde Njaa: .....

Faculty Supervisor: Chandima Ratnayake Mudiyanselage

External Supervisor(s): N/A

Thesis Title: Development and Design of ROV Manipulator

Credits (ECTS): 2x20

Key words:	Pages: 122
ROV Manipulator, Subsea, circular economy,	+ Appendix: 6
product development process, MATE	Stavanger, 15.05.2023

Preface

This bachelor thesis is written between January 4th and May 15th, 2023, at the Department of Mechanical and Structural Engineering and Material Science at the Faculty of Science and Technology, University of Stavanger (UiS). The project was carried out in partnership with UiS Subsea, a student organization that was first founded in 2013. The primary aim of the project was to design and build a fully functional manipulator for a remotely operated vehicle (ROV) to participate in the Marine Advanced Technology Education (MATE) ROV competition in June 2023.

We extend our sincere gratitude to the Faculty of Science and Technology at the University of Stavanger for providing us with the opportunity to participate in the UiS Subsea organization, ROV project, and the MATE competition. The project has been an exceptional learning experience, which has not only allowed us to develop our technical and collaborative skills, but also provided us with the chance to explore our creativity and innovation.

With the support and collaboration of fellow students, sponsors, and family, the project was successfully completed. Our gratitude goes to our supervisor Professor Chandima Ratnayake Mudiyanselage from the University of Stavanger, for guidance and support throughout the project. We would also like to extend our gratitude to our fellow students, sponsors, family members, and the employees at the university who have offered their support and collaboration.

Overall, the project has been an extraordinary experience, providing us with a unique and rewarding opportunity to develop our technical and creative abilities. We are proud of our accomplishments and grateful for the opportunity to participate in this project.

Table of Content

List of Figures

List of Tables

Summary

The thesis is carried out in collaboration with the student organization UiS Subsea. The primary objective of this thesis is to design and develop a manipulator for the ROV, named *YME*, using the product development process (PDP). The end goal is to showcase the final product at the MATE ROV Competition 2023. The importance of sustainability has been highlighted in recent years, and this year, MATE ROV Competition focuses on the United Nations Decade of Ocean Science for Sustainable development (2021-2030), and challenge students to contribute to UNs Sustainability goals by seeking sustainable solutions for their projects.

The product development process consisted of four phases: planning, concept development, concept generation, and product concept selection. The planning process focused on resource allocation, declaring a mission statement, and establishing a good foundation for the process ahead. Gathering benchmarking information and establishing target specifications was a crucial part of the concept development phase, prior to the concept generation process, as the information and specifications served as a guidance and outline for the concepts to be generated. By a circular economy approach, the reuse of old components within UiS Subsea was evaluated, and potential components were located. The circular economy approach influenced design decisions, and resulted in cost and time-efficiency, and contribution towards sustainability in engineering practices. Concepts were generated for both the manipulator arm and end-effector, and the most promising ones were selected for further development. Eventually one concept for the arm, and one for the end-effector, was selected and further developed through detailed design.

Through detailed design, a complete CAD model of the manipulator was made, also material was selected and necessary calculations were performed. The outcome was a three degree of freedom manipulator arm with a rotating end-effector, pitch function,

and a telescope function. Through prototyping and extensive testing, the design was evaluated and deemed sufficient according to customer needs and target specifications. The outcome of the project was a fully functional ROV Manipulator able to perform all the required MATE tasks, and contributed greatly towards the successful qualification to the 2023 MATE ROV Competition. However, there was room for further improvement and optimization of both the manipulator and the process, and hopefully the manipulator can serve as a foundation for future UiS Subsea manipulator projects.

Link to the demonstration video: MATE Demonstration Video 2023 - YouTube

Chapter 1

Introduction

1.1 About UiS Subsea

1.1.1 UiS Subsea Organization

UiS Subsea is a student-organization at the University of Stavanger, and has engaged students in underwater technology since 2013. The primary goal of the organization is to provide students with the experience of working in a team consisting of different engineering disciplines.

The introduction chapter is written by the technical leaders of the project, and is common for all bachelor groups, as it presents the project as a whole.

This year there are a total of nine bachelor groups working together towards a common goal of designing and building a remotely operated vehicle (ROV). The ambitions for this year's ROV project is to build upon the successes and lessons learned from previous years, with focus on improving the vehicle's performance and functionality. The key objectives are to design a more user-friendly ROV, that is easier to maintain, more efficient, and with a software that enables functions more like an autonomous underwater vehicle (AUV). The ROV will not be fully autonomous, but is designed to be capable of competing in a range of autonomous challenges at the MATE competition.

There are two groups of mechanical engineering students within the team. These groups are responsible for design, construction of the chassis, manipulator, and electronics enclosure for the ROV.

There are five groups of electrical engineering students in the team, responsible for developing and implementing various electrical systems on the ROV. These systems include sensors, regulation, connections, circuits, and communication between the ROV and the topside control system.

There are two groups of computer science students, responsible for sending and receiving commands and data, displaying the ROV in a graphical user interface (GUI), and managing controls and image processing.

For several years, UiS Subsea has built ROVs and partaken in international competitions.

This year the main competition is the MATE ROV Competition 2023. This provides a basis for more advanced problem solving and teamwork, with the purpose of creating a positive and healthy environment for learning and developing technical skills. UiS Subsea opens up the opportunity for students to collaborate with industrial companies. Several companies are greatly interested in these projects, providing components and other resources through sponsorship deals. To further improve the relations between the organization and the industry, UiS Subsea annually holds an event called 'Subsea-dagen', where companies from the industry can have their own stand and promote themselves. Both UiS Subsea and the companies gain a lot of exposure from such an event.

In previous years, the organization has suffered from lack of continuity due to a non - existing handover between outgoing and incoming bachelor students. This has resulted in knowledge gaps and steep learning curves for the new students. This year, the previous leader and second leader of UiS Subsea have decided to remain involved in the organization to guide and integrate previous knowledge and experience into the current project.

Figure 1.1: UiS Subsea logo

This years project management consists of the following roles:

- **Project manager:** Joar Rodrigues de Miranda
- **Competition manager:** Thomas Matre
- **Technical leader, Electro:** Jesper A. Flatheim
- **Technical leader, Data:** Filip Sølvberg Herrera
- **Technical leader, Mechanical:** Haakon Aleksander Schei

1.1.2 Computer Science

Image Processing and Artificial Intelligent

The image processing group is responsible for completing sub-tasks for the MATE ROV Competition, which is based upon processing image data to solve tasks. These tasks require camera vision with depth perception and autonomous programming. The tasks are the following:

- **Autonomous Docking**. Maneuver the ROV in front of docking station, and with the help of a pinpoint, autonomously dock the ROV.
- **3D Modelling of sick coral**: This task involves using the main camera to measure the size of a coral, and creating a 3D model of the object. In addition, the software must determine whether the coral is sick or not, based on the amount of white coloring visible on the object.
- **Count frogs along a transect line**. The ROV must follow a transect line and count amount of frogs on the seabed.
- **Monitor/analyze of seaweed growth**. This task involves that the ROV must analyze and compare two fields of seaweed on the ocean floor, and determine if it is positive or negative growth.

GUI

The main task is to develop a system that monitors and controls the ROV. To complete this task, a system that sends commands and control data from topside to the ROV is implemented. This is done in collaboration with the communication team. All of this information has to be displayed on a custom GUI, that presents both vital information and video feeds to the user in real time. Creating a user friendly GUI, control commands and controller settings are essential for a quality of life product.

1.1.3 Electronics

Power Module

The task of the power module team is to regulate and disperse input voltage supplied from the topside system, while ensuring that components are not overloaded, and prevent short circuits. With an input voltage of 48V, it is essential to step - down the voltage to a suitable level for each component.

Communication System

The communication team‘s main task is to create a common system so that electrical circuit boards are connected together and are able to communicate with the rest of the system. By utilizing CAN-bus in addition to C-code, the system is able to aptly convey signals and commands efficiently between each other. In addition, the communication between ROV and topside system has to be solved. Process data and video feed from ROV to topside needs to be processed efficiently with minimal delay. In addition, the internal design of the electronics housing is this groups responsibility.

Regulation System

The task is to create a system for navigation and regulation of the ROV. The most central parts of the system is choice of thruster configurations, manipulator motor and development of circuit board, in collaboration with the mechanical groups. These are essential for the physical limitations and attributes of the ROV and how it interacts with the environment.

The circuit board should be an interface between motor controller and other circuit boards. Thruster and motor choice are limited by competition standards. Another central part of this groups responsibility is the development of a control system. The control system must interpret commands and sensor measurements from topside and other circuit boards, so that the ROV is able to operate and manoeuvre. In addition, regulation needs to be able to maintain stability, orientation and remain at a chosen depth.

Mathematical models and functions are required to be able to digitally simulate the different degrees of freedom of the ROV.

Sensor System

The main task of the sensor system is to maintain and disperse information from the different sensors, and act upon the vital data. These are orientation (IMU), leak and pressure sensor. IMU retrieves angle data and axis relation, and generates data used by the regulation system to control and drive the thrusters. The leak sensors consists of three to four leak probes placed along the inside of the electronics housing to be able to detect leaks and aptly react to the information to minimize damage to critical components. The temperature sensor is divided upon three identical sensors along the enclosure at key points. This is to monitor internal temperature, and the dispersion of it. The pressure sensor is the only sensor mounted externally. It monitors the change in water pressure caused by a change in depth.

Float

The float is the only component not attached to the main ROV. It is essentially its own AUV, with a pre-programmed flight path and own power supply. It is used to gather vital information about ocean health and the underwater environments.

The competition requires that the float completes two vertical profiles: Sink to bottom and return to surface. Afterwards it has to relay time of completion with a ping to topside system, in addition to temperature and pressure. This will be displayed for operator to view.

1.1.4 Mechanical

Design of ROV Frame, Electronics Housing and Float

The main task is to design and build the frame of the ROV, the electronics housing, and the shell of the float, following the product development process. The primary focus of the design is to mesh together all the individual parts into one functional ROV, while also ensuring the ROV being able to perform the tasks in the MATE- and TAC ROV competitions.

In light of the present days environmental challenges, a secondary focus will be sustainability, recyclable materials and design for environment (DFE) in the development process, with the goal being to minimize environmental impact of this process. Effective use of DFE can also help reduce cost and production time, while increasing product quality. Material choice, structural, flow , FEM and buoyancy analysis are tasks to be solved here.

Manipulator

The main task is to develop and design a functional manipulator able perform the required tasks. The goal is for the mechanical arm to be functional according to MATE requirements, while being uncomplicated enough for easy production and maintenance. Creativity and problem oriented solutions are necessary to complete this task. Deciding degrees of freedom, which mechanical principles to implement, and what materials to use are some problems that needs to be solved.

In addition, co-operation with the electrical engineering teams, is essential with regards to manipulator compatibility to the rest of the electrical system.

1.2 About ROV Project

1.2.1 ROV History

Dimitry Rebikoff can be credited for the first remotely operated vehicle (ROV) in 1953, which was called *Poodle*. The *Poodle* is illustrated in Figure 1.2, and was a revolutionary invention, as it allowed researchers and explorers to explore underwater, without the need for humans to enter the waters. The ROV was operated via a tethered connection and controlled from a topside panel, which are used in various modern industries, including oil and gas, scientific research, and marine explorations. [1].

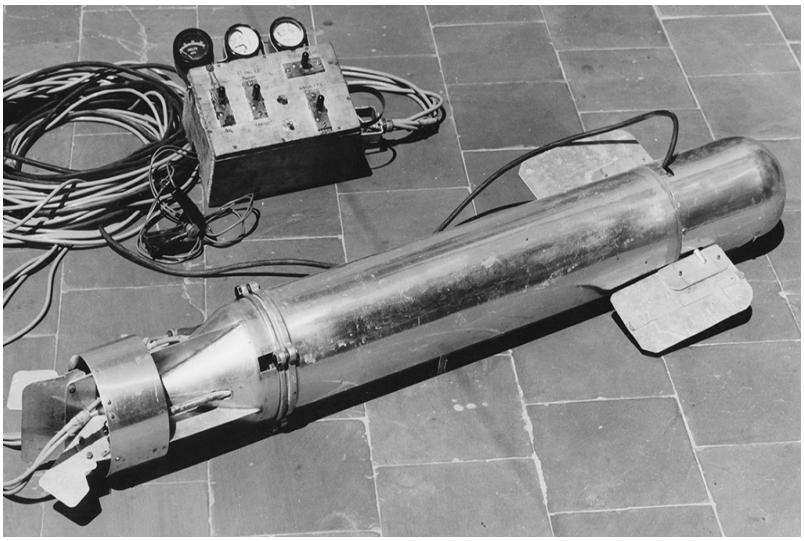

Figure 1.2: The worlds first ROV, *Poodle* [1]

The subsea industry has undergone significant changes since the first ROV in 1953. In the 1960s, the United States Navy used ROVs as recovery drones for underwater equipment, further exploring the development of modern ROV technology. Within two decades, there were over 500 ROVs worldwide, mostly in the commercial market, each with their own unique task and purpose [1].

Modern ROVs are sophisticated and technologically advanced, and equipped with components that make it possible to operate effectively in subsea environments. The specific components vary, depending on the purpose and tasks, but some common components found on ROVs are illustrated in figure 1.3, and listed below [1].

1. Thrusters
2. Tether
3. Camera
4. Lights
5. Frame
6. Pilot controls
7. Buoyancy element

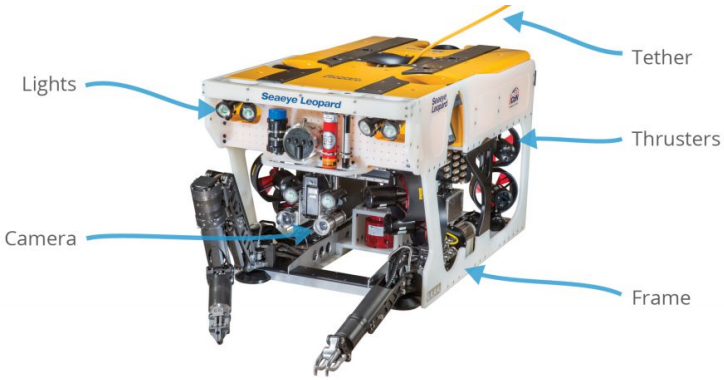

Figure 1.3: Common components for ROVs [1]

Modern ROVs are typically designed upon the given tasks, such as observation and inspection. While some ROVs are designed to perform multiple tasks, others have a more limited scope. There are seven main classes of ROVs classified from I to VII [2]:

I. -Pure observation [3]

II. -Observation with payload option [4]

III. -Work class vehicles [5]

IV. -Seabed-Working vehicles [6]

V. -Prototype or development vehicles

VI. -Autonomous underwater vehicles (AUV) [7]

VII. -High-Speed survey vehicles [8]

Figure 1.4: Different ROV classes

The different elementary functions are divided into classes. There are several benefits and limitations with each class, but the most common classes for ROVs are:

Class I: Known as pure observation vehicles, are highly maneuverable, but are primarily designed for video observation purpose. These vehicles are in general small in size and equipped with a camera, lights and thrusters to navigate in underwater environments. Their compact size make them ideal for conducting service and inspect small areas of the ocean. However, they have limited capabilities and cannot perform other tasks without modifications to the design [2].

Class II: Known as observation vehicles with payload option, have the same capabilities as a pure observation ROV, but usually with additional functionality. In addition to video observation the class II vehicles are equipped with a wide range of additional features

such as manipulator, colour cameras, additional cameras, sonar, and cathodic protection measurement systems. These features make it possible to perform tasks, such as collecting samples and repairing subsea instruments [2].

Class III: Known as work class vehicles, are larger then Class I and Class II vehicles. These vehicles are designed to carry additional sensors and manipulators, making them suitable for more complex tasks, such as installations, maintenance and construction. Class III ROVs also have semi-autonomous capabilities, referred to as multiplexing. This allows the vehicles to operate heavy equipment without loss of functionality. In addition, these ROVs are built to be stable and buoyant enough to carry additional equipment [2].

I. Class III A – Work class vehicles $<$ 100 Hp

II. Class III B – Work class vehicles 100 Hp to 150 Hp

III. Class III C – Work class vehicles $>$150 Hp

Class IV: Known as seabed working vehicles, are designed to perform tasks on the ocean floor. These vehicles are usually larger then Class III ROVs and equipped with traction systems such as belts, wheels, jets or thruster propellers. Seabed working vehicles are the largest and most robust ROVs, designed to do operations in harsh environments. Their primary purpose is to carry out subsea work, including dredging, mining, cable and pipeline trenching, excavation and other types of subsea construction work [2].

Class V: Known as prototype or development vehicles that have not yet been sufficiently tested or are still under development. Most special purpose vehicles or one-off prototypes end up here, since they cannot be categorized by any of the previous classes. In accordance with the Norwegian standard for ROVs, both Class VI and VII ROVs fall under this category, as they are still under development and are only produced by a select few companies. As testing and developing continue, it is possible that these ROVs get categorized into another class eventually [2].

1.2.2 YME

The ROV developed and produced this year is a class II vehicle, with 6 degrees of freedom and a compact design. The goal is to create a vehicle that is based upon well thought existing solutions, whilst still being in accordance with UNs sustainability goals.

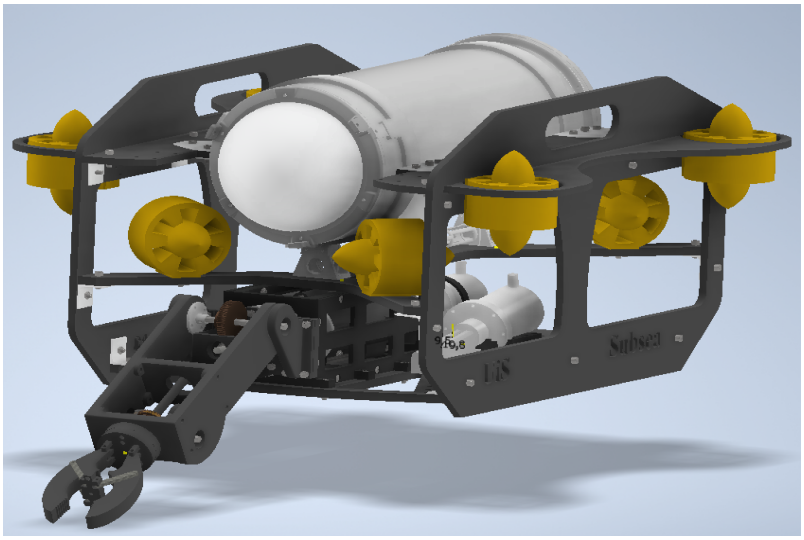

Figure 1.5: 3D model of ROV

YME is a remotely operated vehicle (ROV) that is controlled by a customized graphical user interface (GUI). The ROV is connected to a topside control system via an umbilical cord, making it possible for real time communication and control. The primary object of this project is to compete in the MATE ROV competition, and therefore the ROV is especially designed for this purpose. In addition, the project participants have set a goal of operating at a depth of 50m. The vehicle's modular design enables easy replacement of parts and allows for future students to further develop and customize the ROV to meet their specific needs.

1.2.3 Balder

Balder is a autonomous underwater vehicle (AUV) that is controlled by Bluetooth signals. The primary goal of a float is to track and monitor deep ocean drift currents, with depths up to thousands of meters. These AUVs use a buoyancy engine with pre - programmed heights, allowing them to navigate and collect data. Biogeochemical floats feature an array of optical and chemical sensors, and are therefore capable of collecting valuable

data from otherwise challenging locations [9].

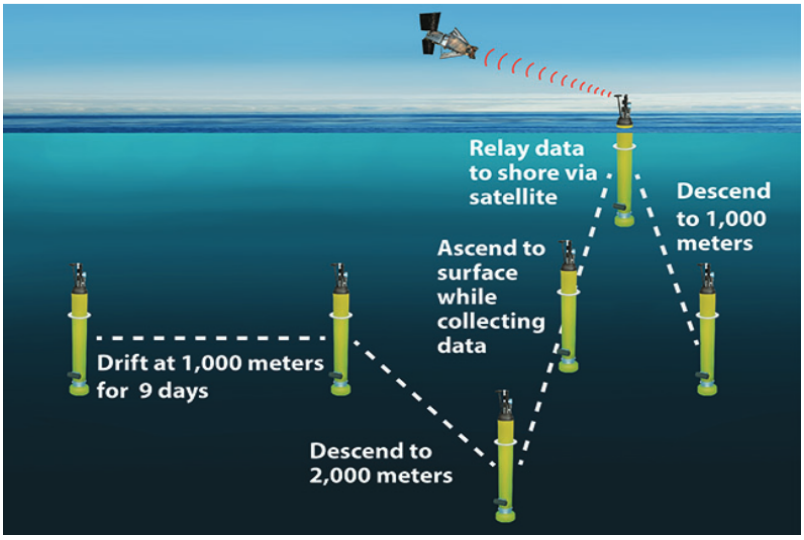

Figure 1.6: Diagram of a float cycle [10]

In Figure 1.6, a typical float cycle is illustrated, where the float descend to a depth of 1000m, drifting for five to ten days while acquiring valuable data. This cycle is repeated again at a depth of 2000m, before the AUV ascends to the surface for transmission of the acquired data. On average, a float typically has a life cycle of about five years.

1.3 MATE - Marine Advanced Technology Education

The information beneath is retrieved from the organization's websites [11] [12].

The ROV created by UiS subsea this year, follows the specification determined by the international competition, *MATE ROV COMPETITION*. This competition is hosted by organization *MATE.The Marine Advanced Technology Education (MATE) Center*, is a partnership of a multitude of American organizations, established in 1997. These partners are mainly comprised of schools, research institutes, governments and marine institutes. This cooperation's main goal is to improve marine technical education, which in turn strengthens the future American workforce for future maritime operations.

Figure 1.7: MATE logo

In 2021, *MATE* transferred the responsibility for student activity over to *Marine Advanced Technology Education for Inspiration and Innovations*, otherwise known as *MATE II*. Their main objective is to motivate student's interest in maritime knowledge, mainly by hosting the *MATE* competition every year. Here, they challenge students to implement engineering principles and knowledge to solve subsea tasks. UiS Subsea is competing in the EXPLORER class, which is reserved for students with higher technical educational background.

Figure 1.8: MATE II logo

1.3.1 MATE ROV Competition

The information about the competition is retrieved from the competition manual [13].

This years competition themes is no different from the previous two where they highlight the importance of the United Nations Decade of Ocean Science for Sustainable Development (2021-2030). Their intention is to increase ocean knowledge and ensure that society implements this knowledge, thus contributing to the UNs sustainability goals. The task this year is to create a ROV and a scientific float. The themes raised this year is the facilitation and production of clean energy, surveillance, and tracking of the oceans biological diversity.

Figure 1.9: MATE Competition logo

Points

Table 1.1, demonstrates the segmentation of the available points. Product demonstration is the first part, where UiS Subsea will solve three practical tasks within 15 minutes. If this is achieved before 15 minutes have passed, additional points are given, 1 per minute and 0.01 per second saved. Additional points are given for ROVs below 25 kg and good team work under the competition. These practical tasks are meant to test the operational characteristics of the ROV. The secondary segment, points are designated for the technical documentation and how the organization portrays themselves. The final points are given based upon the safety of the ROV and how the relevant dangers have been adequately analyzed and addressed .

Table 1.1: Points structure

Product demonstrations	
Tasks	300 points
Time bonus	10 points
Weight restrictions	10 points
Organization efficiency	10 points
Engineering and communication	
Technical documentation	100 points
Product presentation	100 points
Marketing	50 points
Company specification sheet	20 points
Company responsibility	20 points
Safety	
Review of safety documentation	20 points
Safety inspection	30 points
Safety job analysis	10 points
Total	**680 points**

1.3.2 Description of tasks

Task 1: Maritime renewable energy

UNs Sustainability goals:

7 Clean energy for all

12 Responsible consumption and production

The first task is designed to simulate an offshore installation of floating solar panels in an established floating wind farm, removal of bio fouling and piloting the ROV either Autonomously or manually into a underwater docking station

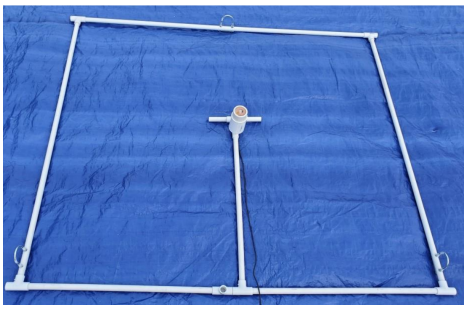

Figure 1.10: Seabed anchor for installation

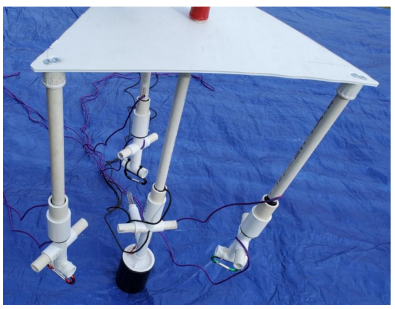

Figure 1.11: Floating solar panel

Figure 1.12: Hook for mooring

- Maneuver the solar panels between three existing wind turbines: 10 points.
- Moor three moorings to the solar panels : 15 points.

- Remove lid from power port entry: 5 points.
- Connect plug from solar panels: 10 points.

Remove bio fouling from the floating wind turbines

Bio fouling is simulated either with red PVC pipes connected with Velcro or chenille pipe cleaners twisted together.

Figure 1.13: Biological material on structure

Figure 1.14: Biological material on rope

- Remove one to two units of bio fouling: 5 points.
- Remove three to five units of bio fouling: 10 points.
- Remove six units of bio fouling: 15 points.

Maneuver the ROV into docking station

Figure 1.15: ROV Docking station

.

- Maneuver autonomously into docking station: 15 points.
- Maneuver manually into docking station: 10 points.

Task 2A: Coral reef and blue carbon

UNs Sustainability goals:

13 Stop climate change

14 Ocean life

The second task is divided into two parts: 2A and 2B. Part A represents scientific tasks: scanning a coral reef, identification of organisms by utilizing eDNA, exposure of UV light on sick coral reefs, inspection and installations of environmentally mooring system to protect seaweed on the seabed.

Measure, model and identification of disease on coral reef

Figure 1.16: Main coral with white spots

.

- Measure diameter on coral reef: 5 points.
- Measure height on coral reef: 5 points.
- Measure area of infection: 5 points.
- Make a 3D model autonomously: 15 points.
- Make a 3D model in CAD manually: 5 points.

All measurements are to be done within two minutes, and can be completed either autonomously or manually with reference objects.

Identify coral reef organisms with eDNA

Figure 1.17: Water - bag connection

Figure 1.18: Connection for sample extraction

- Extract water sample from bottle: 10 points.
- Identify fish species based upon three samples provided by hosts: 5 points.

Administrate Rx to infected coral

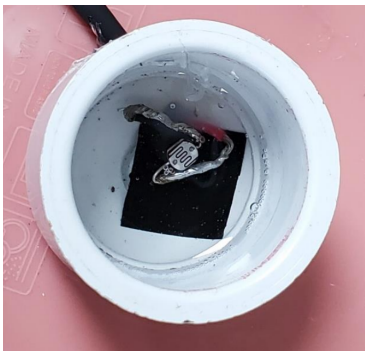

Figure 1.19: Photo resistor

Figure 1.20: Light connection

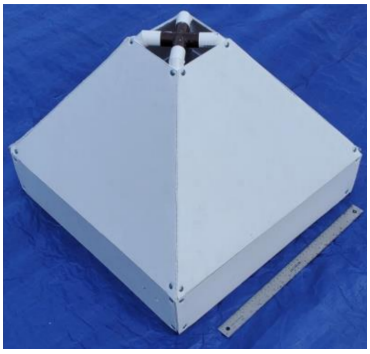

Figure 1.21: Tent

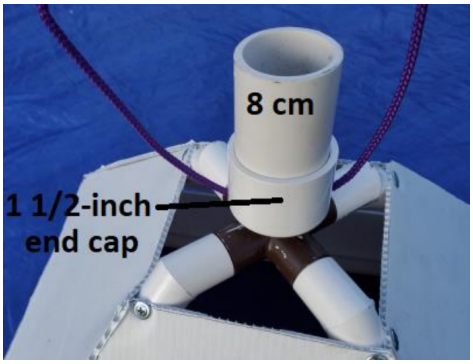

Figure 1.22: Syringe connection

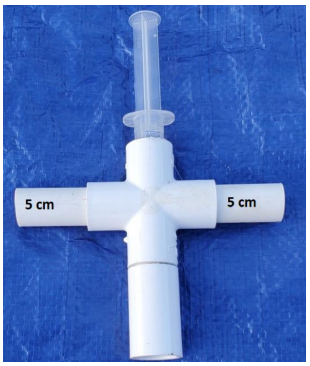

Figure 1.23: Syringe

- Position UV-light above infected area: 5 points.
- Activate light and cure: 5 points.
- Place tent above coral reef: 10 points.
- Place syringe in tent opening: 5 points.
- Remove syringe contents inside the tent: 5 points.

Seaweed habitat protection and surveillance

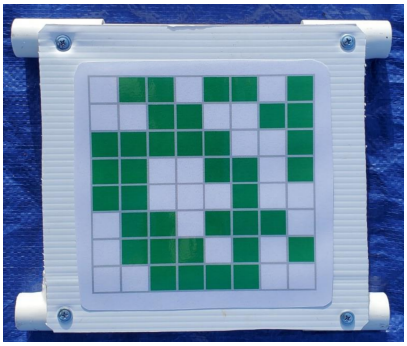

Figure 1.24: Seaweed

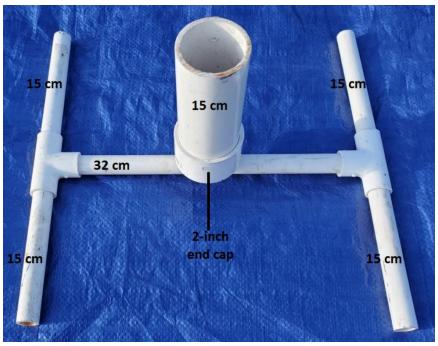

Figure 1.25: Eco - Mooring base

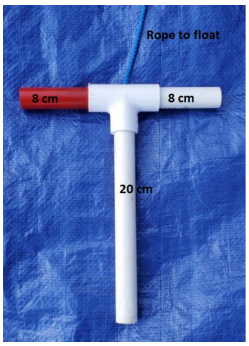

Figure 1.26: Mooring

- Identify if seaweed habitat has been rehabilitated, remained unchanged or worsened, based upon images: 5 points.
- Install Eco-Mooring system on seabed, inside a base and rotate mooring 720°in the base: 10 points.

Task 2B: Lakes and rivers

UNs Sustainability goals:

13 Stop climate change

14 Ocean life

Task 2B is more inclined to work with freshwater bodies. The tasks are to look for fish and determine if they are an invasive species, and release fry where it is safe. There also is rope inspection, clearance of a larger object, follow a transect line, count frogs and install a camera on seabed

Re-introduce endangered species of Northern Red belly Dace fry

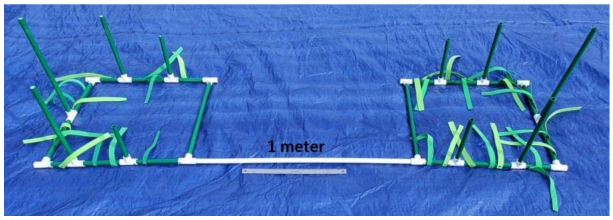

Figure 1.27: Habitat area

Figure 1.28: Fry

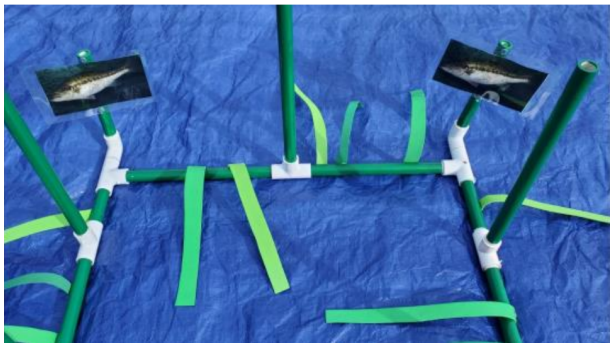

Figure 1.29: Current fish species

- Survey two areas, and identify which is safe to place to release the fry: 10 points.
- Acclimatize fry to safe area: 5 points.
- Release fry in safe area: 10 points.

Ensure the health and safety of the Dillion reserve

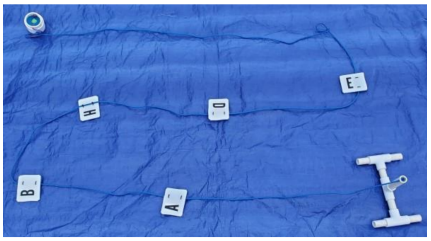

Figure 1.30: Rope with letters

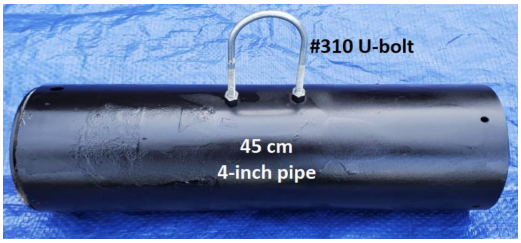

Figure 1.31: Heavy object which is to be removed

- Inspect rope for a buoy and display the ten letters attached: 10 points.
- Display the documentation of the ROVs lifting capacity: 5 points.
- Lift object a maximum of 120 Newton above water: 10 points.
- Return object to land: 5 points.

Surveillance of endangered Lake Titicaca frogs

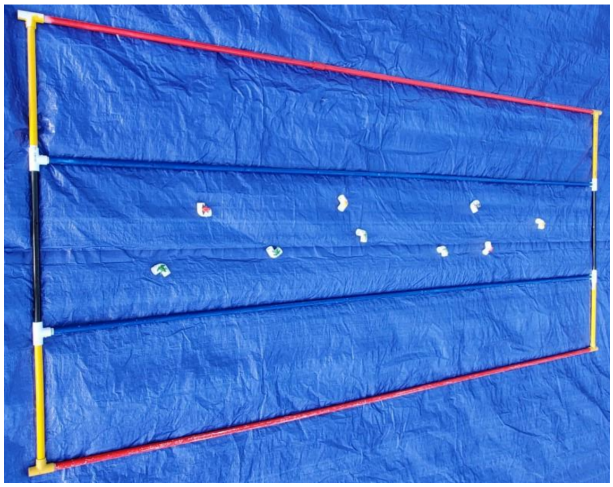

Figure 1.32: The transect line area that the ROV will fly over

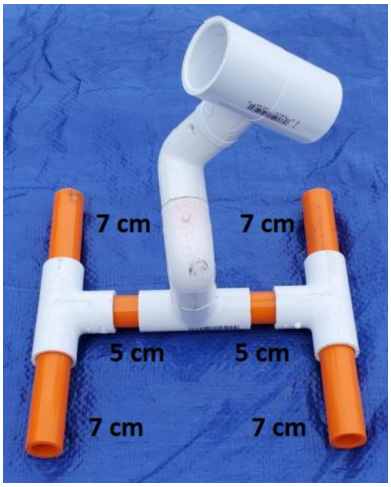

Figure 1.33: The camera which is to be installed

- Fly a transect line and maintain image within area: 10 points.
- Count amount of frogs within an area: 5 points.
- Install a camera on designated area: 5 points.

Task 3: MATE Floats

UNs Sustainability goals:

13 Stop climate change

This task represents the construction of a functioning scientific float, which will transmit date when it reaches the ocean surface.[14]

MATE Floats 2023

- Design and construct a functioning vertical profile float: 5 points.
- Float communicates with land prior to submersion: 10 points.
- Vertical profile one, float sinks and rises after impact with seabed: 10 points.
- Float transmits to land the time of completion after first vertical profile : 10 points.
- Vertical profile two, float sinks and rises after impact with seabed: 10 points.
- Float transmits to land the time of completion after second vertical profile : 10 points.

Restrictions and demands

The competition has certain physical restrictions with size, weight, operational environment and electrical limitations. The only vehicle to be utilized is an ROV

Environment: The ROV must be able to operate in fresh, salt or chloride water, in a temperature span of 15 to 30 °Celsius

Materials: The ROV must be able to operate at minimum four meters depth, whilst being under a maximum of 35 kg.

Tether length: The tether has to be long enough to operate within an area 10 meters from edge and four meters deep. Topside control system can be up to three meters from edge of the pool.

Thrusters: The thrusters needs to be adequately protected and meet IP-20 standards. The thrusters must be designed to operate underwater.

Electrical: The organizer provides power supply for the ROV of 30A and 48 VDC. Conversion to lower voltages has to happen inside the ROV. There have to be implemented an overload protection on 150% of nominal power usage on the ROV.

Float: Batteries utilized must be of the type: AAA, AA, A, A23, C, D, or 9V alkaline batteries.The float shall be protected with a 7.5A fuse. There must be a pressure relief valve with a diameter of minimum 2.5cm.

Chapter 2

Theory

A manipulator is a machine in the field of industrial robotics. An industrial robot is a general-purpose machine with certain anthropomorphic features. The manipulator can be compared to a human arm, consisting of a shoulder, elbow and wrist joint. The modern type manipulator is controlled through computers and programming, where a combination of a controller and software provides the manipulator with an intelligence making it possible for the manipulator to perform a variety of tasks. Industrial robots and manipulators are used as a substitute for human labor, often in hazardous or inconvenient environments. In the offshore industry, a ROV equipped with a manipulator is often used to perform tasks at great depths, where using a human operator would contain very high risks and even impossible in many cases [15, p. 907].

The field of robotics encompasses a vast and intricate landscape. In this thesis, the theoretical section aims to provide a broad perspective, rather than an in-depth analysis. Rather than delving deeply into each aspect of robotic manipulators, this thesis offers a wider-ranging theoretical overview, including a diverse array of core principles that underpin manipulator theory.

2.1 Robot Anatomy

Robot anatomy encompasses the mechanical parts and the construction of a manipulator. Industrial robots typically comprise a mechanical manipulator and a controller, which

work together to perform various tasks and functions. The mechanical manipulator is composed of joints and links that can be positioned and oriented along the manipulator's length. Meanwhile, the controller employs both electric hardware and software to control the movement of the different joints. The joints are coordinated to perform the specified work cycle [15, p. 907-908].

2.1.1 Anatomy Technology

Most industrial robots are attached to a base or floor, with the attachment point being identified as *link zero* and serving as the starting point for the link-joint-link combination of the robot's construction. The combination form the foundation of the manipulator design.

Typically, the manipulator is divided into two assemblies: a wrist assembly and an arm - body assembly. Each assembly has distinct functionality, serving different purposes. The wrist assembly is primarily used to orient or manipulate objects, while the arm - body assembly is used for positioning and manipulation. To perform different functions, it is important that different assemblies meet different criteria. For instance, positioning tasks require large spatial movement to transfer objects from one point to the other, whereas orientation tasks require rotating motions to align objects at desired angles. By combining these two assemblies, the manipulator can perform a wide range of operations [15, p. 908-909].

Several different designs are commonly used for industrial robotics. The five most prevalent anatomies are depicted in Figure 2.1.

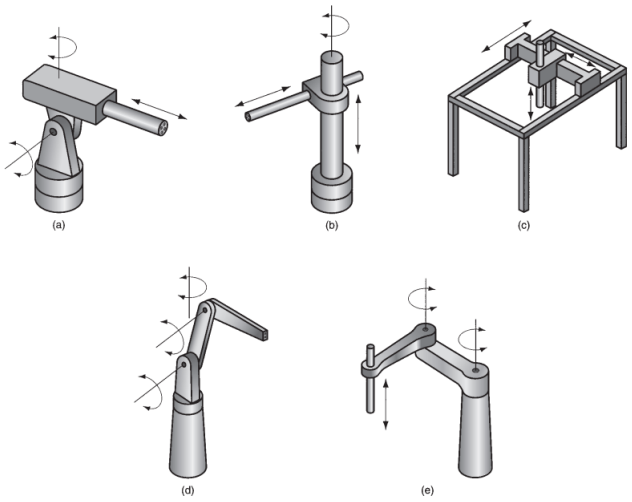

Figure 2.1: Five common anatomies for industrial robots: (a) Polar, (b) Cylindrical, (c) Cartesian Coordinate, (d) Jointed-arm, and (e) SCARA [15, p. 909]

2.1.2 Polar Robot Manipulator

The polar robotic arm is situated on a rotating platform and is capable of tilting up and down, as well as moving forward and backwards. The manipulator employs a two -dimensional coordinate system, with different points on the plane determined by their distance, using what is known as the polar coordinate system [16, p. 13].

2.1.3 Cylindrical Robot Manipulator

The cylindrical manipulator features a rotary joint at the base, and a prismatic joint that connects the links. The manipulator also includes a platform attached to the rotating shaft and the last link where the end-effector is situated. In addition to rotating, the arm can move forwards and backwards. By utilizing the cylindrical robot, it becomes possible to rotate, elevate, and move the arm in a vertical and sliding motion, this enabling a range of complex tasks to be carried out [17].

2.1.4 Cartesian Robot

Cartesian robots are widely used for 3D printing and CNC machining due to their versatility and flexibility. This type of robot allows for precise and speedy adjustments to

be made. The Cartesian coordinate system is employed by this type of robot, enabling movement along the X, Y, and Z axis [17].

2.1.5 Jointed-Arm Robot

Jointed-arm robots, also knows as articulated robots, are designed to move and configure themselves similarly to a human arm. Typically, the arm is composed of two or more rotary joints. The robot also includes a rotary base, allowing for increased flexibility and range of motion [17].

2.1.6 SCARA Robot

SCARA stands for Selective Compliance Assembly Robot Arm. This type of robot is capable of movement along X, Y, and Z axis, as well as rotary motion, making it a highly versatile option for various applications, including assembly, palletizing, and bio-medical tasks [17].

2.1.7 Joints and links

Joints and links for an industrial robot are similar to the links and joints in a human body, providing movement between different parts. The number of links in a robot depends on the number of joints present, with each joint having an input and output link. The output link for one joint serves as the input link for the next, and this series of link-joint-link combinations forms the basis common to all types of manipulators.

A typical industrial manipulator has around five or six joints, with the ability to move, position, and orient objects being critical for performance. For this to happen correctly, the coordinated movement must be accurate. The joints can be classified as either linear or rotating, indicating the motion for the links they control [15, p. 908].

2.1.8 End-Effectors

An end-effector is a specialized tool that connects to the robot‘s wrist, enabling the manipulator to perform the specific tasks. The end-effector is a critical component for a manipulator to function properly. Two general types are tooling and gripping end-effectors.

Tools are frequently employed when the robot needs to carry out a processing operation. Welding tools and automatic screwdrivers are among the most common tools used with an end-effector.

In contrast, grippers are designed to grab and move objects. The objects to be handled can vary from tiny valves to larger debris, and the end-effector must be specifically designed to handle the different objects [15, p. 910]. Figure 2.2 illustrates a common type of end-effector.

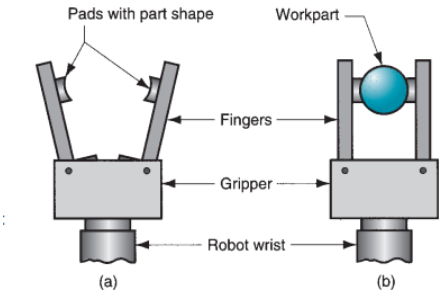

Figure 2.2: Common end-effector [15, p. 910].

2.2 Kinematics

Kinematics is branch of mechanics concerned with the motion of objects, without regard for the forces or fields acting on them. In other words, kinematics is the study of an object’s position and orientation, velocity, and acceleration [18, p. 233].

One of the most critical aspects of a manipulator is the kinematic movement of its arm. To analyze the motion and behavior of the manipulator accurately, it is necessary to formulate the correct kinematic models. This data is especially crucial for remotely operated vehicles to operate effectively. The kinematics of a robot can be divided into two branches: forward

kinematics and inverse kinematics [19, p. 267-268].

2.2.1 Forward Kinematics

Once the joint variables of the manipulator are established, the position and orientation of every link can be determined. A primary characteristic of forward kinematics is that joint numbering starts at the manipulator's base and increases sequentially up to the end-effector link. For robotic arms with a low number of degrees of freedom and subjected to relatively small loads, a geometric approach is often employed to simplify calculations. To relate kinematic information to the robot's components, a local coordinate frame is attached to each link at the corresponding joint. The standard notation for this process is the Denavit-Hartenberg method (D-H).

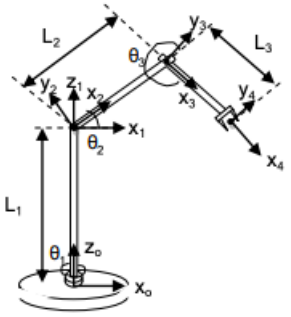

Figure 2.3: Robotic arm with frame assignments for forward kinematics [20]

A robotic manipulator consisting of i links, has $i+1$ joints. The frame assignment procedure using the D-H method goes as follows. The Z_i axis will point along the i-th joint axis, the X_i axis will point along the common perpendicular from Z_i and Z_{i+1} and the Y_i axis is determined using the right hand rule. After the local coordinate frames has been determined, the four D-H parameters are set. [18, p. 235]

The following analysis is based on Figure 2.3.

Link length a_i : The distance along X_i between (Z_i, Z_{i+1})
Link twist α_i : The angle about X_i between (Z_i, Z_{i+1})
Joint distance d_i : The distance along Z_i between (X_{i-1}, X_i)
Joint angle θ_i : The angle about Z_i between (X_{i-1}, X_i)

The parameters are used to determine and compute the transformation matrices using the following formula:

$$ {}^{i-1}_{i}T = \begin{bmatrix} cos\theta_i & -sin\theta_i cos\alpha_i & sin\theta_i sin\alpha_i & a_i cos\theta_i \\ sin\theta_i & cos\theta_i cos\alpha_i & -cos\theta_i sin\alpha_i & a_i sin\theta_i \\ 0 & sin\alpha_i & cos\alpha_i & d_i \\ 0 & 0 & 0 & 1 \end{bmatrix} \tag{2.1} $$

By using using equation 2.1, the homogeneous transformation matrices can be computed. Furthermore, by multiplying these transformation matrices in the right order, the Cartesian coordinates can be obtained. By considering i from 0 to 4, we get the following matrices,

$$ {}^{0}_{1}T = \begin{bmatrix} c_1 & -s_1 & 0 & 0 \\ s_1 & c_1 & 0 & 0 \\ 0 & 0 & 1 & L_1 \\ 0 & 0 & 0 & 1 \end{bmatrix} \tag{2.2} $$

$$ {}^{1}_{2}T = \begin{bmatrix} c_2 & -s_2 & 0 & 0 \\ 0 & 0 & -1 & 0 \\ s_2 & c_2 & 0 & 0 \\ 0 & 0 & 0 & 1 \end{bmatrix} \tag{2.3} $$

$$ {}^{2}_{3}T = \begin{bmatrix} c_3 & -s_3 & 0 & L_2 \\ s_3 & c_3 & 0 & 0 \\ 0 & 0 & 1 & 0 \\ 0 & 0 & 0 & 1 \end{bmatrix} \tag{2.4} $$

$$ {}^{3}_{4}T = \begin{bmatrix} 1 & 0 & 0 & L_3 \\ 0 & 1 & 0 & 0 \\ 0 & 0 & 1 & 0 \\ 0 & 0 & 0 & 1 \end{bmatrix} \tag{2.5} $$

where,

c: cosine of the angle θ_i

s: sine of θ_i

L: length of link i

To get the matrix describing the end-effector frame the following calculation can be performed,

$$ {}^{0}_{4}T = {}^{0}_{1}T\,{}^{1}_{2}T\,{}^{2}_{3}T\,{}^{3}_{4}T \tag{2.6} $$

Which results in the matrix,

$$ {}^{0}_{4}T = \begin{bmatrix} c_1c_{23} & -c_1s_{23} & s_1 & c_1c_{23}L_3 + c_1c_2L_2 \\ s_1c_{23} & -s_1s_{23} & -c_1 & s_1c_{23}L_3 + s_1c_2L_2 \\ s_{23} & c_{23} & 0 & s_{23}L_3 + s_2L_2 + L_1 \\ 0 & 0 & 0 & 1 \end{bmatrix} \tag{2.7} $$

Where s_{23} and c_{23} are the the sine and cosine of the sum of θ_2 and θ_3 respectively.

The first three rows in the last column of ${}^{0}_{4}T$ gives the X, Y, and Z coordinate of the end-effector.

$$ x = c_1c_{23}L_3 + c_1c_2L_2 \tag{2.8} $$

$$ y = s_1c_{23}L_3 + s_1c_2L_2 \tag{2.9} $$

$$z = s_{23}L_3 + s_1L_2 + L_1 \tag{2.10}$$

This analytical procedure of matrix calculations to obtain the Cartesian coordinates of the end-effector frame is the forward kinematics analysis.

2.2.2 Inverse Kinematics

Inverse kinematics is the reverse of forward kinematics and begins at the end-effector, progressing towards the manipulator's base. The goal of inverse kinematics is to determine the joint variables of each joint as a function of the desired X, Y, and Z coordinates of the end-effector.

In contrast to forward kinematics, there is no specific method for solving inverse kinematic problems, which are typically more complex. This is because inverse kinematics problems do not have a unique solution but rather multiple solutions for the same input.

To find the joint angle we divide Equation 2.9 by 2.8

$$\frac{y}{x} = tan\theta_1 \tag{2.11}$$

Then θ_1 is expressed as

$$\theta_1 = arctan2(\frac{y}{x}) \tag{2.12}$$

By combining and rearranging Equation 2.8, 2.9, and 2.10 for c_3 you get

$$c_3 = \frac{x^2 + y^2 + z^2 - (L_1^2 + L_2^2 + L_3^2) - 2L_1(z - L_1)}{2L_2L_3} \tag{2.13}$$

Then from the Pythagorean trigonometric identity

$$s_3 = \pm\sqrt{1 - c_3} \tag{2.14}$$

Equation 2.14 reveals that there are two solutions available. These solutions correspond to the two distinct pathways or configurations that the manipulator can adopt to reach a particular point. In other words, one solution involves moving the elbow of the manipulator upwards, while the other moves it downwards. This illustrates the increased complexity involved in using inverse kinematics compared to forward kinematics. Unlike forward kinematics, which typically has a single solution to the kinematic equation, inverse kinematics often has multiple solutions, requiring a range of different approaches to compute the inverse kinematic solution [20].

2.3 Angled End-Effector

When using an angled end-effector, the fingers must exert a force to hold an object in place. In the case of vertical downward force being applied, the force is evenly split between the two fingers. Refer to Figure 2.4 for a visual representation.

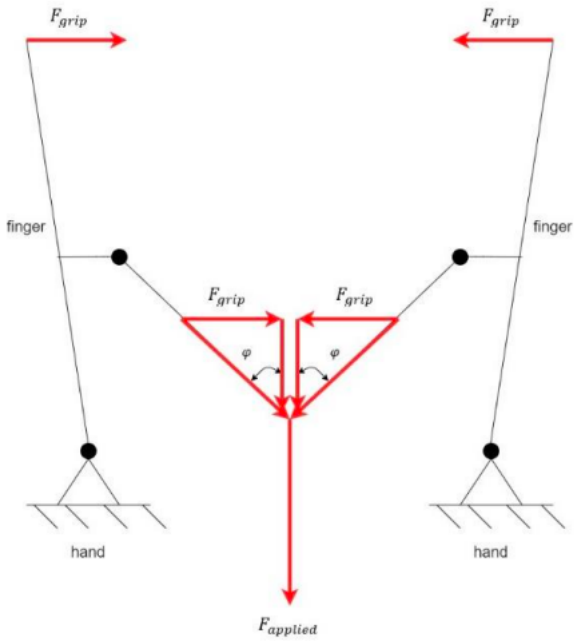

Figure 2.4: Angled end-effector forces [16, p. 21].

The formula for the resulting grip force is,

$$F_{Grip} = \frac{F_{Applied}}{2} tan\varphi \tag{2.15}$$

An important note to make concerning this formula is that the angle φ will diverge towards infinity as the angle approaches 90°. There can be mechanical constraints that prevent the angle from becoming ideal for the maximum grip force.

2.4 Mechanical Elements and Motors

A robotic manipulator consist of several mechanical components and systems that are essential for its functionality and capacity to execute repetitive and automated tasks. Additionally, motors are used to power these mechanisms. This section will explore a variety of components and mathematical concepts used in the design and operation of robotic manipulators.

2.4.1 Worm-Gear Pairs and Spur Gears

There are four primary types of gears, namely: helical, bevel, spur, and worm gears. Each gear type possesses distinct characteristics, and the choice of which to use is determined by the intended application. Meshing gears transmit force, enabling the provision of torsional moments to shafts for generating rotational motion. The meshing process also exerts forces on the corresponding shafts and bearings, potentially leading to material failure. Consequently, it is important to select the appropriate dimensions and materials for gears, shafts, and bearings [21, p. 674-675].

This section will focus primarily on worm-gear pairs and touch upon spur gears, as they are most relevant to the thesis.

A worm-gear pair consists of a worm and a worm gear. This type of gearing system is commonly used in conjunction with electric motors, providing a high reduction ratio and increased output torque to facilitate the transmission of rotary motion. This thesis will specifically address cases where the angle between the shafts is 90°.

During the design of a worm-gear pair, several decisions must be made that will influence

its rotation and overall performance. Firstly, the direction of rotation depends on whether the worm teeth are cut with a right-hand or left-hand orientation. Moreover, the rotational direction of the worm gear is contingent upon the rotational direction of the worm. The worm's shape also affects the efficiency of the pair. One method, called enveloping, shapes the worm in a manner that allows the teeth of one or both components to wrap around the other. There are two types of enveloping: single and double. A single-enveloping worm gear pair features a cylindrical worm and a throated gear partially wrapped around the worm. In contrast, for double-enveloping pairs both components are throated and wrapped around each other.

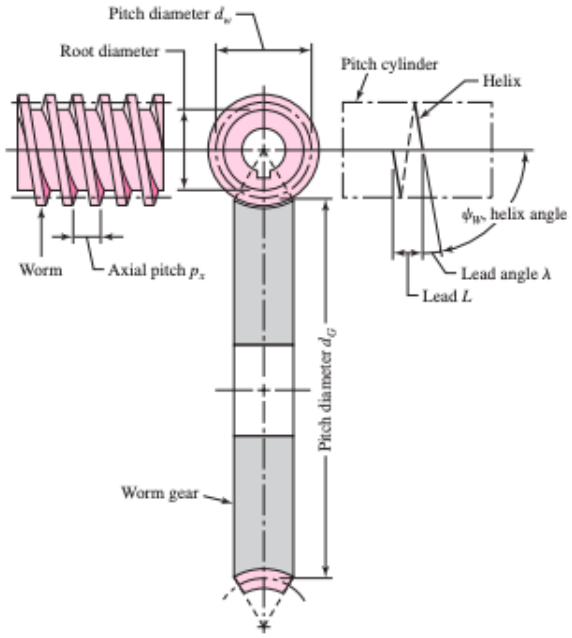

Figure 2.5: Nomenclature of a single-enveloping worm gearset [21, p. 695]

.

In Figure 2.5, a standard single-enveloping worm-gear pair is depicted. A notable characteristic for a worm-gear pair is that the helix angle on the worm is typically quite large, while the angle on the gear is comparatively small. For a 90° shaft angle, these two angels are equal. The pitch of a worm-gear pair is generally denoted by the axial pitch p_x and the circular pitch p_t. These two values are also equal for a 90° shaft angle.

The pitch diameter of the worm gear is the same as for a spur gear, and is given by,

$$d_G = \frac{N_G p_t}{\pi} \tag{2.16}$$

where,

d_G: Pitch diameter

N_G: Number of teeth gear

The worm pitch diameter is not related to the number of teeth, it can in theory have any pitch diameter. Regardless, this diameter should be equal to the hob diameter used to cut the worm-gear teeth. The diameter should be in the interval,

$$\frac{C^{0.875}}{3.0} \leq d_w \leq \frac{C^{0.875}}{1.7} \tag{2.17}$$

where,

C: Center distance

d_w: Pitch diameter worm

The *lead* L and *lead angle* λ of the worm are related as follows,

$$L = p_x N_w \tag{2.18}$$

where N_w is the worm's number of teeth, and lead angle λ is,

$$tan\lambda = \frac{L}{\pi d_w} \tag{2.19}$$

In worm gearing, the pressure angles used depends on the lead angles. One criteria for these angles is that they must be large enough to prevent a phenomenon called undercutting. Undercutting occurs when two meshing gears cut deeper than the involute tooth curve. The primary approach to avoiding undercutting involves designing gears with a number of teeth greater than 16, assuming the standard pressure angle of 20° is used. Tooth depth, or addendum and dedendum, is also crucial for ensuring proper meshing and functionality of the worm-gear pair. The relationship between the pressure angle and tooth depth is outlined in Table 2.1.

Table 2.1: Relationships between angles and tooth depth for worm gearing

Lead Angle λ , degrees	Pressure Angle ϕ_n, degrees	Addendum, α	Dedendum b_G
0-15	14.5	$0.3683p_x$	$0.3683p_x$
15-30	20	$0.3683p_x$	$0.3683p_x$
30-35	25	$0.2865p_x$	$0.3314p_x$
35-40	26	$0.2546p_x$	$0.2947p_x$
40-45	30	$0.2228p_x$	$0.2578p_x$

The analysis of forces on a worm-gear pair is based on the formulas presented in Shigley's Mechanical Engineering Design [21, p. 714-718]. The force exerted by the gear on the worm is noted by F and can be decomposed into F_x, F_y, and F_z. If the friction is neglected, the decomposed forces will be,

$$\begin{aligned} F_x &= F cos\phi_n sin\lambda \\ F_y &= F cos\phi_n \\ F_z &= F cos\phi_n cos\lambda \end{aligned} \tag{2.20}$$

To differentiate between forces acting on worm and gear, subscripts W for worm and G for gear will be used.

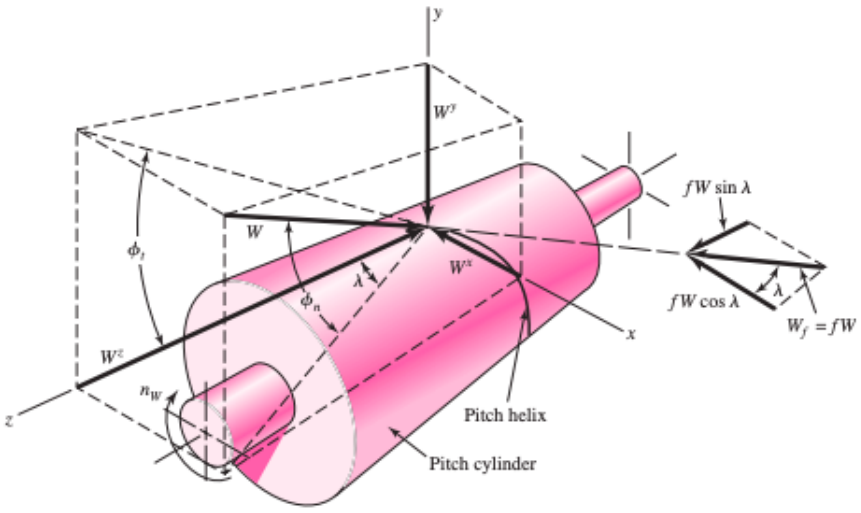

Figure 2.6: Forces on worm exerted by worm gear [21, p. 715].

With reference to figure 2.6 and assuming 90° shaft angle, the gear forces are opposite to the worm forces. This relationship is given as follows,

$$\begin{aligned} F_{Wt} &= -F_{Ga} = F_x \\ F_{Wr} &= -F_{Gr} = F_y \\ F_{Wa} &= -F_{Gt} = F_z \end{aligned} \tag{2.21}$$

Because the relative motion between a worm and worm gear is pure sliding, the friction plays a significant role and is important to include in the calculations. As a result, the coefficient of friction is introduced, μ. By considering friction, Equation 2.20 can be given as follows,

$$\begin{aligned} F_x &= F(cos\phi_n sin\lambda + \mu cos\lambda) \\ F_y &= F sin\phi_n \\ F_z &= F(cos\phi_n cos\lambda - \mu sin\lambda) \end{aligned} \tag{2.22}$$

To find the frictional force F_μ, we insert $-F_{Gt}$ from Equation 2.21 for F_z in Equation 2.22.

$$F_\mu = \mu F = \frac{\mu F_{Gt}}{\mu sin\lambda - cos\phi_n cos\lambda} \tag{2.23}$$

A useful relationship of the tangential forces of the worm and gear is given by the equation,

$$F_{Wt} = F_{Gt} \frac{cos\phi_n sin\lambda + \mu cos\lambda}{\mu sin\lambda - cos\phi_n cos\lambda} \tag{2.24}$$

The tangential component of the worm can be given by the following equation,

$$F_{W_t} = \frac{2T_{in}}{d_w} \tag{2.25}$$

where d_w is the worm diameter and T_{in} is the input torque.

The efficiency of the gearset is given by the equation,

$$\eta = \frac{cos\phi_n - \mu tan\lambda}{cos\phi_n + \mu cot\lambda} \tag{2.26}$$

The output torque of the worm gearset is given by,

$$T_{out} = F_{Gt} r_{Gp} \tag{2.27}$$

where r_{Gp} is the pitch radius of the worm gear.

A useful property of worm-gear pairs is their ability to be self locking. This property is especially useful in applications where it is necessary for a robotic arm to hold a certain position. If the system is self locking, an applied torque to the output shaft will not be able to rotate the worm. Theoretically, a worm gearset is self locking if the static friction μ_s is larger than the lead angle of the worm.

$$\mu_s \geq tan\lambda \tag{2.28}$$

For two meshing spur gears transferring motion and moment by friction assuming no slip, the tangential speed at the contact surface is identical and given by the following formula [22, p. 103-104],

$$v = w_1 r_1 = w_2 r_2 \tag{2.29}$$

where w is the angular velocity and r is the pitch radius. Furthermore, assuming there is no slip between, gear ratio i is given by,

$$i = \frac{w_{in}}{w_{out}} = \frac{Gear_1}{Gear_2} \tag{2.30}$$

where $Gear_1$ is the number of teeth of the driving gear and $Gear_2$ is the number of teeth of the driven gear.

Equation 2.30 can be rewritten in terms of input and output torque as follows,

$$i = \frac{T_{out}}{T_{in}} \tag{2.31}$$

2.4.2 Shafts

Shafts are rotating members, often featuring a circular cross section. They provide the axis of rotation and can be mounted with components like gears and bearings to transmit power and motion. Shafts accommodating gears and bearings are subjected to bending and shear forces. To minimize the deflections and bending moments, the shafts should be designed as short as possible. When a shaft is fitted with a worm gear, the forces exerted by the gear must be considered. These forces will influence the choice of bearings for the shaft, as they must withstand the reaction forces. Furthermore, the shaft diameter depends on the tolerances and specifications of the components to ensure proper assembly. For instance, the shaft diameter must align with the bore diameter of the gear and its tolerances.

In determining the axial layout of the components of the shaft, several factors must be considered. Generally, load-bearing components should be placed between two bearings. To minimize bending moments and deflection, it is beneficial to position these components near bearings or shaft shoulders, if possible. A stepped cylinder shaft design with shoulders is common in many cases. However, if axial loads are relatively low, shaft shoulders can be overlooked. In such instances, the use of press fits, set screws, and other fit methods are sufficient to maintain the axial location of the shaft.

After determining the components, materials, and dimensions of the shaft, an analysis can be conducted to obtain shear and bending moment diagrams, allowing for the determination of forces at the bearings.

2.4.3 Bolts, Screws, and Fasteners

Bolts and screws are often mistakenly considered synonymous, however, despite their similar appearances, they are distinct fasteners with unique applications.

The Machinery's Handbook clarifies that bolts are employed to assemble unthreaded parts, often in combination with nuts. In contrast, screws are utilized to join parts with threads. In instances where screws serve as fasteners, threads may not always be premade. Screws possess the capability to create threads during installation. In summary, the key distinction between bolts and screws lies in their usage: bolts assemble unthreaded parts, while screws join threaded components. There are thousands of bolt and screw varieties, differing in terms of material, size, and shape. Common types of bolts include anchor bolts and hexagonal bolts [23].

2.4.4 Rolling Bearings

There is a wide variety of rolling bearings available. The term "rolling bearings" refers to bearings with rolling elements, which can be either balls or rollers. These diverse bearings are designed to accommodate pure radial load, pure axial load, or a combination of both. One commonly used bearing in the industry is the single-row deep groove ball bearing, which will be covered in this section. The formulas for sizing and selecting bearings are based on the guidelines provided by SKF. These bearings can handle both radial and some axial load, and consist of four main components: The outer ring, inner ring, balls, and separator. Refer to Figure 2.7 for an illustration.

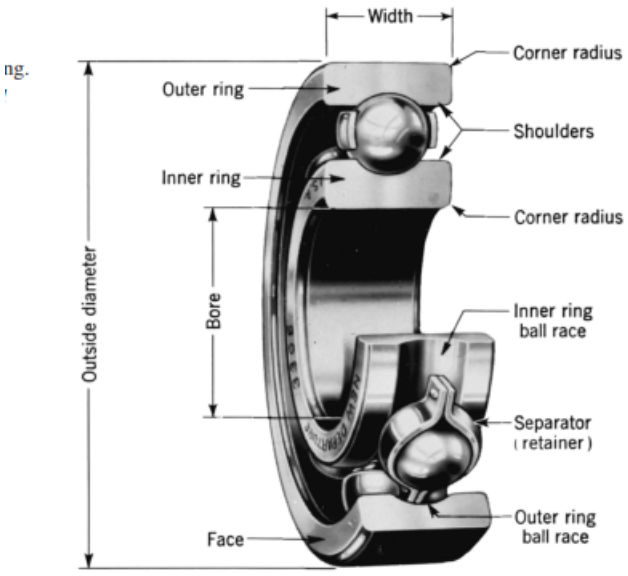

Figure 2.7: Nomenclature of a standard ball bearing [21, p. 571]

Contact stresses arise during the rotation of bearings, fluctuating between minimum and maximum values. Given this variation in stress during rotation and the expectation that a bearing will perform millions of revolutions, it is essential to design bearings with fatigue failure in mind. Significant plastic deformations can occur in bearings due to static loads. Static loads are particularly critical for slow-rotating bearings, as they can significantly impact their performance for longevity.

For a bearing subjected to both axial and radial load, the equivalent static bearing load is given by the following equation,

$$P_0 = X_0 F_r + Y_0 F_a \tag{2.32}$$

where,

P_0: Equivalent static bearing load

F_r: Radial bearing load

F_a: Axial bearing load

X_0: Radial load factor for the bearing

Y_0: Axial load factor for the bearing

The values for X_0 and Y_0 vary for each type of bearing.

To check if a bearing can handle the equivalent static load, it needs to be compared to the basic static load rating C_0. To avoid permanent deformations the following condition must be met,

$$s_0 P_0 \leq C_0 \tag{2.33}$$

where s_0 is the static safety factor. The value for s_0 depends on the different bearings usage and its purpose.

For single-row deep groove ball bearings, axial bearing load should not surpass 50 percent of basic static load rating.

$$F_a \leq 0,5C_0 \tag{2.34}$$

When choosing a bearing, one must also consider the dynamic bearing load. The equivalent dynamic bearing load is given by the following equation,

$$P = XF_r + YF_a \tag{2.35}$$

where,

P: Equivalent dynamic bearing load

X: Radial load factor

Y: Axial load factor

The dynamic load factors is a function of the relationship f_0F_a/C_0, where f_0 can be found in the SKF catalogue and depends on the inner and outer diameters of the bearing.

Once the equivalent dynamic bearing load is known, it is possible to calculate the bearing's service life.

$$L_{10} = \left(\frac{C}{P}\right)^a \tag{2.36}$$

where,

L_{10}: Basic rating life at 90 percent reliability

C: Basic dynamic load rating

P: Equivalent dynamic bearing load

a: Exponent for the life equation

The value for a has a standard value for ball bearings and roller bearings. For ball bearings $a = 3$, and $a = 10/3$ for roller bearings.

The service life of a bearing can also be given in terms of operating hours. If the bearing

operates at constant revolutions per minute, the following equation gives the operating hours for a bearing at 90 percent reliability,

$$L_{10h} = \frac{10^6}{60 * n} L_{10} \tag{2.37}$$

where n is revolutions per minute.

2.4.5 Mechanical Compression Springs

Mechanical compression springs are coiled components that possess valuable characteristics. When subjected to an applied force, these springs compress and subsequently produce a counteracting force, allowing them to return to their original length.

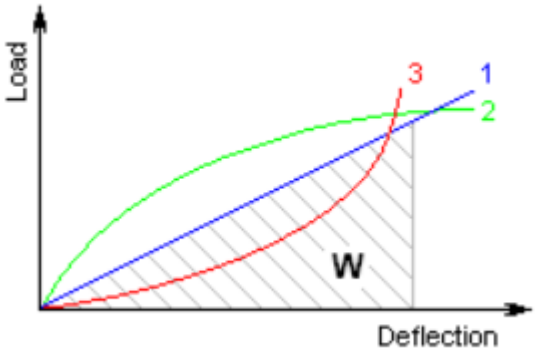

Figure 2.8: Load compared to deflection [24]

The relationship between the force applied to the spring F, and the deformation of the spring δ, can be described by Hooke's Law. Hooke's Law states that the force F required to compress or extend the spring is proportional to the deformation δ.

Hooke's Law can be expressed mathematically as,

$$F = k\delta \tag{2.38}$$

where,

F: Spring force

k: Spring constant

δ: Displacement

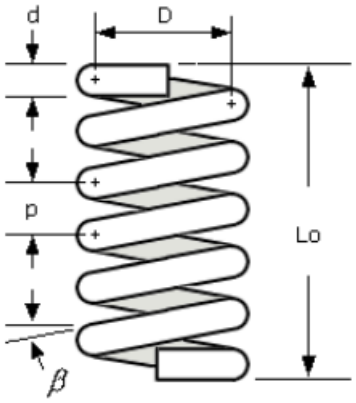

Figure 2.9: Compression spring nomenclature [22, p. 142]

Figure 2.9 presents important nomenclature for a compression spring.

where,

L_0: Unloaded length of spring

D: Mean diameter

d: Wire diameter

p: Spring pitch

β: Helix angle

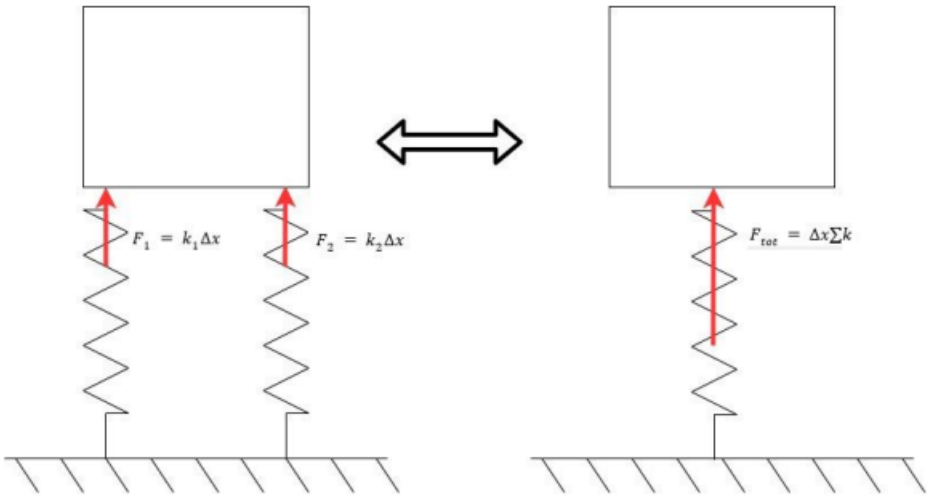

Figure 2.10: Two active spring forces [16, p. 23]

The compression force is given by the following equation,

$$F_{tot} = \Delta x \sum k \tag{2.39}$$

The maximum shear stress of a spring refers to the highest stress the spring can endure before experiencing deformation. When considering the curvature of the spring, the shear stress can be expressed as,

$$\tau_2 = \frac{16FD}{\pi d^3}(\frac{2C+1}{4C-3}) \tag{2.40}$$

where C is,

$$C = \frac{D}{d} \tag{2.41}$$

and F is,

$$F = \frac{Gd\delta}{8nC^3} \tag{2.42}$$

where,

G: The pressure the material can withstand

n: Number of active coils

The various cases for n , can be determined from Figure 2.11.

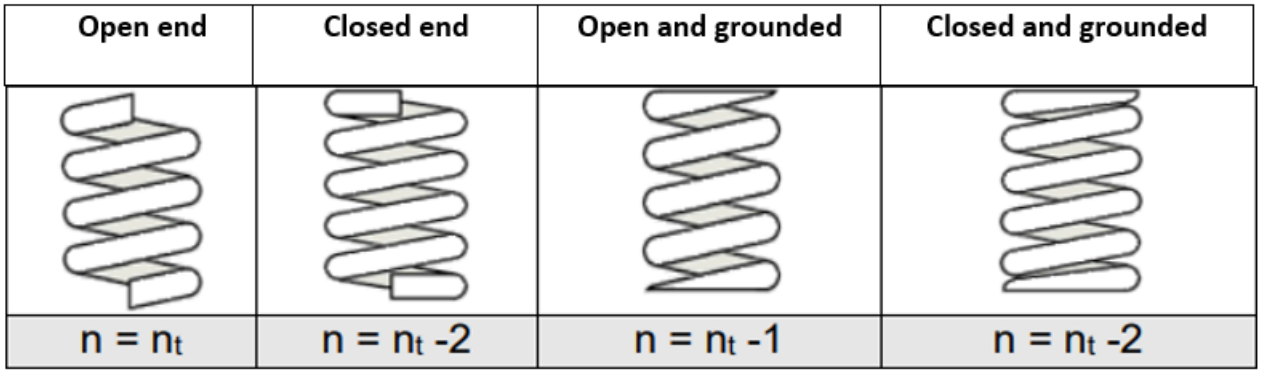

Figure 2.11: Different cases for n [22, p. 143].

2.4.6 Shaft and Housing Fits

A proper fit is critical to ensure the desired function of a joint for shafts and holes, and to minimize the use of additional fasteners. Fits can be classified into three types: interference fit, transition fit, and clearance fit, all of which are commonly used for bearing-housing and bearing-shaft assemblies, as well as for the assembly of other mechanical components. When selecting fit, standardized tolerances provide precise values for the diameters of the shaft and hole required to achieve the desired fit and function.

An interference fit involves the fastening of a shaft and hole due to normal forces. By slightly decreasing the hole diameter compared to the shaft diameter, the tight fit produces a joint held together by friction. Several methods exists to assemble a press fit, such as the use of hammers, hydraulic rams, and shrink fitting by cooling one component.

In a transition fit, the hole diameter is smaller than the shaft diameter, similar to an interference fit. The difference between the two is that, for a transition fit, the tolerance zone of the shaft lies between the lower and middle part of the tolerance zone of the hole. In other words, the difference between the hole tolerance and shaft tolerance is not as large as in an interference fit.

A clearance fit entails a gap between the shaft and the hole. Transition and interference fits are often used when rotary movement is involved. Conversely, a clearance fit is commonly used for linear movement, where there is no requirement for the hole to move with the shaft [21, p. 395-397].

Figure 2.12 illustrates different types of fits, while Figure 2.13 shows classifications for bearing fits.

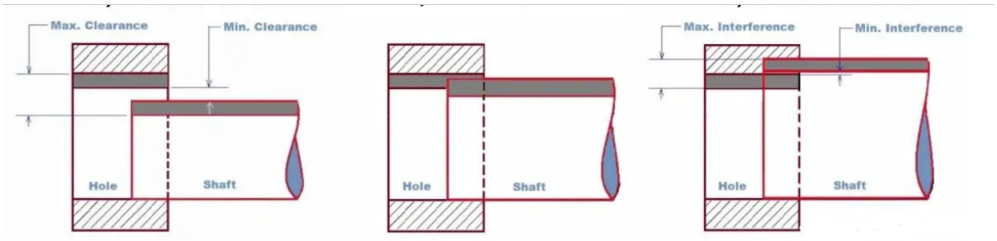

Figure 2.12: From left to right: Clearance fit, Transition fit, Interference fit [25].

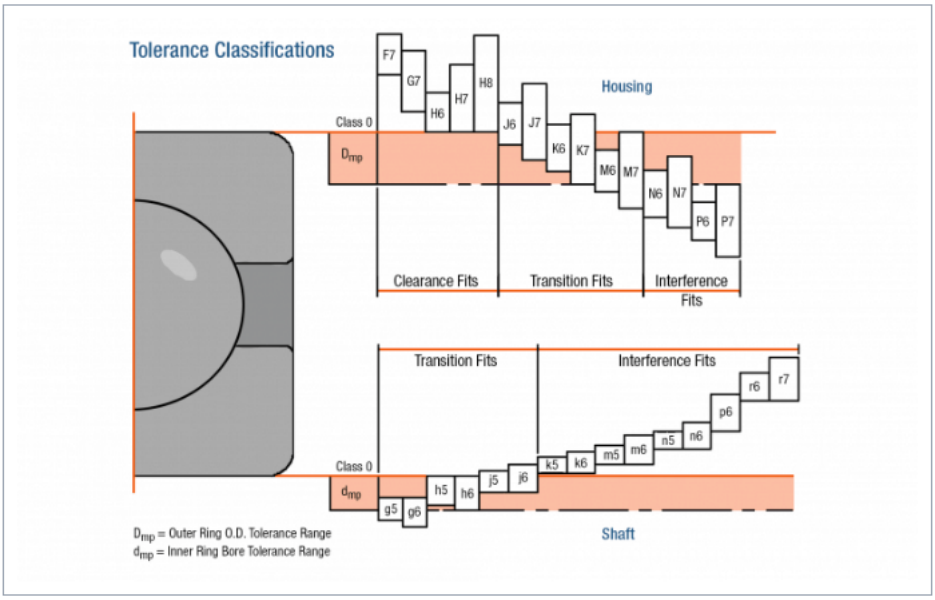

Figure 2.13: Shaft and housing tolerances for bearings [26].

In an interference fit, stresses can occur. These stresses can lead to potential failure such as buckling of a shaft or malfunctioning of a bearing. If the shaft and hole are made of different materials, and the shaft is a solid cylinder with uniform internal pressure, the shear stress at a given point on the face of interference can be calculated. Formulas relevant for these calculations can be found in Appendix B: Additional Theory.

2.4.7 Buckling

Buckling refers to the deformation of a structure when subjected to a load. As the load on a structure increases, it reaches a critical point where the structure undergoes deformation. Depending on the type of support, the deformation can occur in different directions. There are four Euler cases with regards to the length of the structure, which are illustrated in Figure 2.14 and the effective length factor is presented in Table 2.2.

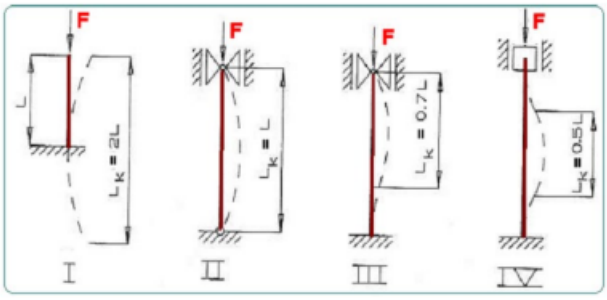

Figure 2.14: The four Euler cases illustrating effective length factors [22, p. 33].

Table 2.2: Theoretical and recommended effective length factors [22, p. 33]

Euler case	I	II	III	IV
Theoretical value	0.5	1	$\sqrt{2}$	2
Recommended value	0.5	1	1.1	1.1

The Euler stress is given by the following equation,

$$\sigma_E = \frac{F_E}{A} = \frac{\pi^2 EI}{AL_k^2} = \frac{\pi^2 Ei^2}{L_k^2} \tag{2.43}$$

where,

F_E: Critical buckling load

A: Cross section

E: Modulus of elasticity

L_k: Critical length

I: Moment of inertia

i: Radius of gyration

The compressive load that a column can withstand depends on the ratio between its length and diameter, which is also knows as the slenderness ratio, λ, and can be calculated as follows,

$$\lambda = \frac{L_k}{i} \tag{2.44}$$

Where the i is,

$$i = \sqrt{\frac{I}{A}} \tag{2.45}$$

Eurocode 3 is a design standard that provides guidelines for determining the buckling resistance of steel structural members, taking into account the effects of stress, defects, and deflection caused by shear forces. The critical buckling stress depends on the material properties of the structural member and is a function of the buckling factor and the

yield strength of the material. The buckling reduction factor χ, and the non-dimensional slenderness $\bar{\lambda}$ can be calculated as follows,

$$\chi = \frac{\sigma_k}{R_e} \tag{2.46}$$

where σ_k is the buckling stress, and R_e is the yields strength. The non-dimensional slenderness is,

$$\bar{\lambda} = \frac{\lambda}{\lambda_F} \tag{2.47}$$

The critical slenderness λ_F is,

$$\lambda_F = \pi\sqrt{\frac{E}{R_e}} \tag{2.48}$$

The factor of safety for buckling, denoted as n_k, is a key parameter in ensuring the safety of a structure against failure. Typically n_k ranges from 1.5 to 3, indicating the level of safety required for the specific application. The factor of safety is a measure of the safety margin of a structure against failure. A higher safety factor indicates lower risk of failure. The maximum allowable axial force with a given factor of safety can be calculated using the following equation[22, p. 36],

$$F_{allowed} \leq \frac{\sigma_k * A}{n_k} \tag{2.49}$$

Figure 2.15 depicts the Eurocode 3 buckling curves, which are functions of the non-dimensional slenderness and the buckling reduction factor. The selection of the appropriate buckling curve also depend on the type of cross section and other design considerations illustrated in Figure 2.16.

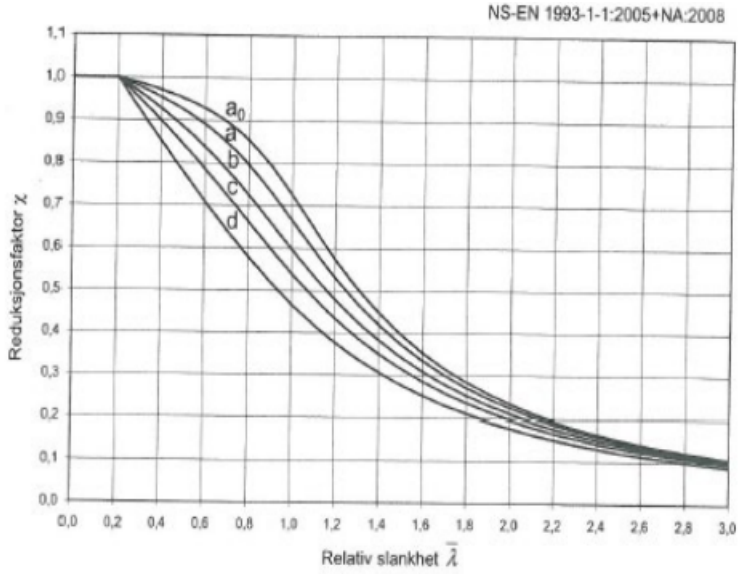

Figure 2.15: Eurocode 3 buckling curves [22, p. 37]

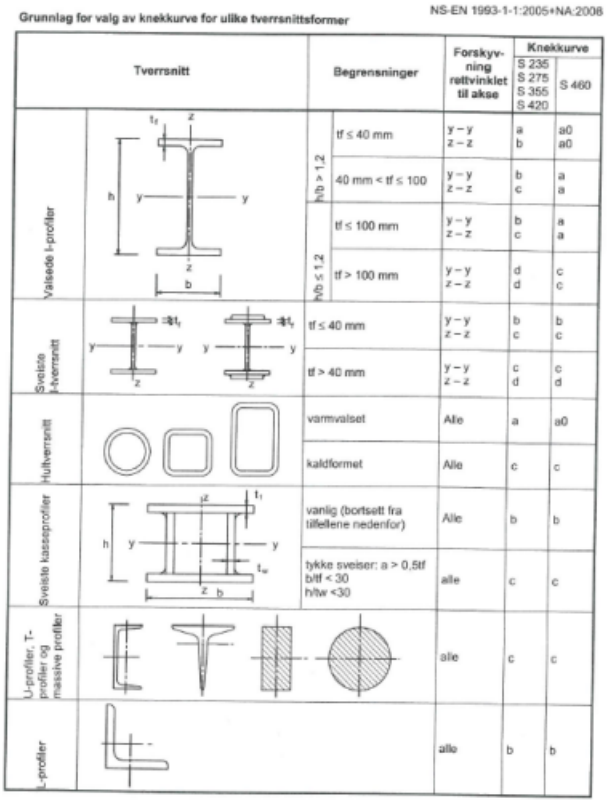

Figure 2.16: Selection of buckling curve for a cross section [22, p. 38]

2.4.8 Motors

An electromechanical energy conversion device, commonly known as an electric motor, converts electrical energy into mechanical output energy. A manipulator used on a ROV

requires motors that are waterproof and that provides desired mechanical output. Two types of electric motors are stepper motors and BLDC motors. The primary differences between the two types is that a BLDC motor is optimized for high speed applications, while stepper motors exceed in applications requiring precision [27].

BLDC Motors

The Brushless Direct Current (BLDC) motor is an electric motor that operates without brushes. It uses an electric controller to switch DC currents to the motor coils, creating a rotating magnetic field, which the permanent magnet rotor follows. Unlike traditional motors, BLDC motors do not require brushes and commutators, since their coils are fixed. As a result, they require little maintenance and can easily be made waterproof with epoxy, making them suitable for subsea manipulator operations. However, one disadvantage of the BLDC motor is that it does not provide a holding torque, and an external source, such as a worm-gear, is required to hold positions. Figure 2.17 illustrates the interior for a BLDC motor.

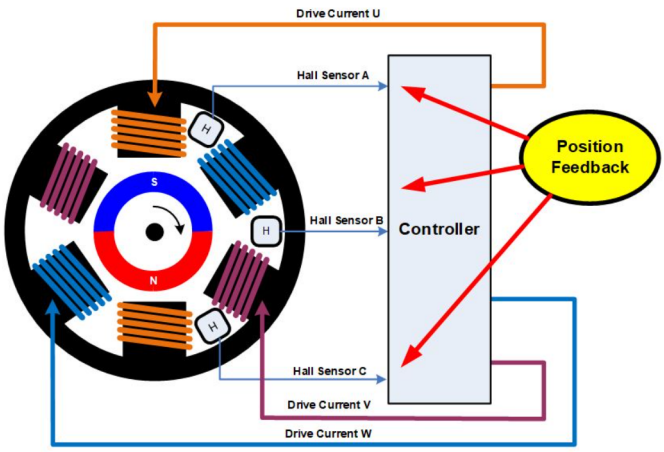

Figure 2.17: BLDC motor interior [28].

The RPM of certain BLDC motors, with a given KV-rating, is given by the following equation,

$$RPM = KV * Voltage \tag{2.50}$$

The effect, Q, can be calculated as follows,

$$Q = V * A \tag{2.51}$$

The maximum input torque can then by calculated by the following equation,

$$T_{max} = \frac{Q}{w_{max}} \tag{2.52}$$

where w_{max} is the maximum angular velocity.

Stepper Motors

A stepper motor is an electrical motor that divides its movement into discrete steps, with a constant angular distance between each step. The motor achieves this by using windings inside the motor as magnetic poles when electrical input energy is supplied. These wire windings are evenly spaced on the stator. The rotor, on the other hand, is made up of magnet pairs in a gear shape, which align with the magnetic poles on the stator. Figure 2.18 illustrates the interior of a stepper motor [27].

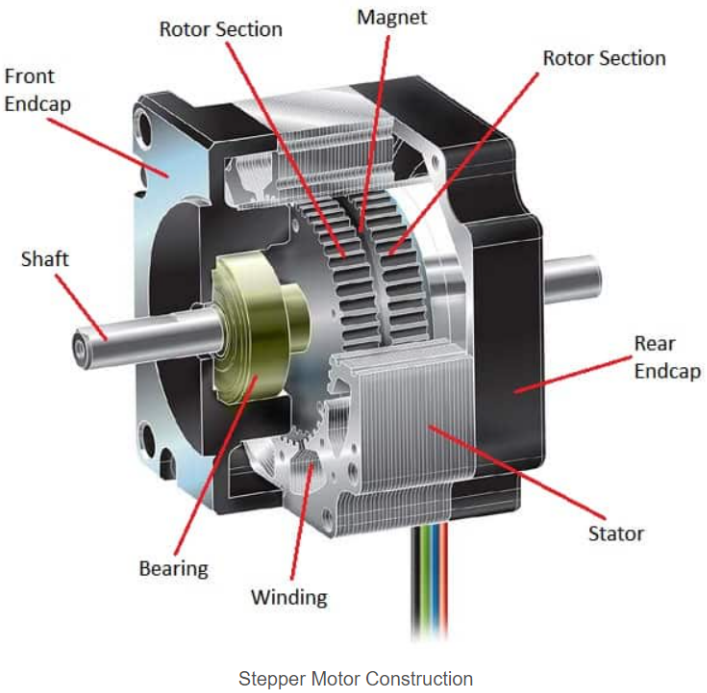

Figure 2.18: Stepper motor interior [29].

A motor controller is used to control the movement of a stepper motor. The controller switches the current to the windings, creating a magnetic field that moves the rotor from one pole to another. The step angle and the number of steps can be controlled by the motor controller, making stepper motors highly accurate. Moreover, stepper motors can provide holding torque, making them ideal for applications that require precise positioning and holding certain positions. This feature is particularly useful for a ROV manipulator, where accuracy is crucial and specific positions must be maintained [27].

2.5 3D printing

3D printing is a revolutionary technology that uses additive manufacturing to create parts. Unlike traditional subtractive manufacturing, which involves carving out a block of raw material, 3D printing adds material layer by layer to create a part. This process allows for the creation of complex geometries that would be otherwise difficult and impossible to manufacture using traditional methods.

The process of 3D printing starts by creating a CAD model of the part that needs to be printed. This model is then exported as an STL file and uploaded to a slicing software. The software converts the model into G-code, which is then uploaded to the 3D printer. Once the printer receives the G-code, it begins the printing process, creating the part layer by layer.

3D printing technology is rapidly advancing, with printers becoming faster and more affordable. As a result, they are becoming widely used in the engineering world for both production and prototyping. The benefits of 3D printing extend beyond just creating complex geometries; it also allows for the creation of customized parts with ease, reducing the need for costly tooling and mold-making. With 3D printing, parts can be quickly and easily produced on-demand, making it a versatile and powerful tool in modern manufacturing [30].

While 3D printing is commonly associated with low-cost materials such as PLA and ABS, there are now printers available that can work with a wide range of materials, including steel and carbon fiber. There are different types of 3D printers on the market. For

instance, the Original Prusa i3 printers are affordable, making them ideal for prototyping, but may not be as suitable for producing detailed products requiring high strength [31]. On the other hand, printers like the Ultimaker S5 are capable of printing parts of stronger material which can be used beyond just prototyping [32].

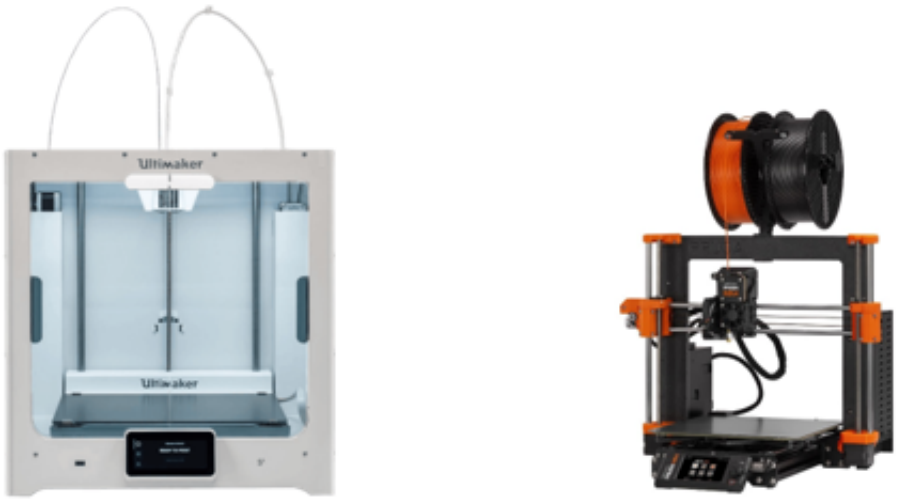

Figure 2.19: From left to right: Ultimaker S5 and Original Prusa i3 3D printers [31] [32].

Chapter 3

Product Development Process

The product development process was the method utilized for this project. The PDP is a common step by step method serving as a great tool in structuring and breaking down tasks for the project. The generic process consists of a six step plan that takes the project from an idea and initial concept to the final product. PDP is not necessarily a fixed process where the process is fully followed. This project used the PDP as a tool and guidance to achieve a structured approach, and only the relevant steps of the generic process were used in this project. These were planning, concept development, detail design, testing and refinement, and production [33, p.57].

Figure 3.1: Generic product development process [33, p.57].

3.1 Product Planning

The planning phase precedes the product development process, and parts of it was not included in the thesis. The first two steps were to identify opportunities and evaluate and prioritize projects. These two steps had already been performed when UiS Subsea was first founded, and were therefore not included in this thesis. The planning phase for this project was primarily allocation of resources, plan timing, and complete pre-project

planning including the missions statement.

3.1.1 Allocation of Resources and Plan Timing

The allocation of resources and plan timing process was heavily influenced by the limited time and resources available. During the first weeks of the project, the teams responsibilities throughout the project were determined. Summarized, the responsibilities of the team included creating the manipulator for the ROV, as well as choosing and waterproofing its motors. This process was extensive as all the teams had to cooperate and through communication declare the constraints and limitations. The manipulator was assigned a budget, and deadlines and weekly goals were established. A dynamic project plan was created, and based on the requirements from MATE and UiS Subsea a needs matrix was created. The needs matrix included requirements and their relative importance for the projects. Moreover, each need was assigned an estimated degree of difficulty to better allocate resources and time. A GANTT chart was also utilized, which is a project management tool serving as a project plan illustrating the phases of the project and their respective activities. Furthermore it illustrates the work completed in relation to the time planned for the product. A GANTT chart undergoes several revision throughout a project. Figure 3.2 shows an early revision of the GANTT chart. The needs matrix is illustrated in Figure 3.3.

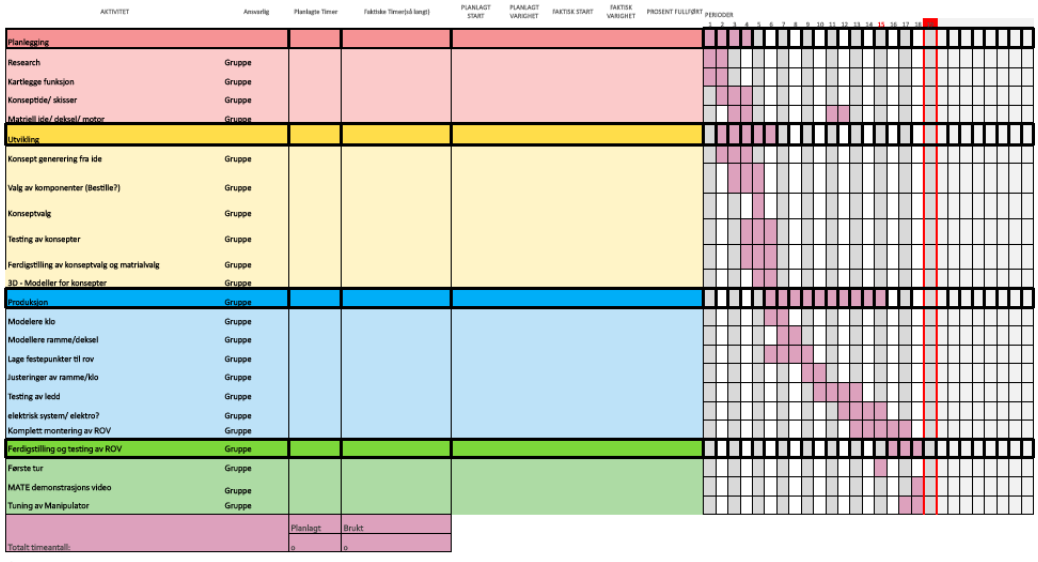

Figure 3.2: GANTT chart

	Ansvarlig person	Beskrivelse	Vansklighetsgrad	Avklaring	Prioritet	Begrunnelse	Verifisering
1	M - Manipulator	Manipulatorklo må kunne gripe og håndtere	Middels/Høy	Fra 2 mm til 30mm. Gripekraft må være minst 10N	Høy	Mate krav	3D Print og testrigg
2	M - Manipulator	Bæreevne	Middels	Må kunne transportere FLOAT og andre gjenstander gitt av MATE og TAC.	Høy	Mate krav	
3	M - Manipulator	Mobilitet	Middels	Må kunne gripe 90 grader opp fra ROV og 90 grader på havbunnen.	Høy	Mate krav	
4	M - Manipulator	Vanntett	Middels/Høy	El - system og motorer skal ikke eksponeres for vann	Middels/Høy	Nødvendig for å sikre komponenter i system	
5	M - Manipulator	Topologi	Middels	Redusere vekt ved å fjerne unudvendig materiale	Middels	Manipulator må veie minst mulig for å ikke overskride kravene fra mate om vekt	
6	M - Manipulator	Material	Middels	Valg av riktig material for å unngå rust	Middels/Høy		
7	M - Manipulator	Drivkraft/ motor	Middels/Høy	Motorkraft må være tilstrekkelig for å opperere mainipulator oppgaver og gi nødvendig holdemoment for klype og ledd	Middels/Høy		
8	M - Manipulator	Kamera	Lav	Kamera montert arm. Må sende bilde til overflate	Middels/Høy	For å kunne se gripeklo og utføre oppgaver fra overflate	
9	M - Manipulator	Vannprøve på 50 ml	Lav	Vannprøve skal tas ved hjelp av ventil på manipulatorarm	Høy	Mate krav	

Figure 3.3: Needs matrix

3.1.2 Mission Statement

As the planning phase concluded, the team drafted a mission statement for the project, providing clear development guidance. This statement enabled the team to create a more detailed product description, determine product benefits, establish key business goals, identify the primary targets, assumptions and constraints. Additionally, stakeholders were identified, allowing the team to consider their needs and expectations. The mission statement served as a summary of the direction to be taken during the concept development phase and the entire development process. The missions statement can be found in Table 3.1.

Table 3.1: Mission statement

Product Description Manipulator	A fully functional ROV Manipulator capable of performing all necessary tasks
Benefit proposition	• Easy assembly, disassembly, and maintenance • Capable of performing the tasks given by MATE • Size and weight within limits • Easy maneuverability and efficient movement • Environmentally friendly product
Key Business Goals	• Ready for water test by April 11^{th} • Product build complete by May 15^{th} • Price of components and manufacturing within given budget • Perform well in the competitions • Build a foundation for future manipulator projects
Primary Market	• Subsea operations • Education and student competitions
Assumptions and constraints	• Submerged and operates in chlorinated water • Budget of 8000 NOK • Experience and knowledge of the group • Time span from 05.01.23 - 15.05.23 • Operates at a depth of 4 meters • Subjected to low loads • Driven electrically
Stakeholders	• UiS Subsea • University of Stavanger • UiS Subsea sponsors • Future UiS Subsea members • MATE ROV Competition

3.2 Concept Development

After completing the product planning phase, the next major phase was the concept development. This phase involved identifying customer needs, establishing target specifications, and generating, selecting and testing concepts. This thesis will not cover every step of the concept development process, and will focus on the key steps relevant to the development of the manipulator.

3.2.1 Identifying Customer Needs

The initial step involved identifying the customer needs. The primary customer was from the start known to be MATE, and the MATE ROV Competition manual provided the raw data. This manual contained an extensive array of information and data that could be perceived as customer needs. However, it was important to express the customer needs according to certain guidelines [33, p.87],

- The needs had to be expressed based on what the manipulator had to do, not how it might do it.
- Needs had to be expressed at the same level of detail as the raw data and as an attribute of the product.
- Use of positive phrasing only, while also avoiding words such as *must* and *should*.

The next step of the process was to organize the customer needs in terms of their importance. See Table 3.2.

Table 3.2: Customer needs manipulator

No.	Need	Imp.
1	The manipulator can grab objects between 2-30mm	5
2	The manipulator can transport objects of 1kg	5
3	The manipulator functions at a depth of 4 meters	5
4	The manipulator is safe and not environmentally hazardous	4
5	The end-effector of the manipulator can hold an object with a load of at least 10N	5
6	The manipulator can be submerged for 15 minutes	4
7	The manipulator can operate in chlorinated water at temperatures between 15-30°C	4
8	The manipulator can perform a water sample test of 50ml	5
9	The weight of the manipulator will not lead to the total ROV weight exceeding 35kg	5
10	The end-effector of the manipulator can grip an object with a force greater than 10N	4
11	The manipulator is easy to assemble, disassemble and maintain	3
12	The manipulator has three degrees of freedom	3
13	The manipulator can perform all necessary MATE tasks	4
14	The weight distribution of the manipulator is balanced	3
15	The manipulator has a modular build	3
16	The manipulator can be produced within a budget of 8000NOK	4
17	The manipulator material is water and chemically resistant	4
18	The material of the manipulator is environmentally friendly	3
19	The manipulator can be submerged in water for 1 hour	2
20	The manipulator can be submerged in salt water	2
21	The manipulator can operate at a depth of 50m	1

In Table 3.2, need number 1 through 10 were directly derived from the MATE Competition requirements. Needs 11 through 21 were needs from within the UiS Subsea team, and their ambitions. Upon inspection, it became apparent that some needs were redundant. For instance, need 3 and 21 both emphasized operational depth. This was because MATE required a depth of four meters, while UiS Subsea aimed for a depth of 50m. Similarly, need 6 and 19 were redundant. Needs 17 and 7 both highlighted that the manipulator should be able to function in chloride or chemical environments, making need 17 unnecessary. Additionally, both need 11 and 15 focused on the manipulator's assembly. If the build was modular, it was likely that the manipulator could be easily assembled, disassembled, and maintained.

The next step involved removing these redundant needs, assigning importance ratings to them and arraigning them hierarchically. Table 3.2 illustrates that the needs provided by MATE had the highest relative importance. The team's aspirations were merely an added

advantage and an opportunity to potentially exceed in the competition. This approach of arranging the needs in a hierarchical list ensured that the manipulator's development was centered around MATE's requirements, and no crucial needs were overlooked. The list also acted as a reference for the team regarding how to prioritize the various needs.

Table 3.3: Customer needs for manipulator, rated by importance

No.	Need
1	The manipulator can grab objects between 2-30mm
2	The manipulator can transport objects of 1kg
3	The manipulator functions at a depth of 4 meters
5	The end-effector of the manipulator can hold an object with a load of at least 10N
8	The manipulator can perform a water sample test of 50ml
9	The weight of the manipulator will not lead to the total ROV weight exceeding 35kg
4	The manipulator is safe and not environmentally hazardous
6	The manipulator can be submerged for 15 minutes
7	The manipulator can operate in chlorinated water at temperatures between 15-30°C
10	The end-effector of the manipulator can grip an object with a force greater than 10N
13	The manipulator able to perform all necessary MATE tasks
11	The manipulator easy to assemble, disassemble and maintain
12	The manipulator has three degrees of freedom
14	The weight distribution of the manipulator is balanced
16	The manipulator can be produced within a budget of 8000NOK
18	The material of the manipulator is environmentally friendly
20	The manipulator can be submerged in salt water

3.2.2 Search For Information and Benchmarking

By conducting research and benchmarking of products both internally within UiS Subsea and externally, valuable information was gathered and existing products were mapped and compared. This enabled the identification of potential solutions that catered to customer needs and the challenges at hand, while also providing inspiration for further innovation for the manipulator.

During the external search, the team looked up various manipulators used in the subsea industry. Two commonly used manipulators are the Schilling Robotics TITAN 4 Manipulator and the Subsea Tech ATOM ROV Manipulator. The TITAN 4 is a versatile servo-hydraulic manipulator typically used for ultra-heavy work class ROVs. It has a

nominal maximum lift capacity of 454kg, and can operate at a depth of up to 4000 meters [34]. In contrast, the Subsea Tech ATOM ROV Manipulator is a more compact manipulator designed for use on smaller ROVs. It is suitable for light-duty tasks such as inspection and sampling and can operate at a depth of up to 300 meters [35]. It is worth noting that the majority of industrial manipulators are based on hydraulics. Hydraulics would pose significant challenge for this project, as it is complex and expensive. Additionally, the use of oil-based components possibly causing spillage, goes against the customer need emphasising the environmental friendliness.

To address this, the team studied previous UiS Subsea manipulators, specifically the one from 2015 and 2021, to extract relevant information on their solutions and challenges. Unfortunately, documentation on the manipulators between 2015 and 2021 was not available. Furthermore, the manipulator designed in 2022 did not work properly, and was not used in the competition. However, one promising concept from 2022 was the implementation of lead screw actuation and a telescope function for the manipulator. Benchmarking information for the 2015 and 2021 manipulator is shown in Table 3.4.

Table 3.4: Benchmarking information

Benchmarking Information		
Products	Manipulator 2021 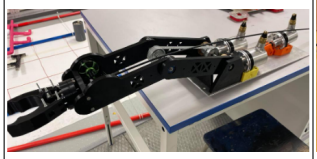	Manipulator 2015 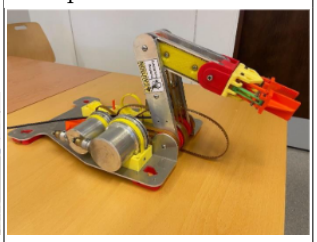
Placement in MATE	NA	19th
Weight(g)	4855	8802
Active reach (mm)	450	450
Frame material	PLA	Aluminum
Gripping function	Steel wire	Steel wire
Motors	4	6
Pros	x Motors close to mass center x Easy to assemble x Light weight x 3 degrees of freedom	x High lift capacity x Easy to assemble x Robust x Easy to handle
Cons	x Unstable x Loose cables x Limited lift capacity	x Heavy x Belt slack x Poor grip

3.2.3 Establishing Target Specifications

While the established customer needs were helpful in developing a clear understanding concerning MATE, they provided little direction on how to design and engineer the manipulator. The way forward was open, and therefore, it needed to be narrowed down and made more specific. Hence, the customer needs were transformed into target specifications. A specification was composed of a metric and its value. The target specifications provided a comprehensive and measurable description of what the manipulator needed to accomplish, without specifying how to achieve these specifications. The target specifications were determined early in the development process, without considering limitations such as technology and time constraints. However, they did represent the team's aspirations and goals for the project. The target specifications outlined a manipulator that the team anticipated would perform well in the competition. The process of establishing the

target specifications involved the following steps: preparing a list of metrics, gathering benchmarking information, and defining ideal and marginally acceptable target values [33, p. 96-98].

The first step was to prepare a list of metrics. Each metric satisfied one or more of the customer needs, followed by the relative importance, unit, as well as ideal and marginal values. Ideally, there is only one metric for each need, but there were cases where each need had several metrics. Some metrics were not measurable, or could not be quantified. The unit of these metrics were assigned the unit "Subj." as these were subjective. The metric "easy assembly" was important to the team, but could not be quantified. The team came to the agreement that the best way of evaluating subjective metrics was by benchmarking and testing. These were verified during the assembly and by submerging the manipulator in water.

The ideal values for the metrics were set hand in hand with the ambitions of UiS Subsea, and was the best outcome the team could hope for. The ideal values for some metrics were set with the ambition of improvement from earlier years. Last years manipulator only had two degrees of freedom, and the team had a goal of exceeding this by setting the ideal value to three or more. The marginal acceptable values were set according to the MATE requirements. Those that were not corresponding to a competition requirement, were set by considering benchmarking information and theory. The target specifications for the manipulator are illustrated in Table 3.5.

Table 3.5: Target specifications for manipulator

Metric No.	Needs No.	Metric	Imp.	Unit	Marginal Value	Ideal Value
1	1	End-effector grip range	5	mm	2-30	2-30
2	2,5	Lift capacity	5	N	>10	>15
3	3,21	Operational depth	4	m	>4	>50
4	4	Environmental impact	4	Subj.	OK	OK
5	6,19	Time submerged	5	min	>15	>60
6	7	Operational temperatures	4	°C	15-30	15-30
7	9	Length of manipulator	3	mm	400-450	400-450
8	9	Width of manipulator	3	mm	100-110	100-110
9	8	Water sample container volume	5	ml	>=50	>=50
10	9	Weight of manipulator	4	kg	<9	<8
11	11,15	Easy assembly	4	Subj.	OK	OK
12	12,8	Degrees of freedom	4	DOF	2	>3
13	13	Manipulator tasks MATE	4	pts.	0-680	680
14	16	Manipulator budget	4	NOK	<8000	<8000
15	5	End-effector grip force	5	N	>10	>10
16	17,20	Material properties	5	Subj.	OK	OK
17	13	Maneuverability	4	Subj.	OK	OK
18	4,18	No sharp or dangerous edges and parts	4	Subj.	OK	OK
19	9,14	Balanced weight distribution	4	Subj.	OK	OK
20	17	Waterproof	5	Subj.	OK	OK
21	12	Manipulator reach	3	mm	300-400	300-400
22	2,10	Rigid manipulator	4	Subj.	OK	OK

3.3 Generation of product concepts

A product concept is a brief description of the how product will look, its working principles, and technology. The product concept gives a description of how the product will satisfy the customer needs. By considering the already set customer needs and target specifications, the team looked at already existing product concepts by UiS Subsea from earlier years to see if parts of them could be adapted to the new product. Furthermore, new concepts were considered, primarily based on benchmarking information of products with similar functionality, presented in Table 3.4, and by using external information and solutions as inspiration. For the process of creating product concepts, the manipulator was divided into two subsystems, the manipulator arm and the end-effector. The con-

cepts created for the two different subsystems were rough and simple three-dimensional models, which served as an outline and direction for potential further development of the concepts.

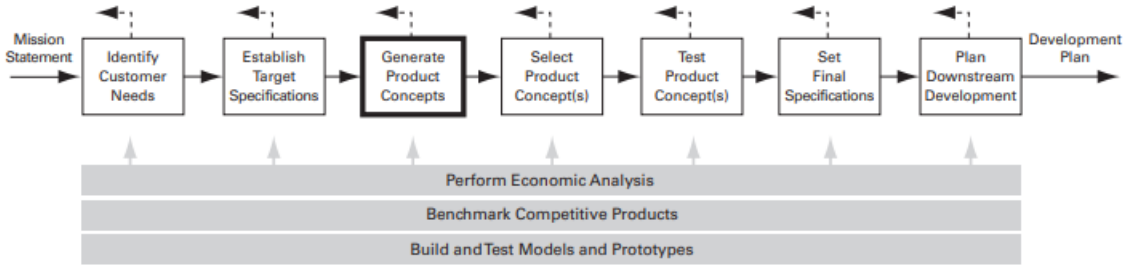

Figure 3.4: Concept development phase in the PDP [36, p.118]

3.3.1 Manipulator Arm Concepts

A total of five different concepts were developed for the manipulator arm, represented by three-dimensional models labeled A through E in Figure 3.5.

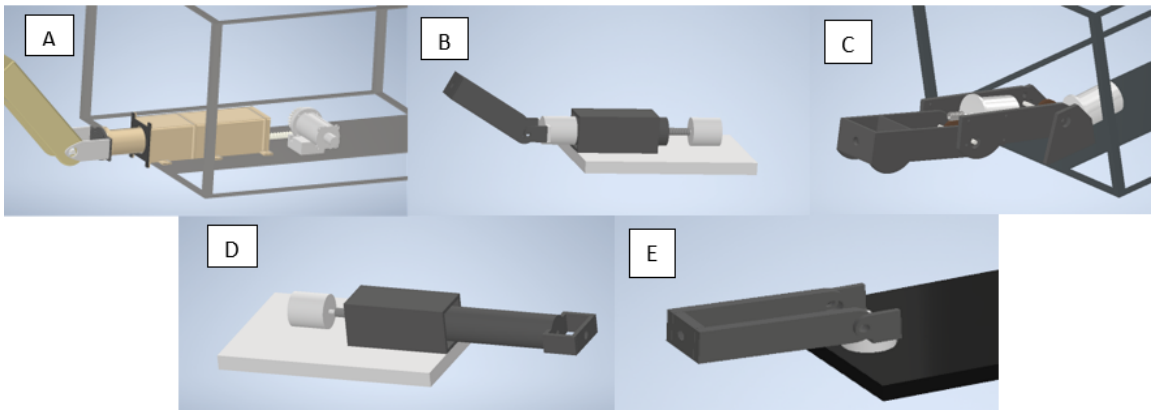

Figure 3.5: Manipulator arm concepts

The manipulator arm concepts developed by the team were relatively similar to each other due to the requirements and limitations they faced. The target specifications allowed for a marginal value of two degrees of freedom, and the ideal value was set to three or more. Concepts A through C were capable of three degrees of freedom, while concepts D and E only two. The majority of the concepts featured an open arm solution with parallel arm links, chosen for easy assembly, disassembly, and maintenance, and to minimize weight and production cost. All concepts were able to fit an end-effector that could rotate 360°.

Concepts A, B, and D featured a cylindrical section in the back to support linear movement and protect electrical cables and components. The circular shape of the arm allowed for easier assembly of the stepper motor housing. The main differences between the concepts were primarily in the joints and movement mechanisms. Concepts A, B, and D had a telescope feature or prismatic joint for linear movement, while concept C had shoulder and elbow joints. Concept E had a unique revolute joint that would reduce the required movement of the ROV while operating in the horizontal plane.

Concept C was inspired by the UiS Subsea manipulator from 2021 but with modifications to avoid the use of belts and pulleys that had caused issues for the previous manipulator. Concept A used a rack and pinion drive for linear movement, while concepts B and D used lead screw actuation. These differences in joint and movement mechanisms resulted in distinct design choices for each concept.

3.3.2 End-Effector Concepts

Compared to the development of the manipulator arm concepts, the process of creating end-effector concepts was relatively straightforward. The team decided early on to use earlier concepts from UiS Subsea as a starting point, given their proven effectiveness for the intended purpose. The primary area of improvement in the previous manipulators was the mobility and stability of the arm, not the end-effector's functionality. As a result, a larger portion of the product development phase was devoted to the arm. Consequently, the end-effector concepts developed were not very different from those of previous years. Concepts A through D are shown in Figure 3.6.

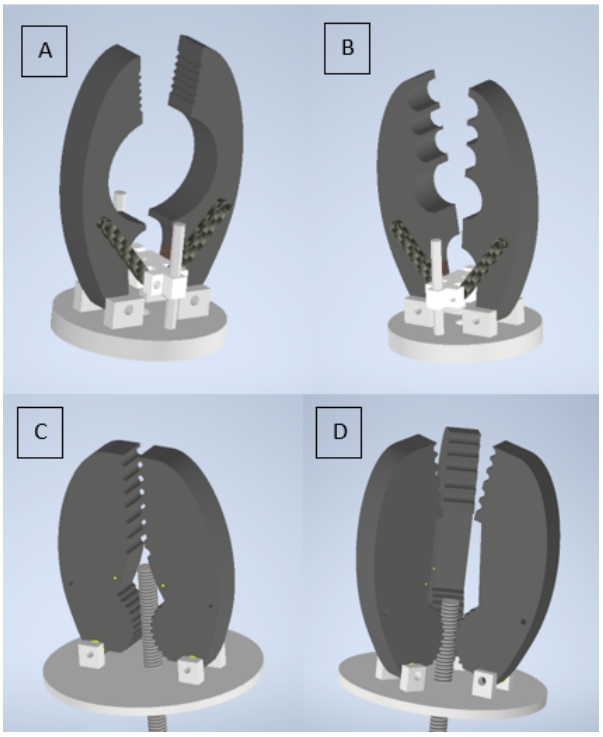

Figure 3.6: End-effector concepts

The gripping mechanisms in the generated concepts were divided into two types. Concepts A and B featured a steel wire mechanism, while concepts C and D used a lead screw mechanism. Concept D stood out with its three fingers, a new concept for UiS Subsea. The inspiration behind this was a common issue in previous manipulators where the end-effector would grab an object, but it would slip as the end-effector rotated due to insufficient grip force and friction. With three fingers, this risk was significantly reduced. The main difference between the concepts was the geometrical shape of the fingers, and the team generated different shaped end-effectors. The team aimed to create concepts that were well-suited for grabbing and holding objects typically used in MATE tasks previously.

3.4 Product Concept Selection

After the concepts for the manipulator arm and end-effector were created, each one was evaluated based on customer needs and target specifications. The most promising concepts were then selected for further development. A system of lists and matrices was created to compare the concepts to each other, and this process of concept screening served as

helpful guidance for selecting the best concepts for further development. This process of concept screening helped ensure that the selection criteria were met. By using a systematic approach to evaluate and compare the concepts, the group was able to make informed decisions and ultimately achieve their design goals.

To rate the concepts, a simple coding system was used. Each criteria for every concept was given a rating of "better than" (+), "worse than" (-), and "equal to" (0). The scores for each concept were calculated by summing the +'s, -'s. and 0's. Depending on the score, the concepts were given a rank, and the team decided which concepts qualified for continued development.

Table 3.6: Concept screening matrix manipulator arm

Criteria	**Concepts**				
	A	**B**	**C**	**D**	**E**
Good maneuverability	0	0	0	0	0
Produced within budget	+	+	+	+	+
Easy assembly, disassembly and maintenance	0	0	0	0	0
Can lift items of 10N	0	0	0	0	0
Can be submerged for minimum 15 minutes	0	0	0	0	0
Can operate at depth of 50 metres	0	0	0	0	0
No sharp or dangerous edges or parts	0	0	0	0	0
Weight balanced	0	0	-	0	0
Able to perform MATE tasks	0	0	0	0	0
Manipulator reach of 300-400mm	+	+	0	0	-
Manipulator fit on ROV	0	0	0	0	-
Operates in fresh and chlorinated water, (15-30°C)	0	0	0	0	0
Three degrees of freedom	0	0	0	-	-
Minimize required ROV movement	+	+	+	-	-
Rigid and little risk of failure	-	+	-	0	0
Sum +'s	3	4	2	1	1
Sum -'s	1	0	2	2	3
Sum 0's	11	11	11	12	11
Net Score	2	4	0	-1	-2
Rank	2	1	3	4	5
Continue to develop	Yes	Yes	No	No	No

Table 3.7: Concept Screening Matrix End-Effector

Criteria	Concepts			
	A	**B**	**C**	**D**
Good maneuverability	0	0	0	0
Produced within budget	+	+	+	+
Easy assembly, disassembly and maintenance	0	0	0	0
Can hold items of 10N	0	0	0	0
Can be submerged for 15 minutes	+	+	+	+
Can operate at depth of 50 metres	0	0	0	0
No sharp or dangerous edges or parts	+	+	+	+
Balanced weight distribution	+	+	-	-
Able to perform MATE tasks	0	0	0	0
End-effector fit on manipulator	0	0	0	-
Operates in fresh and chlorinated water (15-30°C)	0	0	0	0
Minimize required ROV movement	+	+	+	+
Can grab objects between 2-30mm	+	0	-	-
End-effector geometry suited for MATE tasks	+	-	-	-
Rigid and little risk of failure	0	0	0	0
Sum +'s	7	5	4	4
Sum -'s	0	1	3	4
Sum 0's	8	9	8	7
Net Score	7	4	1	0
Rank	1	2	3	4
Continue to develop	Yes	No	No	No

Following the concept screening process, concepts A and B for the manipulator and concept A for the end-effector were selected for further development and testing. Concept A and B for the manipulator arm were similar in many respects, with the main difference being the mechanism of the telescope function.

After improving the 3D models and studying the two concepts more closely, the group discovered some issues with the rack and pinion drive in concept A. One problem was

ensuring that the manipulator was securely fastened to the ROV and that its movement was stable. In the event of the ROV tilting, the group had to ensure that the rack and pinion drive would not slip or experience unexpected forces and stresses that could lead to failure. To address this issue, the team explored various solutions and ultimately explored the possibility of attaching bearings to the cage, which would function as wheels to support the telescope motion and make it more stable. See Figure 3.7.

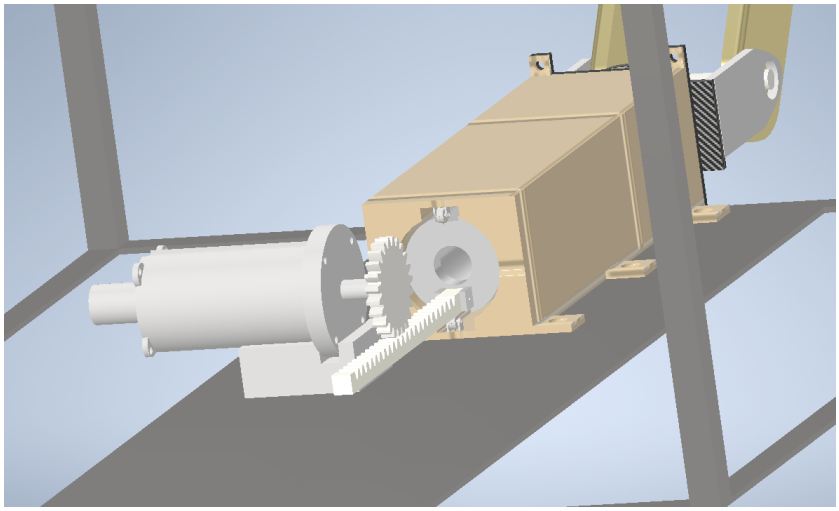

Figure 3.7: Bearings used for stabilization for concept A

After a brainstorming session, the team concluded that the rack and pinion drive in concept A was too risky, and the process of fail-proofing the mechanism would be more expensive and result in more weight compared to the lead screw mechanism used in concept B. Additionally, concept B would take up less space on the ROV as the motor for the lead screw could be placed closer to the manipulator arm than the rack and pinion. After discussing within the team and with other members of UiS Subsea, it was decided to move forward with concept B for the manipulator arm and concept A for the end-effector. With this decision, the team had completed the concept development phase and could move on to the detailed design.

Summarized, this process of evaluating and selecting the most promising concepts helped the team make informed decisions and ensure that the design met the customer needs and specifications. By choosing the best concepts, the team was able to streamline the design process and focus their efforts on the promising options.

3.5 Circular Economy

The circular economy is a production and consumption model that emphasizes the reuse, repair and refurbishment of existing materials and products to increase their life cycle [37]. The team used a circular economy approach during the development and design of the manipulator. By searching UiS Subsea's storage and old manipulators collecting dust, components viable for reuse were identified. The availability of these components influenced the detailed design process of the project and ultimately impacted the final outcome. This approach resulted in significant resource and time savings, as long delivery times and manufacturing complications were avoided. Moreover, this approach promoted a closed-loop system where materials and products were reused rather than disposed, reducing waste and contributing to a more sustainable future.

Table 3.8 presents the reused parts harvested from old manipulators and UiS Subsea's storage, also specifying if parts would have to be modified or not.

Table 3.8: Reused components

Reused Parts	Modified	Not modified
Steel wire	X	
Steel wire protective cover	X	
Motor housings		X
Trapezoidal lead screw and nut	X	
Worm	X	
Electrical connectors		X
O-ring		X
Shaft seal		X
BLDC motor		X
Shafts	X	
Compression springs		X

Chapter 4

Detailed Design and Calculations

The outcome of the planning and concept development was the selection of concepts for both the manipulator arm and the end-effector. These concepts primarily demonstrated the shape and form of the manipulator and did not serve much structural, functional, or aesthetic purpose. In the following sections, the selected concepts will be integrated and further developed through detailed design. Final specifications for geometry, material, and production methods will be determined. Additionally, all mechanical components of the manipulator will be identified and tested if necessary.

A target for the manipulator was to be able to handle a small load of 10N. Due to the manipulator's dimensions being based primarily on component compatibility, rather than external forces, conducting a complete finite element analysis of the concepts was deemed unnecessary. In fact, if the group were to optimize the manipulator based on FEA, it would likely be too small to accommodate critical components such as motors, bearings, and shafts. This has been the case in previous manipulator projects for UiS Subsea as well.

As a result, the manipulator arm was designed to be oversized when considering external forces. Testing was primarily done through specific component calculations, prototyping, and physical testing covered in the sections to follow and Chapter 5.

4.1 End-Effector

The detailed design process of the end-effector involved defining final specifications for geometry, dimensions, actuation, and material. The end-effector is a crucial component of the manipulator design as it is the part of the ROV that directly interacts with objects. A poorly designed end-effector could result in unfavorable outcomes in the MATE ROV Competition. However, due to assumptions made considering the low external loads, the design primarily focused on functionality. Based on research conducted on earlier manipulators from UiS Subsea, the end-effector's structural capabilities were deemed to be more than adequate.

4.1.1 Geometry and Dimensions of Fingers

One design change made to the end-effector concept design was to alter the dimensions of the finger geometry to meet the target specifications. The most crucial part of the finger is the contact face that interacts with objects. The circular middle section of the finger was replaced with an ellipse shape instead. Since objects are rarely perfectly circular, the half-ellipse section provided an increased contact surface area between the finger and objects with unequal semi-major and semi-minor axis. This section proved too large in the concept design, and different dimensions were tested before settling on a radius of 36.25mm. To assess the intersection between various objects and the surface, different objects were constrained to the surface in Autodesk Inventor.

The smaller circular extrusions in the top section of the fingers were also modified according to the target specifications. Each half-circle extrusion was given a radius of 1.25mm. The end-effector was required to pick up an object with a 3mm diameter, and when the end-effector was completely closed, the half-circles combined to form a full circle with a diameter of 2.5mm. Initially, the group set the radius to 1.5mm, which would have resulted in the object barely touching the surface of the fingers when the end-effector was closed. By reducing the radius to 1.25mm, the contact pressure between the finger and the object increased, thereby reducing the risk of the object slipping. Figure 4.1 illustrates the first revision of the end-effector finger.

Figure 4.1: End-effector finger revision 1

4.1.2 End-Effector Base

The purpose of the end-effector base was to connect the fingers to the end-effector system and support the gripping motion. Initially, the fingers were to be placed between two fastening brackets on the base, as depicted in concept A of Figure 3.6. To enhance the rigidity of the assembly, a third bracket was added in the middle, necessitating a revision of the finger design. Fillets were added to decrease stress concentrations and remove sharp edges. Additionally, holes were added to the base to facilitate connection between the base, fingers, and the rest of the end-effector.

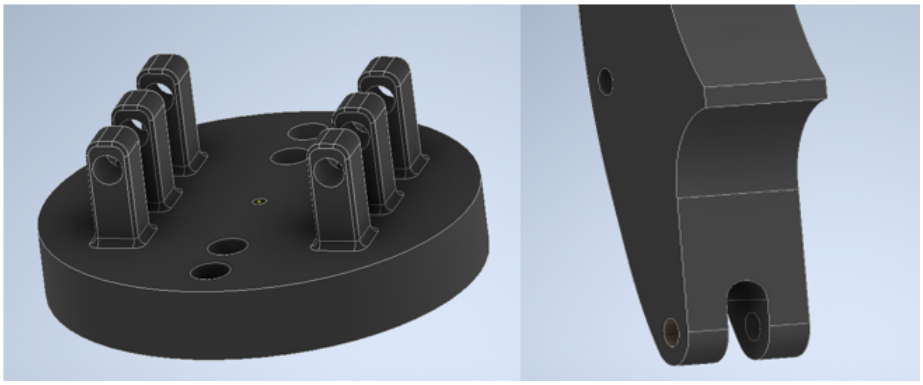

Figure 4.2: Revision of base and finger

4.1.3 Wire Actuation

The design of the end-effector was based on an electrical actuation system utilizing a stepper motor, with a steel wire serving as the power transmission mechanism. The stepper motor was strategically positioned on the ROV frame, contributing to the weight balance of the manipulator. The stepper motor featured a lead screw shaft, and a hollow threaded cylinder was used as the coupling between the motor and the steel wire. The steel wire was fixed at one end of the cylinder, and as the motor rotated, the cylinder and wire traveled backwards along the lead screw. At the end-effector, the steel wire was attached to the connecting actuation bracket depicted in Figure 4.3.

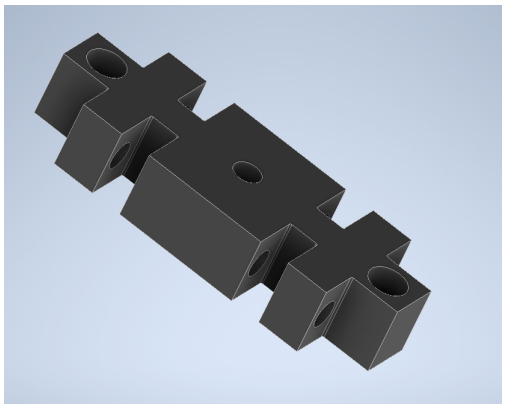

Figure 4.3: Wire actuation bracket

The actuation bracket was a central component of the end-effector system, responsible for merging the actuation mechanism with the end-effector. The steel wire used had a diameter of 2mm with a nut of 4mm at the end. By inserting the wire through the counterbore hole of the bracket, the nut rested on the seat, which prevented the wire from passing through, consequently closing the end-effector when the wire was pulled. Figure 4.4 displays a 3D model of the final design, including the shaft connecting the end-effector to the manipulator arm. The actuation bracket was secured to two M5 bolts with a compression spring and nut to hold it in place. The compression spring played a crucial role in the end-effector design by enabling a smoother closing motion and, more importantly, ensuring that the wire nut would not leave its seat, thereby achieving the correct open position for the end-effector.

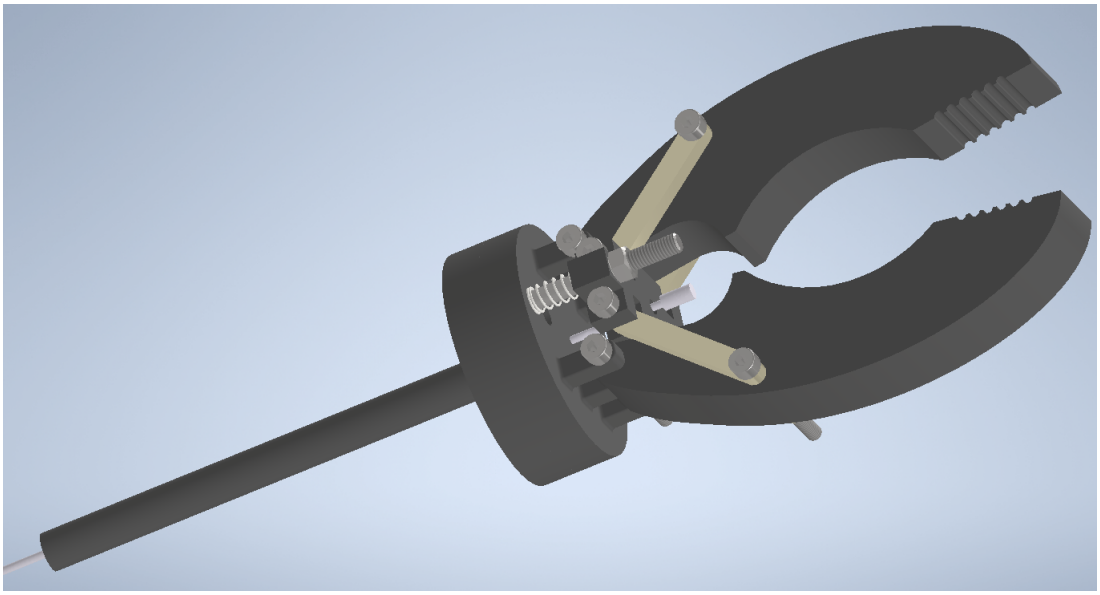

Figure 4.4: End-effector with steel wire

The target specifications stated that the end-effector was required to hold a load of 10N. The grip force was generated by the NEMA 17 stepper motor that pulled the wire. To calculate the grip force, it was necessary to determine the pull force of the stepper motor, which can be challenging to estimate by calculations and thereby required experimental testing. See Section 5.2.1. Additionally, precise measurements of various dimensions of the end-effector in different positions were required to accurately calculate the group and spring forces. See Figure 4.5.

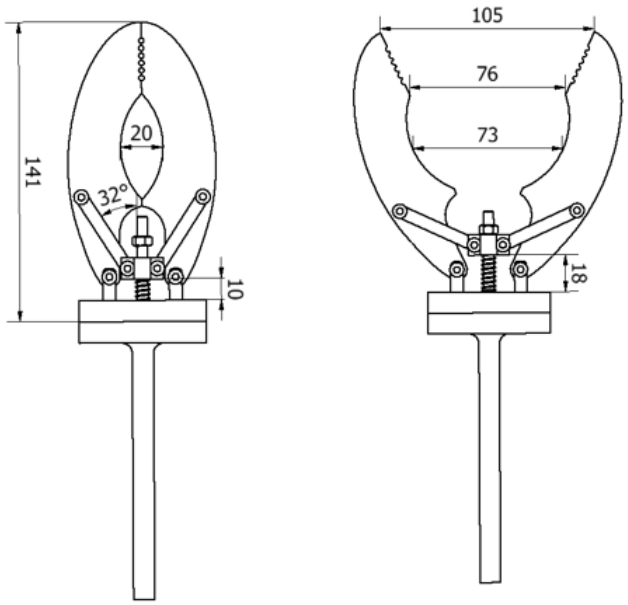

Figure 4.5: Measurements of end-effector

The compression springs used were identical to those used on the 2021 manipulator [16, p. 65]. These were of stainless steel with a spring constant of $k = 0.11\frac{N}{mm}$ and a length of 25mm. As shown in Figure 4.5, the spring was measured to be 18mm in length when the end-effector was in an open position. The spring length ensured that it was always in a slightly compressed state, resulting in some degree of force acting at all times, which is a design choice that stiffened the end-effector.

To calculate the compression force, the theory presented in Section 2.4.5 was applied. Since two compression springs were used, Equation 2.39 was used to calculate the compression force. If the end-effector was in the open position, then,

$$F_{open} = (25 - 18)mm * 2 * 0.11\frac{N}{mm} = 1.54N \tag{4.1}$$

and if in a fully closed position,

$$F_{closed} = (25 - 10)mm * 2 * 0.11\frac{N}{mm} = 3.3N \tag{4.2}$$

To protect the steel wire during operations, a flexible polymer cable used for gearing on bicycles was used to encase the wire. The friction between the steel wire and the protective cable was minimal. Thus, the calculated forces would be sufficient to open the end-effector correctly. When considering the springs, the maximum grip force in a closed position could be calculated using Equation 2.15.

$$F_{grip,max} = \frac{(363 - 3.3)N}{2} tan(32^\circ) = 112.4N \tag{4.3}$$

The manipulator would have to hold a load of 10N, and therefore the motor would be sufficient in order for the end-effector to exert enough force on the object and prevent the fingers from opening. The fingers might not open, but the object could slip between the fingers if there was a lack of friction. To prevent this, layers of silicone or another

material providing friction could be added. Also, by having a rotating end-effector, it can position the object in a horizontal manner, preventing vertical slip.

The minimum force that the motor must apply to hold 10N is

$$F_{applied,min} = 2\left(\frac{10}{tan(32°)} + \frac{3.3}{2}\right)N = 35N \tag{4.4}$$

The motor torque required to exert 35N to the wire can be calculated. The method of calculation is inspired by the manipulator thesis from 2021. A M5 bolt and nut was used for the mechanism, and only the motor specifications differ. The torque required from the motor is given by the following equation [16, p. 67].

$$T_{grip,min} = F_{applied,min} * r * \left(\frac{\mu_s + tan\gamma}{1 - \mu_s tan\gamma}\right) \tag{4.5}$$

where the dimensions of the bolt is,
Radius, $r = 2.5mm$
Lead angle, $\gamma = 3.04°$
Friction coefficient steel/steel, $\mu_s = 0.42$

Inserting the values into Equation 4.5 gives the torque required, $T_{grip,min} = 42Nmm$. By comparing the result from Equation 4.5 to the torque curve given in Figure 4.6, the motor will be able to apply this torque at all operating levels.

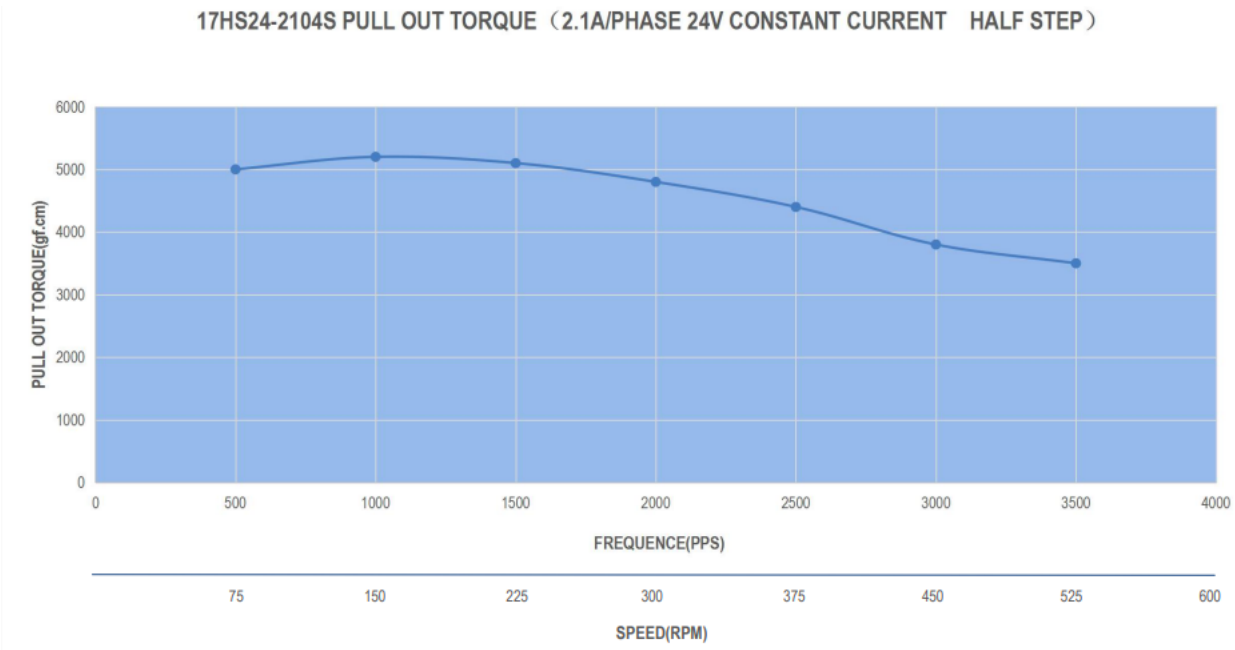

Figure 4.6: Pull out torque NEMA 17 [38]

4.2 Manipulator Arm

The design process of the manipulator arm was iterative and required multiple revisions to ensure compatibility of all necessary components. The concept design of the manipulator arm primarily ensured the target specifications regarding degrees of freedom and functionality could be achieved. As the design process progressed, it became increasingly important to consider the components and mechanisms of the arm, as well as ensuring compatibility with the end-effector and the rest of the ROV.

4.2.1 Lead Screw Actuation and Stability

The telescope function was designed to minimize the required horizontal movement of the ROV during operations. The system consisted of a trapezoidal lead screw and nut, a stabilizing cage, a cylindrical arm link, and a stepper motor. Considering the circular economy approach, the team wanted to reuse a 10x2 trapezoidal lead screw and suitable nut already owned by UiS Subsea. This was possible by lathing one end to the same diameter as the motor shaft and connecting them by a shaft coupling. As the motor ran, the manipulator arm would move linearly along the lead screw. Forces acting on

the system were negligible, and functionality and stability were the main priorities of the design process. Based on benchmarking and consultation with members of UiS Subsea that were part of the 2022 project, the team was made aware of the problems concerning the previous attempt for a telescope function. The issues encountered were instability and difficulties using a BLDC motor due to their high RPM and limited configuration options. In contrast, the new design included a stepper motor, which could be set to the desired RPM, providing more control of the movement. While stepper motors are heavier than BLDC motor, it was concluded a benefit for this design as it contributed to a more balanced weight distribution and increased overall stability of the ROV.

The manipulator cage design was further developed to achieve a modular build and stability for the linear movement and manipulator as a whole. The dimensions of the cage were determined according to requirements from the ROV-Design. The dimensions were set to ensure it would fit on the ROV, and also based on the fact that it would have to support the electronics enclosure. The cage dimensions were set to 270x105x105 millimeters. To meet the target specifications of a modular design, the cage was divided into six individual parts. This modular build facilitated easy assembly, disassembly, and maintenance. As the cage was not subjected to significant forces, material was removed to reduce weight. The team explored various design possibilities to stabilize the linear movement of the arm and to increase rigidity. The best solution was inspired by 3D printers, particularly the PRUSA printers used at UiS, which use lead screw actuation, and stabilize the movement using shafts and a housing part. See Figure 4.7.

Figure 4.7: 3D-Printer lead screw actuation

The concept from the PRUSA 3D printers was adapted to stabilize the linear movement. Four stainless steel shaft, each measuring 8mm in diameter and 270mm in length, were attached to the cage. Although smaller diameter shafts could have been used considering the loads, it would be more cost-effective to use the same 8mm shafts that were needed for other parts of the end-effector. Both ends of the shafts were assigned a diameter of 6mm and inserted into 6.1 mm holes in the cage. This difference in diameter served as a mechanical stop and made it possible to avoid the use of tight press fits. The shafts connected the manipulator arm to the cage and were inserted into housings on the cylindrical section of the arm. Sleeve bearings were used to reduce the friction and tear between the shaft and the housing, thereby ensuring a smoother linear movement. This design ensured stability both vertically and horizontally. 3D models of the cage, the cylindrical arm link, and the assembly, are shown in Figure 4.8.

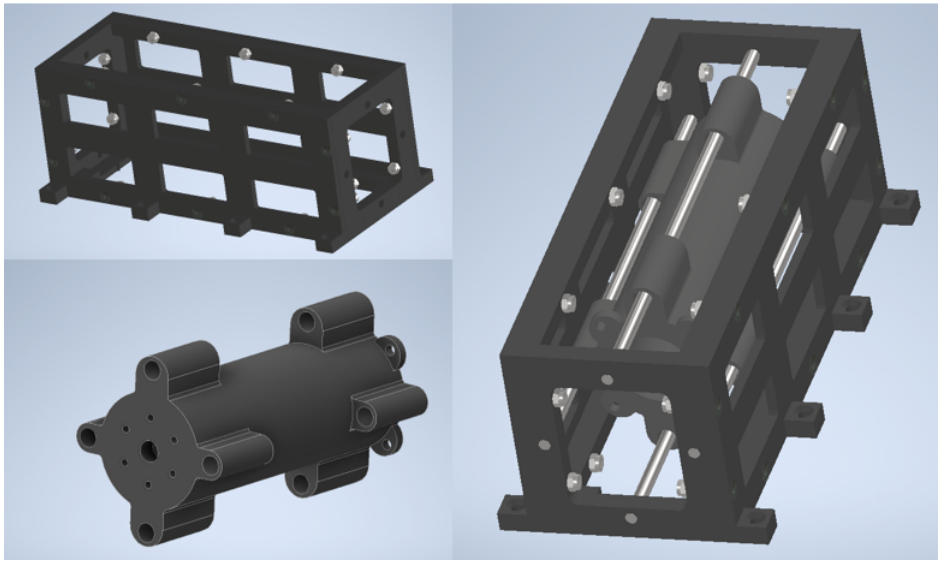

Figure 4.8: 3D models of the cage, cylindrical arm link, and the assembly with shafts.

To align the the lead screw and the lead screw nut attached to the arm, a motor mount was designed. The motor mount dimensions were set in order to elevate the motor to a height where the lead screw and the nut would be in spirit level. An additional stabilizing component was placed between the motor and the arm to reduce vibrations. See Figure 4.9 for the full assembly of this section.

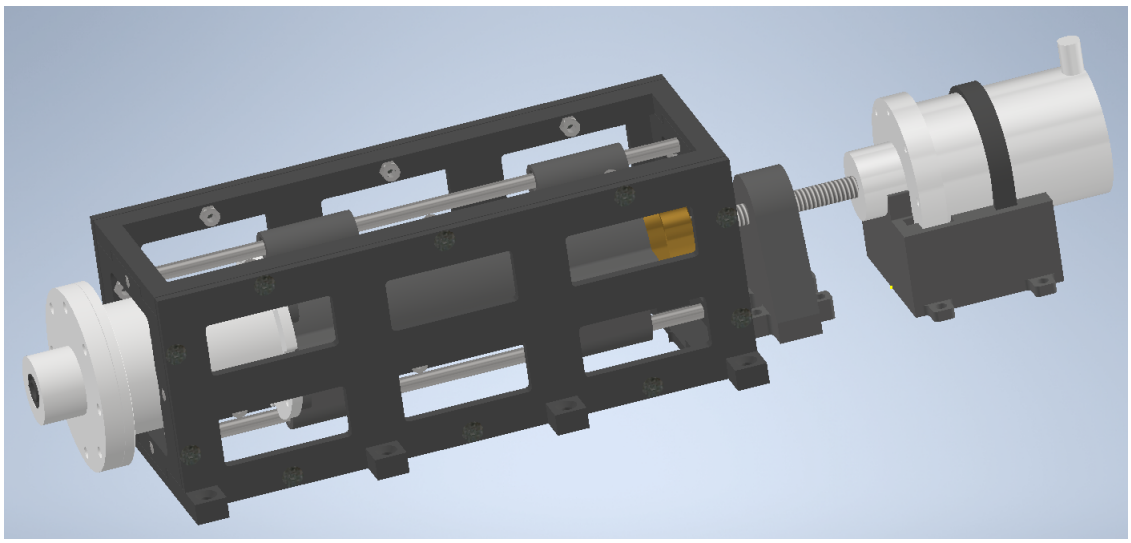

Figure 4.9: 3D model of the lead screw actuation system

4.2.2 Pitch Function

The elbow joint was responsible for the pitch function of the arm. The ability to tilt was important in terms of achieving the target specifications and meeting customer needs. This function let the arm tilt 90° downwards and 90° upwards. To increase the output torque and slow down the movement, a worm-gear pair was implemented. The worm was directly attached to the stepper motor shaft, and the worm gear to the shaft connecting the side-plates. See Figure 4.10.

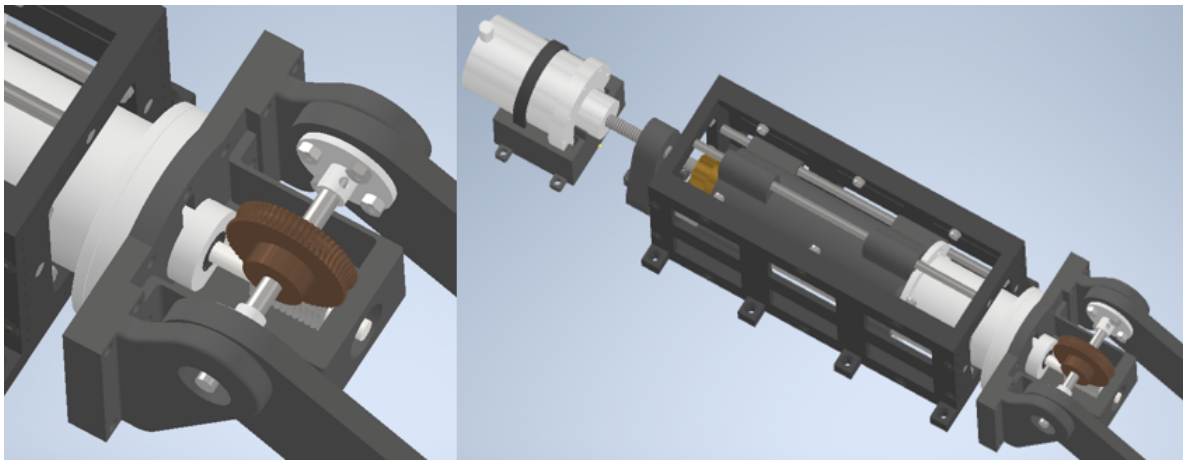

Figure 4.10: 3D Model of the elbow-joint system

As illustrated in Figure 4.10, this section of the manipulator arm consisted of several components that ensured compatibility and functionality of the manipulator. Firstly, a bracket is attached to the motor housing lid to connect the upper and lower section

of the arm. Additionally, two angular brackets serving as shaft housings were required. These brackets were designed to position the shaft carrying the worm gear high enough to provide sufficient room for the worm. Furthermore, a component accommodating a bearing to support the worm shaft is fastened to the connecting bracket. Two shaft couplings properly connect the shaft to the side plates to ensure a reliable transmission of torque between the gear shaft and side plates.

It is not possible to calculate the exact torque of a stepper motor. The data sheet of the NEMA 17 motor was used. See figure 4.6. By inspection, the maximum torque of the stepper motor was around 0.5Nm. The worm-gear pair consisted of a SUW0.8-R1 worm and a BG0.8-60R1 worm gear. See Table 4.1 for their respective dimensions.

Table 4.1: Worm [39] and worm gear [40] dimensions

Type	**Unit**	**SUW0.8-R1**	**BG0.8-60R1**
Material	-	Stainless Steel	Bronze
Number of teeth	-	1	60
Module	[mm]	0.8	0.8
Diameter	[mm]	14	48.08
Reference angle	[deg]	20	20

The lead angle for the worm in contact with the worm gear is calculated by solving Equation 2.19 for λ.

$$\lambda = tan^{-1}\left(\frac{0.8 * 1}{14}\right) = 3.27^{\circ} \tag{4.6}$$

The coefficient of friction between bronze and steel is approximately 0.34. By inserting values into Equation 2.28, the self locking property can be checked. In Section 2.4.1, the relationship between angles and tooth depth was presented. The worm-gear pairs used for this project were stock gears from the renowned gear manufacturer KHK Gears. The relationship was therefore reasonable to assume being within limits.

$$0.34 \geq 0.06 \tag{4.7}$$

This result confirmed that the worm-gear pair was self-locking, which was crucial for the manipulator arm to maintain different positions.

Based on the relationship between gear and worm forces covered in Section 2.4.1, the following values were obtained for the tangential forces,

By Equation 2.25 the tangential force on the worm is,

$$F_{W_t} = \frac{2 * T_{in}}{d_w} = \frac{2 * 0.5Nm}{0.014m} = 71.43N \tag{4.8}$$

By inserting this value into Equation 2.24 and rearranging for F_{G_t}, the value obtained was $F_{G_t} = 166.97N$. From these values the output torque of the stepper motor was calculated from Equation 2.27.

$$T_{out} = F_{G_t} * r_G = 166.97N * 0.07m = 4.01Nm \tag{4.9}$$

The maximum reach of the manipulator from the elbow joint to the end-effector was approximately 350mm. By inserting the output torque of the worm-gear pair and the reach into the following equation, the maximum lift force was calculated,

$$F_{lift,max} = \frac{T_{out}}{reach_{max}} = \frac{4.01Nm}{0.35m} = 11.45N \tag{4.10}$$

This proves that the NEMA 17 motor combined with the worm-gear pair can lift 10N at at 350 mm reach.

Using Equation 2.21 and 2.22, the radial, axial and tangential forces from the gear were calculated. The material of the worm-gear shaft was stainless steel with a diameter of 8 mm and length of 120 mm. The worm gear was centered on the shaft. Using the forces applied to the shaft from the worm-gear set, strength calculations were performed. The values for the forces from the worm-gear set on the shaft are given in Table 4.2.

Shaft dimensions:

Table 4.2: Magnitude of forces on worm gear shaft

Force	Axial (N)	Radial (N)	Tangential (N)	Torque (Nm)
Value	69.96	60.88	166.97	4.01

Cross-section: $A = \frac{\pi}{4} * 8^2 = 50.26$

Moment of inertia: $I = \frac{\pi}{64} * 8^4 = 201.0$

Radius of gyration: $i = \sqrt{\frac{201}{50.26}} = 2.0$

If assumed Euro Case 2, then the critical length is,

$$L_k = L * 1.0 = 0.12m \tag{4.11}$$

And the slenderness is,

$$\lambda = \frac{120mm}{2} = 60 \tag{4.12}$$

The yield strength of stainless steel is 205 MPa and Young's Modulus is 196 GPa. Using these values the critical slenderness can be calculated,

$$\lambda_F = \pi \frac{196 * 10^3}{205} = 97.14 \tag{4.13}$$

Then, the non-dimensional slenderness is,

$$\bar{\lambda} = \frac{60}{97.14} = 0.62 \tag{4.14}$$

From Figure 2.15, the reduction factor is $\chi \approx 0.78$, and the buckling stress is given by Equation 2.46.

$$\sigma_k = 0.78 * 205MPa = 159.9MPa \tag{4.15}$$

Furthermore the axial force allowed before buckling is

$$F_{allowed} \leq \frac{159.9Mpa * 50.26mm^2}{n_k} = \frac{8036.57}{n_k} \tag{4.16}$$

The axial force on the shaft is very low relative to the allowed force, which gives a high factor of safety against buckling, n_k. These calculations are an approximation to reality and factors not considered could change the values. Nevertheless, considering the high factor of safety the shaft would in theory not buckle.

The load values were also inserted into the software SkyCiv. The maximum deflection of the shaft and the Von Mises stress was obtained. See Figure 4.11 for the maximum deflection.

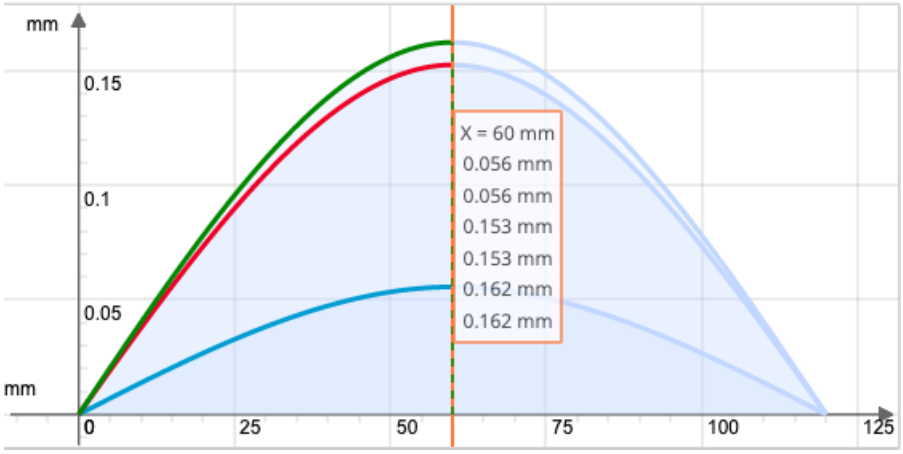

Figure 4.11: Deflection of the elbow joint shaft. Blue curve represent XY-plane, red XZ-Plane, and green the sum.

The maximum deflection of the beam was 0.162mm. A rule of thumb states that the deflection should not exceed the length of the shaft divided by 360.

$$0.33 \geq 0.162 \tag{4.17}$$

This implies that the displacement of the shaft was not severe and within the critical limit. The Von Mises stress was less than the yield strength of the stainless steel shaft. According to the Von Mises hypothesis the shaft will not yield if the Von Mises stress is less than the yield limit. The max Von Mises stress is 106.07 which is less than the yield

limit. See Figure 4.12 for Von Mises stress distribution.

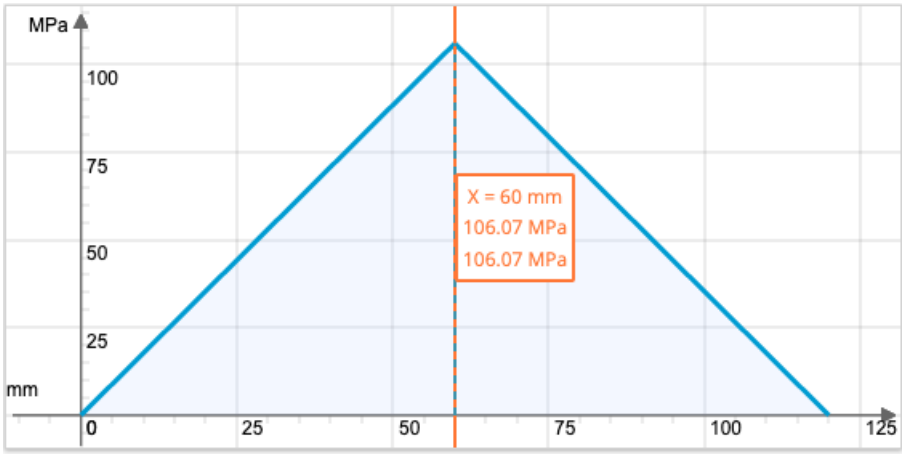

Figure 4.12: Von Mises stress for the worm gear shaft.

Section 2.4.4 covered several factors and equations that usually has to be taken into account when selecting bearings for an application. In this case, the bearings used for the shaft accommodated relatively small loads. Thus, the selection of bearings were primarily based on dimensions, price and delivery time. The bearings selected for the elbow joint of the manipulator arm were 608-2RSL SKF bearings. See Table 4.3 for bearing dimensions and specifications.

Table 4.3: Specifications and dimensions for 608-2RSL SKF Bearing

Specification	**Value**
Bearing Type	Deep Groove Ball Bearing
Bore Diameter (d)	8 mm
Outer Diameter (D)	22 mm
Width (B)	7 mm
Basic Dynamic Load Rating (C)	3.45 kN
Basic Static Load Rating (C0)	1.37 kN
Fatigue Load Limit (Pu)	0.057 kN
Reference Speed	70,000 r/min
Limiting Speed	36,000 r/min
Mass	0.012 kg
Sealing	Low Friction Rubber Seals (2RSL)

Based on the bearing data and the reaction forces, see Figure 4.13, there would in theory be no chance of the bearings malfunctioning, or any issues occurring in the shaft-bearing system. While selecting the bearings, the team took advantage of the SKF Bearing Selection Tool. Based on the input data, the SKF Bearing Selection Tool calculated

the different important values like dynamic and static bearing load and bearing life, and checked whether the bearing would be sufficient for its application [41].

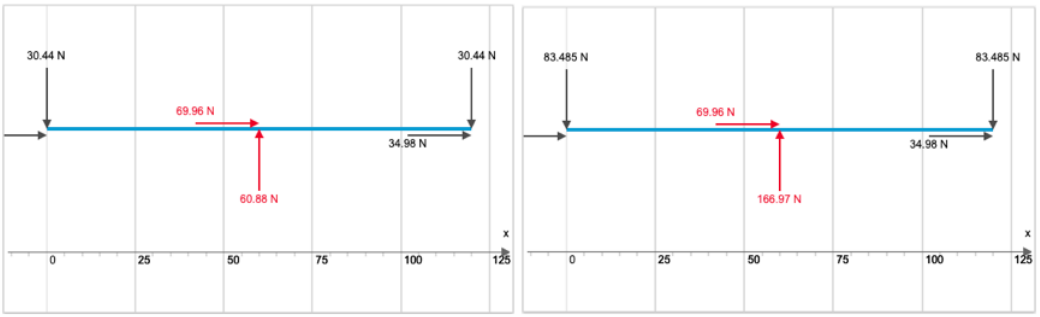

Figure 4.13: Reaction forces at bearings in XY-plane and XZ-plane, respectively.

Selecting the correct tolerances was crucial to prevent failure. Although the theoretical calculations for the shaft and bearings indicated no risk of failure, selecting the right tolerances was important. The 2021 manipulator encountered problems during assembly of the bearings to the shafts due to tolerances being too tight, resulting in the shaft buckling because of the static forces [16, p.78]. For the new design, the tolerances were changed to prevent the same problems while still ensuring functionality. It was decided to avoid using tight press fits, and instead use transition fit with a small clearance. A h8 tolerance was chosen for the shafts. This provided less interference while still ensuring an adequate fit between shaft and inner ring of bearing for the intended function. A transition fit tolerance was also chosen for the housing, and the use of a retaining compound would prevent the outer ring from rotating. This design solution did not only reduce the chance of buckling and failure during assembly, but also made the assembly process easier as tight press fits require specific tools and expertise to be done correctly.

Transition fit tolerances were also assigned to the gears and worms to avoid the potential complications of tight press fits. Given the low RPM and forces involved, the use of set screws was deemed sufficient for this application.

4.2.3 Rotating End-Effector

To fulfill the target specifications concerning degrees of freedom, a mechanism was designed to allow the end-effector to rotate. Ideally a stepper motor's holding torque would be convenient for this mechanism, but due the required position of the motor and the

size and weight of a stepper motor, a BLDC motor was deemed the best option. The major problem concerning the use of a BLDC motor was its high, fixed RPM. The motor selected was a Eaglepower LA3508 KV390. This motor was already in possession of UiS Subsea, and had already been made waterproof. The motors theoretical RPM is given by Equation 2.50,

$$RPM_{max} = 390KV * 12V = 4680RPM \tag{4.18}$$

and then, the theoretical max angular velocity is,

$$w_{max} = 4680PRM * \frac{\pi}{30} = 490\frac{rad}{s} \tag{4.19}$$

To reduce the high angular velocity of the BLDC motor and achieve a reasonable rotational speed for the end-effector, a gearing system was implemented. The system included two spur gears and a worm-gear pair. The bearings and shafts used for this system had the same diameter as those used at the elbow joint, but the shafts were shorter. Additionally, the gears were smaller in size and placed closer to bearings, which minimized vibrations and bending. Based on the strength calculations performed in Section 4.2.2, the mechanical components of the system were assumed to not contain any risk of failure due to the high factor of safety. Design decisions for this mechanism were based on available space and the required gear ratio to achieve a reasonable rotational speed.

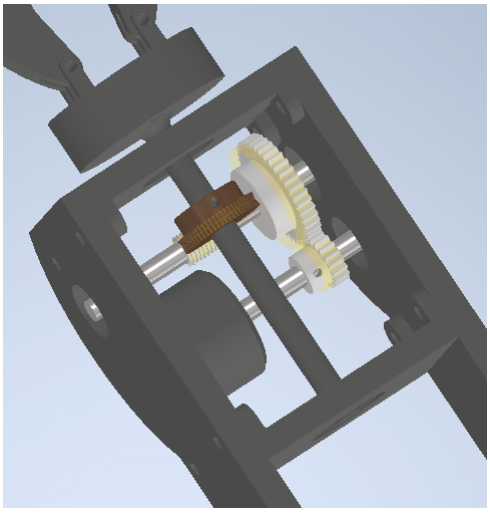

Figure 4.14: Gear system for rotation

Table 4.4 and 4.5 contain the gear dimensions.

Table 4.4: Worm [42] and worm gear [43] dimensions

Type	**Unit**	**SUW0.8-R1**	**BG0.8-60R1**
Material	-	Stainless Steel	Bronze
Number of teeth	-	1	60
Module	[mm]	0.5	0.5
Diameter	[mm]	11	30.03
Reference angle	[deg]	20	20

Table 4.5: Spur gear dimensions [44] [45]

Type	**Unit**	**SUW0.8-R1**	**BG0.8-60R1**
Material	-	Bronze	Bronze
Number of teeth	-	40	18
Module	[mm]	1	1
Diameter	[mm]	40	18
Reference angle	[deg]	20	20

To obtain values for the output RPM and torque, the following calculations were made:

The gear ratio was calculated using Equation 2.30,

$$i = \frac{60}{1} * \frac{40}{18} = 133.3 \tag{4.20}$$

This meant that for every 133,3 rotations of the motor, the end-effector would rotate once.

and the output RPM can be calculated by dividing the input RPM by the gear ratio i as follows,

$$RPM_{output} = \frac{4680RPM}{133.3} = 35RPM \tag{4.21}$$

From Equation 2.51, effect is given by

$$Q = 12V * 15A = 180W \tag{4.22}$$

and max torque from the motor is given by Equation 2.52,

$$T_{max} = \frac{180W}{490\frac{rad}{s}} = 0.37Nm \tag{4.23}$$

From Equation 2.31 output torque can be calculated,

$$T_{out} = 133.3 * 0.37 = 49.3Nm \tag{4.24}$$

The RPM was significantly reduced through this gear train, and the value was reasonable. In contrast, the output torque was increased. See Figure 4.15 for a 3D model of the complete and final design.

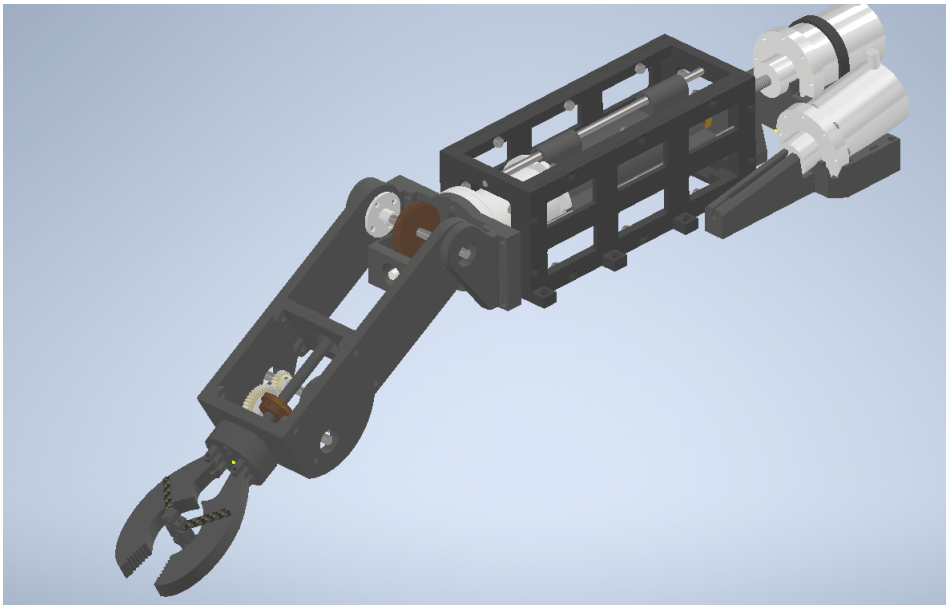

Figure 4.15: Complete 3D model of the manipulator

4.3 Waterproof Housing for Stepper Motors

The choice of using stepper motors meant having to waterproof them. A total of three stepper motors were used, but only two motor housing were available for reuse. The team searched for documentation and technical drawings for the motor housings, but without luck. This resulted in having to design and produce a new motor housing from scratch.

The motor housing assembly consisted of three parts. The first part was the base cylinder

where the stepper motor would be placed, the second part was the lid and the third part was a stabilizing component that attached the stepper motor to the housing and kept the motor in position. Figure 4.16 and 4.17 shows the 3D model of the assembly and the exploded view respectively.

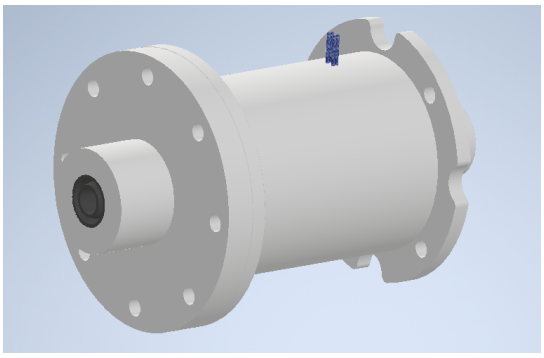

Figure 4.16: Stepper motor housing assembly

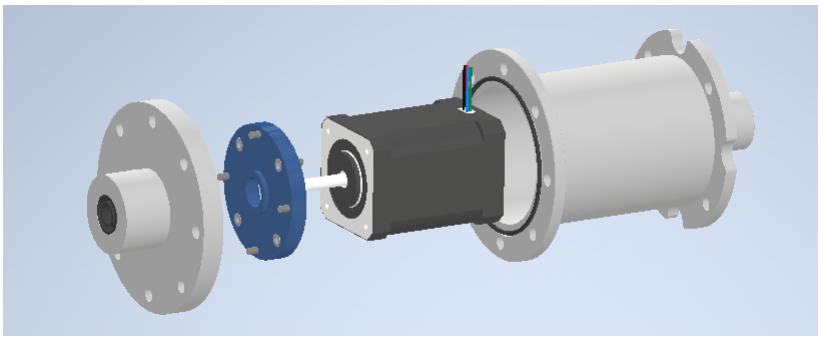

Figure 4.17: Stepper motor housing exploded view. From left to right: lid, stabilizer, motor, base cylinder

Prior to designing the new motor housing, the team disassembled an old one for inspiration and to identify possible areas of improvement. One issue with the old design was the limited space for bolts and nuts, which made the assembly process challenging, as bolts and nuts had to be forced into place. This problem is clearly visible in Figure 4.18. In the old motor housing, the stabilizer was assembled to the inner extruded circle of the lid, and the outer holes on the stabilizer were too close to the edge. To address this problem, the extruded circle was removed from the lid, which allowed for an increase in the diameter of the stabilizer. To make the housing waterproof, and O-ring groove was added to the new design. The groove was placed between the outer bolts and the inner diameter of the base cylinder. Similarly to the old housing, a shaft seal was used to ensure waterproofing where the shaft exits the house.

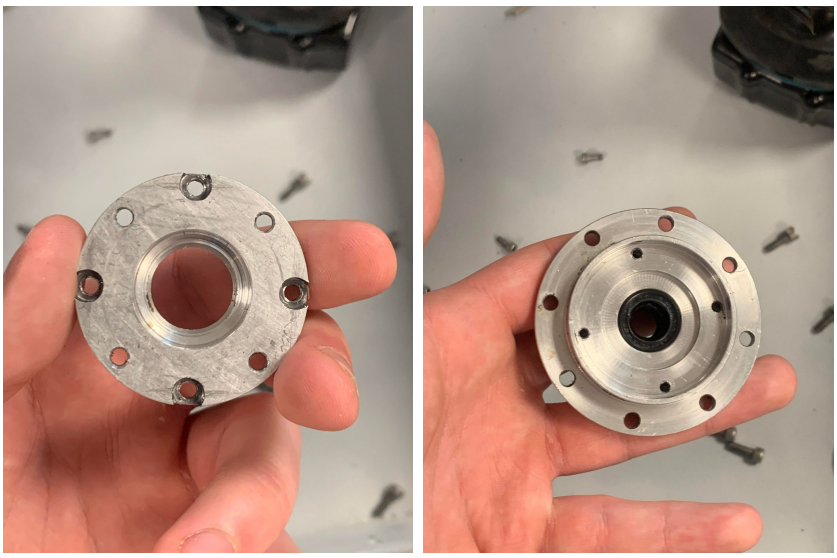

Figure 4.18: Stabilizing component and lid from old motor housing from left to right respectively

The design of the motor housing was optimized to simplify and accelerate the manufacturing process. To provide power to the stepper motor, an electrical connector needed to be assembled to the motor housing. In the previous design, the connector was assembled to an extrusion on the cylindrical surface of the base cylinder, necessitating the extrusion to be welded onto the surface. See Figure 4.19. In the new design, the extrusion for the connector was located on the flat back-surface of the base cylinder. This design change allowed for the entire base cylinder to be manufactured from a single block of raw material. This was also the reasoning behind the design of the attachment points on the back side of the base cylinder.

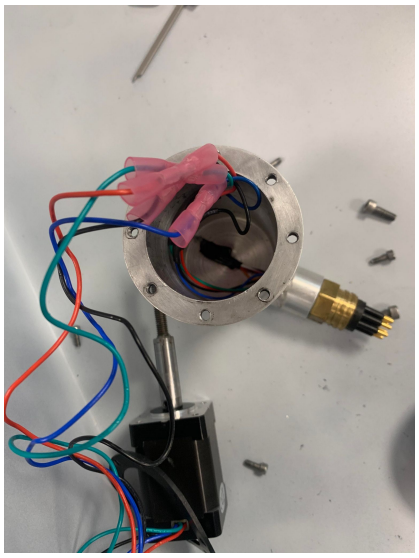

Figure 4.19: Old base cylinder design

Extensive research of materials for the motor housing was conducted. Stepper motors generate a considerable amount of heat. It was therefore important to choose a material with good thermal conductivity to prevent overheating. Initially, the team considered 3D printing the motor housing, which would reduce the manufacturing time. However, the thermal conductivity of filaments available at UiS were poor. The best available option was CPE with a thermal conductivity of $0.381 W/M * K$. In contrast, aluminum was found to have an thermal conductivity of $237 W/M * K$, and great mechanical properties in terms of strength and weight. Stainless steel was also considered, but rather quickly discarded. Although stainless steel has higher tensile strength, the lower thermal conductivity and higher weight deemed aluminum superior for the application. See Table 4.6 for a comparison of the considered materials.

Table 4.6: Comparison of material properties for Aluminum [46], CPE [47], PLA [48], and Stainless Steel [49].

Material	Heat Conductivity ($\mathrm{W\,m^{-1}\,K^{-1}}$)	Density ($\mathrm{kg\,m^{-3}}$)	Tensile Strength (MPa)
Aluminum	237.00	2700	70
CPE	0.381	1020	38
PLA	0.13	1240	50
Stainless Steel	15.00	8000	500

Technical drawings for the motor housing can be found in Appendix A: Technical Drawings.

4.4 Material Choice

In order to meet the target specifications considering weight, budget and also respecting the time constraint, the group wanted to 3D print as many of the parts as possible. Plastic materials are light and 3D-printers are capable of printing parts of complex geometry and fine tolerances. If the group were to print these parts at an external company, the list of possible materials would be greater, and it would be more likely to find a better material for the intended purpose. Nevertheless, it would be expensive and also the delivery time in the sector was long during this period. Delivery time was between five to eight weeks, and without knowing the exact price, the group decided to 3D-print at UiS instead to save resources at the cost of a more limited selection of materials and print quality. The group had a meeting with the 3D-printing lab staff at UiS to figure out what materials were

available, and what could be done with respect to the limited budget. 3D-printing can be expensive and the very high-end materials were off limits for the team. After researching, consulting staff at the printing lab, and members within UiS Subsea, the list of possible materials reduced to three. These materials were PLA [48], CPE [47], and ABS [50]. Table 4.7 shows mechanical properties, pros, and cons of the different materials.

Table 4.7: Comparison of 3D-printing materials

Property	**PLA**	**CPE**	**ABS**
Density (g/cm^3)	1.24	1.16	1.10
Tensile Strength (MPa)	50.0	38.0	39.0
Hardness (Shore D)	84	72	76
Elongation at Break (%)	5.2	8.2	4.8
Pros	Easy to print	Chem. resistant	High strength
	Biodegradable	UV resistant	Good heat resist.
	Inexpensive	Good layer adhesion	Durable
	Fast printing	Good mechanical resistance	
	Good detail quality	Good flexibility	
Cons	Brittle	High print temp.	Potential warping
	Low heat resist.	Moisture sensitive	Harmful fumes
	Degrade in water	Costly	Poor UV resistance

When selecting the material for the 3D printed parts, mechanical properties, environmental impact, and availability was in focus. Firstly, PLA was considered due to its low cost and quick production process using the PRUSA printers at UiS. However, PLA has been a frequently used material for earlier UiS Subsea manipulators, and has been proven to be inadequate in many cases. Although PLA is biodegradable which is positive concerning environmental impact, it absorbs water and degrades rapidly. If compared to CPE and ABS, PLA has a shorter service life. Additionally, failures or breakage of PLA parts lead to material waste, increased cost, and time lost. After comparing the materials, the group determined that PLA was only suitable for prototyping.

CPE and ABS were both deemed viable options. They both possess good mechanical properties and durability. A common downside with the two materials is that they are not fully water resistant. Nevertheless, this would not be an issue given the short time the manipulator would be submerged. Eventually, CPE was chosen. It was chosen due

to chemical resistance which was convenient considering chlorinated water, and also since its flexibility reduced stress concentrations. Another deciding factor was that the printing cost of CPE would be covered by UiS.

4.5 Product Cost

Due to limited resources, the team used a circular economy approach, and contacted companies for sponsorship to realize the project. The group used circular economy principles to maximize resource efficiency and reduce waste. Table 3.8 illustrates the different parts reused and modified from earlier years. The limited budget was challenging due to significant expenses. By comparing the costs of the entire manipulator (approximately 30.000kr) to the budget (8.000kr), we observe a difference of 22.000kr, which is around 300% over budget. Table 4.8 provides an overview of the various components and respective expenses. Based on the actual product cost, the customer need and target specification concerning the budget was achieved.

Component	**Value**	**Actual Cost**	**Sponsored**
BLDC motor	588	-	-
Stepper motor	1150	-	-
3D prints	8000	-	8000 (University of Stavanger)
Shafts	200	-	200 (University of Stavanger)
Gears	10143	4470	5673 (Alf I. Larsen)
Connectors	2000	-	-
Wire	240	240	-
Springs	20	-	20 (University of Stavanger)
Fasteners	500	-	500 (Seam)
Lead screw	800	-	-
Bearings	1500	750	750 (TESS)
Motor housing	4500	-	4500 (University of Stavanger)
Total	**29641**	**5460**	**19643**

Table 4.8: Product Cost

Chapter 5

Production, Assembly and Testing

The components of the manipulator were produced, assembled, tested, and revised. In order to ensure the intended functionality of the manipulator, this process was crucial. The detail design of the manipulator was done thoroughly to minimize prototyping in order to save resources as 3D printing is costly. Even though the group performed a detailed design of every component, and the assembly from Autodesk Inventor indicated a working manipulator, there can always occur issues or possible points of improvement through assembling and testing the product.

5.1 Production

All the components of the manipulator were manufactured in-house at UiS. While the majority of the parts were 3D printed, some components such as shafts and the motor housing had to be manufactured the traditional way. The group encountered challenges during the printing process, causing significant delays. Specifically, there were issues with the Ultimaker S5 printer in the lab. Fillets and finer dimensions of the parts were not printed correctly, and were not viable for the final product. Fortunately, the printing issues were eventually solved, and the remaining parts were successfully printed. See Figure 5.1.

The choice of infill for the parts was carefully considered. The group decided to use an infill between 50-90% based on the target specification of easy assembly and disassembly.

While it was suggested by the printing lab staff that a lower infill could suffice considering the operational forces exerted on the parts, the group opted for a higher infill to minimize the risk of parts breaking during the assembly process. Furthermore, a higher infill reduced the volume between the layers in the print, addressing an issue stated by the ROV-Design team, where the buoyancy was too high. Despite a slight increase in weight to the higher infill, the functionality of the manipulator was not compromised. In fact, the additional weight, even though minor, served as ballast to further enhance the ROV stability.

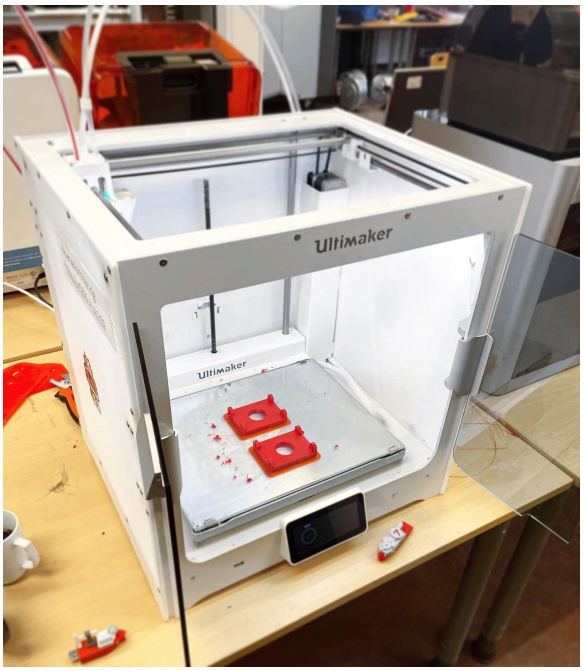

Figure 5.1: 3D printing of plates for the manipulator arm

Even though the design process was done to the best of the team's ability, there were instances of failure for the printed parts. The first component printed was the end-effector, because of its crucial role in the manipulator's ability to perform the MATE tasks. It was quickly realized that certain components of the end-effector were structurally too weak. Specifically, the shaft responsible for the rotational motion, and connecting the end-effector to the arm, failed when subjected to load. To rectify this issues, fillets were added to reinforce the shaft, and the diameter was increased from 7mm to 10mm to further enhance its strength.

Due to an unexpected delay in the delivery of the gears, the team decided to attempt printing them instead. The intention was to be able to start modular testing of the end-effector rotation before the actual gears arrived. The gears were printed using PLA as filament on the PRUSA printer. Unfortunately, the print was unsuccessful as the gear

teeth dimensions were not printed correctly and the overall result would not be viable for testing. For visual reference, see Figure 5.2 which illustrates the first prototype and final version of the end-effector, as well as the unsuccessful printing attempt for the gears.

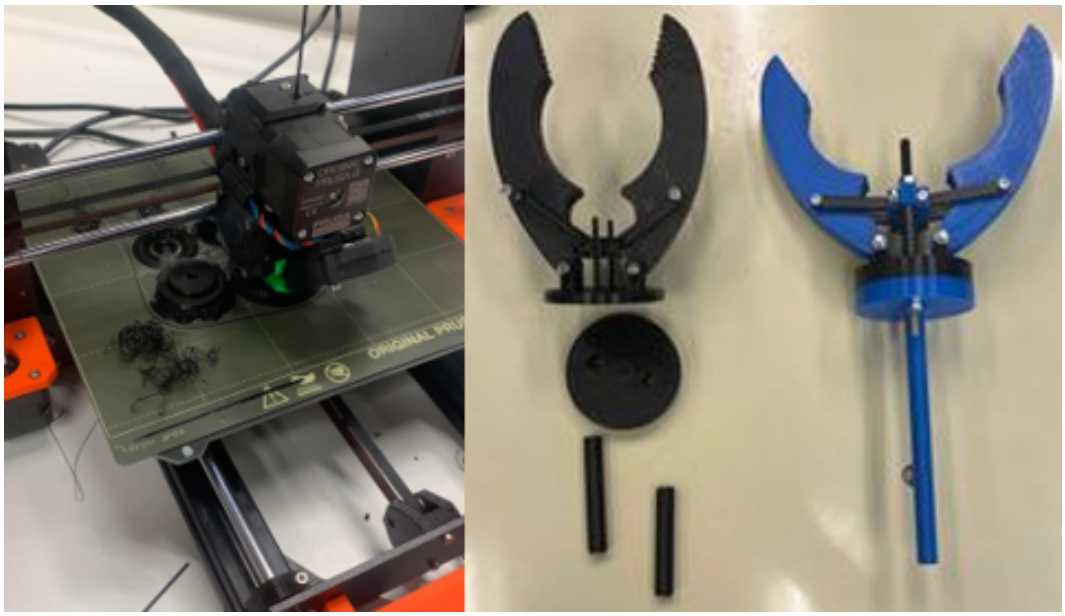

Figure 5.2: Failed gear print and end-effector

The production of the motor housing faced delays due to high activity in the workshop. The electronics enclosure for the ROV was still not manufactured when the team was ready to produce the stepper motor housing. As the completion of the electronics enclosure was essential for the water testing of the ROV, which could be done without the manipulator, it was given priority. Consequently the production of the stepper motor housing was delayed.

To address this inconvenience and to be able to assemble the arm, a temporary solution was devised. A prototype of the motor housing was 3D printed in PLA, although it was not adequate for the intended proper use. See Figure 5.3. Its primary purpose was to allow the arm to be assembled, and consequently letting the group verify that the different components fit, while also allowing some limited testing. Due to the high temperatures generated by the motor and the low thermal conductivity of PLA, this motor housing prevented proper testing of the arm's pitch function. Nonetheless, the housing prototype was useful, as it allowed completion of the assembly and testing of other functions with a full assembly.

Figure 5.3: 3D printed motor housing

Eventually the final motor housing was produced by CNC machining and lathing. The outcome was promising, but a misunderstanding between the team and the workshop staff led to misalignment of the holes in the lid and base cylinder. The displacement of the holes were approximately 20-30° from their intended position set in the technical drawings. This posed a challenge when assembling the connecting bracket to the motor housing lid. Considering the limited time available and the fast approaching testing deadline, the group deliberated on potential solutions. One option was to refine and re-print a new bracket that would match the hole placement on the motor housing. However, determining the exact displacement of the holes was challenging without precise measurements. Eventually, the group decided to drill new holes in the existing bracket, aligning them with hole positions on the housing. Although this decision impacted the aesthetics, it was deemed a sufficient temporary solution that allowed for testing and the MATE qualification. There was a window of time between May 15th and the MATE competition where a new bracket with the correct dimensions could be made. Nevertheless, the new motor housing resolved the assembly and disassembly challenge, discussed in Section 4.3. The design changes made were clearly an improvement. See Figure 5.4 showing the motor housing components.

Figure 5.4: Motor housing components with O-ring and shaft seal.

The last step of the production process involved adjusting the shafts and gears to the right dimensions, and modifying the components that were a part of the circular economy approach. While shafts were ordered with the appropriate tolerance, they did not accommodate the required holes for bolts and setscrews. Additionally, the bore diameter of the gears had to be increased. Since none of the team members had extensive workshop experience, achieving correct results required patience and extreme precision. To determine the best approach for this task, the team engaged in discussion. Ultimately, considering the limited experience, it was decided to use the pillar drill, which was one of the easier machines to operate. See figure 5.5.

Figure 5.5: Use of pillar drill to increase bore diameters

The circular economy approach allowed for some production failure. The first attempt of increasing the bore diameter of the worm for the pitch function failed. The hole was not

drilled perfectly straight which was a problem considering the teeth contact between the worm and the gear. Due to the design taking into account adaptability of components from earlier manipulators, an old worm of the same type was available in-house. The second attempt was a success and the bore was centered.

5.2 Assembly and Testing

When all the parts had been 3D-printed, manufactured and delivered from suppliers, the manipulator was ready to be assembled and tested. The different subsystems of the manipulator was first assembled individually in order to perform modular testing of each system important for its functionality. Modular testing allowed the group to easily isolate problems and points of improvement as well as not having to disassemble the whole manipulator to identify and fix problems. Through testing, the performance of the manipulator was compared and assessed according to the design calculations covered in Chapter 4.

5.2.1 End-Effector

The first component tested was the end-effector and its gripping mechanism. The team recognized the importance of measuring the pull force of the NEMA 17 motor responsible for the gripping mechanism, as this data was required for the force calculations covered in Section 4.1.3. Consequently, this test was conducted relatively early compared to other tests. Since the lead screw and nut of the system was reused from 2021, the test could be done as soon as the stepper motor was ready.

To perform the test, the team used an approach involving a fish weight. One end of the steel wire was attached to the fish weight, while the other end was connected to the motor. The fish weight had a maximum capacity of 40kg, but was more than enough for this test. The test commenced gradually, and the pull force increased steadily until the weight displayed 37kg. At this point, the test was stopped to avoid damaging the fish weight, but the pull force of the motor was deemed more than adequate. The recorded value corresponded to approximately 363N of pull force. See Figure 5.6 showing the test

rig.

Figure 5.6: Testing of NEMA17 pull force

The first important component of the manipulator to be assembled was the end-effector. The different components of the end-effector were assembled using stainless steel M3 and M4 bolts and nuts. Initially standard hexagonal nuts were used to fasten the bolts, but seemed to loosen as the end-effector components moved. Lock nuts were implemented to avoid such issues when forces were applied. The shaft of the end-effector still seemed mildly vulnerable to radial forces at the intersection of the plate and shaft. In order to further strengthen the shaft, an additional circular plate was added to support the fillet.

The assembly process required little time and few tools, which fulfilled the target specification of easy assembly. When fully assembled, weight and objects of geometry relevant for the MATE competition was attached to the end-effector. Both larger and smaller objects were successfully held by the end-effector. During this test, a weight of $\approx 1.1kg$ was placed on the end-effector, without complications. Furthermore, the wire actuation mechanism successfully closed and opened the end effector as intended. Thus, the design was proven to meet the important customer needs and target specifications concerning the end-effector. See Figure 5.7.

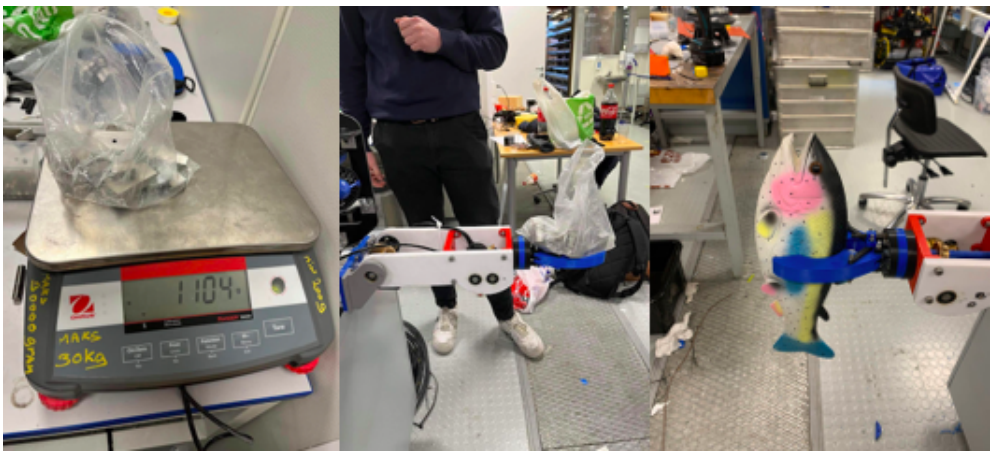

Figure 5.7: Weight and objects placed on end-effector

5.2.2 Manipulator Arm

The manipulator arm was assembled in two separate sections. It was divided by the elbow joint, which made it possible to individually test the telescope function and the rotation of the end-effector before connecting the two sections for testing of the pitch.

Upper Section

The assembly of the upper section of the arm, which included the rotation mechanism for the end-effector, was a challenge. To ensure functionality of the system, the components had to be assembled carefully and in the correct order to achieve compatibility and prevent damages. The worm and gears were attached to the shafts using setscrews. For the modular testing it was decided not to utilize the bearing retainer preventing the outer rings of the bearings from rotating. This decision was made in anticipation of potential issues that might have required disassembling of components. The retainer could have complicated this process and both bearings and 3D printed components would be at risk of damage due to more force required to disassemble. Despite the absence of the retainer, the outer ring of the bearings remained stationary, enabling the group to conduct the modular tests required.

Another challenge encountered was the attachment of the shaft to the BLDC motor. The BLDC motor was a reused component, and its original shaft had been cut of at some point. To resolve this issue, a 3D printed coupling with threaded holes was attached to

the motor, and an M3 bolt and nut was used to effectively attach and connect the shaft to the motor.

After assembling all the components of the upper section of the arm, tests were conducted to evaluate both the rotational speed and torque. However, the initial test revealed instability and difficulties with the meshing spur gears. The reason behind this issue was discovered to be related to the setscrews on BLDC motor shaft becoming loose, due to the lack of threaded area between the setscrew and the hole. This resulted in axial displacement and high vibrations. To address this issue, set screws of longer length were used. Additionally, a retaining compound was used, effectively securing the set screw and allowing smooth rotational motion. To measure the rotational speed of the end-effector, a stopwatch was utilized, resulting in a measured speed of approximately 0.5-0.6 rotations per second. This result aligned with the theoretical calculations, and officially marked a manipulator with a fully functional and stable rotational function.

To assess the output torque, a test rig was created, involving the manipulator holding and rotating an M6 bolt. The end-effector was able to hold and rotate the bolt. This functionality proved advantageous for tasks such as rotating a valve, which has been a common task in earlier competitions. The required torque of the system was not exceptionally high, and the main purpose of the feature was to improve mobility and ease completion of certain tasks. Previously, similar tasks required rotation of the entire ROV, consequently proving the new design beneficial. See Figure 5.8 for assembly and testing of rotation.

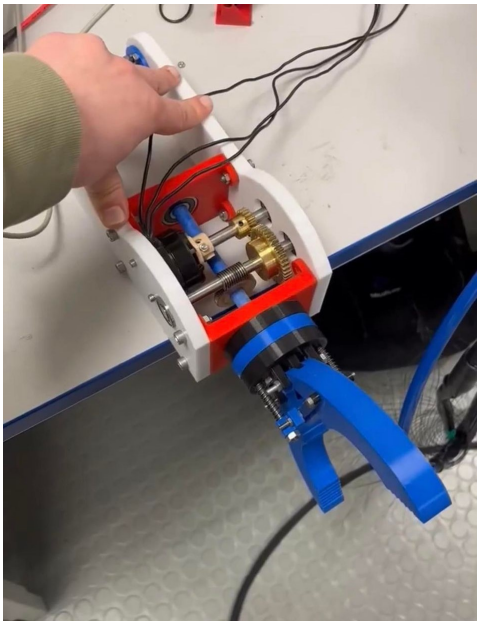

Figure 5.8: Assembly and test of end-effector

Lower Section

The lower section of the manipulator arm was assembled, and the performance and stability of the lead screw actuation was evaluated through testing. During the assembly of the plastic bearings supporting the stabilizing shafts, the flange of the bearing broke and the sleeve cracked. See Figure 5.9. This was despite using the correct tolerances specified by the supplier for the shaft and the housing. The likely cause of this issue was an observed unevenness and imperfection in the circularity of the housing print. As a result, the desired clearance was not achieved, leading to high friction and static forces between the shaft and bearing. Consequently, a significant amount of force was required to move the shaft linearly, which was insufficient in terms of desired functionality.

Figure 5.9: Broken plastic bearing

Fortunately, spare bearings were available, and the inner surface of the housing was carefully filed down to achieve the appropriate level of force required to assemble the bearing. This solution would not be ideal for heavy industries applications, as it deviated from the specified tolerances. Nevertheless, it served as a temporary fix with respect to the limited time available, and was deemed adequate considering the low forces and linear speed. Furthermore, the rest of the components were assembled, and a test rig was set up to evaluate the lead screw actuation. See Figure 5.10 for the connection of the motor and test rig. Note that the length of the trapezoidal lead screw was not of correct length for this specific test.

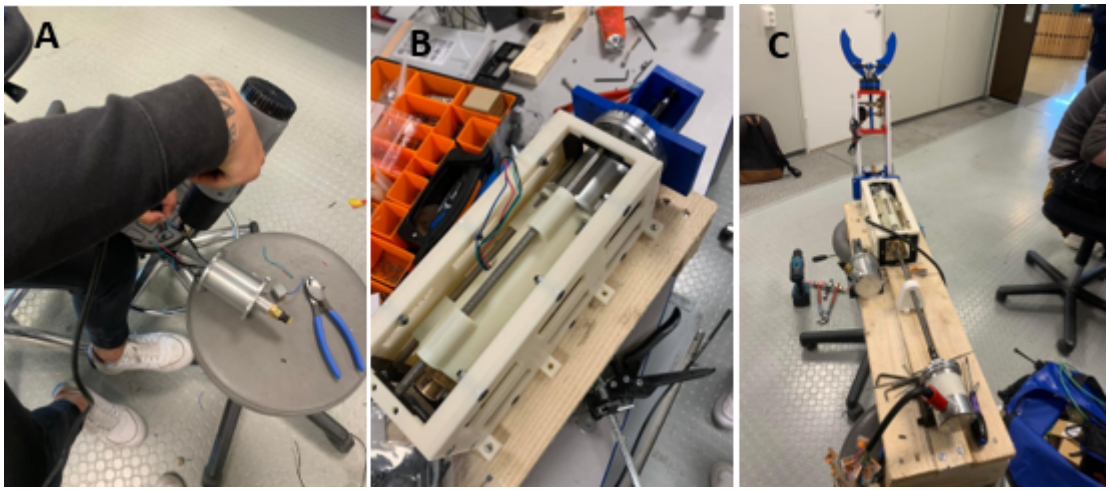

Figure 5.10: (A) Connection of motor (B) Lower section assembly (C) Test rig

The lead screw actuation was initially tested with only the lower section of the manipulator arm assembled, and later with complete assembly as shown in Figure 5.10 (C). The first test was successful, and the manipulator moved as intended at both lower and higher speeds. Thereafter, the upper section of the manipulator arm was assembled to evaluate the system's functionality with additional weight up front and to ensure that the intended functionality was achieved. However, upon starting the motor, no movement occurred. The shaft struggled to rotate, and the manipulator arm was unable to move linearly. The group initially considered the length of the lead screw being a potential issue. The length of the screw could have potentially led to vibrations and bending, causing misalignment between the lead screw and the nut. Consequently, the lead screw was cut to the specified length of 150mm. Despite the adjustment of the length, the system remained non-functional.

In an effort to troubleshoot the problem, the group decided to disassemble the upper section of the manipulator, and repeat the initial test with only the lower section assembled, which had been completed successfully earlier. This was done to determine if the issue was mechanically related or caused by another factor. However, even with only the lower section assembled, the system did not function. This indicated that the problem was not related to the mechanical design or assembly.

The team responsible for the electric regulation was contacted, and the problem was identified. It was discovered that the motor was receiving bugged data, which made it try to rotate in both directions simultaneously. By debugging and fixing the code, the system

was operational once again. The upper section of the arm was reassembled, and the test was redone with successful results. The linear actuation system of the manipulator arm was fully functional, and from starting position it was able to move the manipulator approximately 8cm linearly.

Pitch Function

Once the manipulator was fully assembled, the pitch function was tested. Similar to the issue encountered with the telescope function, the motor would not rotate properly. Fortunately, the cause of the problem was quickly identified to be the same, and the issue was quickly fixed.

A primary purpose of the test was to determine the frequency for the motor that yielded the best performance. The frequency was initially set 500Hz, based on the output torque graph provided in the motor's data sheet. See Figure 4.6. However, at this frequency, the tilt motion of the arm was not ideal, and seemingly moved in steps rather than evenly. Through collaboration with the regulation team, several frequencies were tested, and the frequency that provided the most even and stable movement was eventually determined to be 900Hz.

Once the motion of the tilt was sufficient, loads were gradually added to the arm to test its lift capacity. The manipulator had no issues lifting lighter object, but as the weight increased to around 1kg, it began to struggle. The step-like motion reappeared. Upon inspection, it was concluded that shock loads were a possible cause. When a relatively high load was applied abruptly, a force was exerted on the gear shaft, which reduced the clearance between the teeth of the gear and worm responsible for the tilt movement. An increased interference of the teeth increase the resistance and friction, causing the worm-gear pair to not function properly. However, this issue was not considered highly problematic. It was expected that the shock loads would decrease when the manipulator was submerged in water, and that the manipulators ability to perform the required task was not compromised. Due to time constraints and the deadline for the MATE qualification video, this issue was not fully resolved at the time of writing this thesis.

Nevertheless, the self-locking property of the worm-gear pair proved to be sufficient, suc-

cessfully holding a weight of 1.1kg without any problems, and the manipulator demonstrated rigidity. Through the tests performed, the target specifications of load capacity, rigidity, and degrees of freedom were achieved. See Figure 5.11 showing the manipulator in different positions.

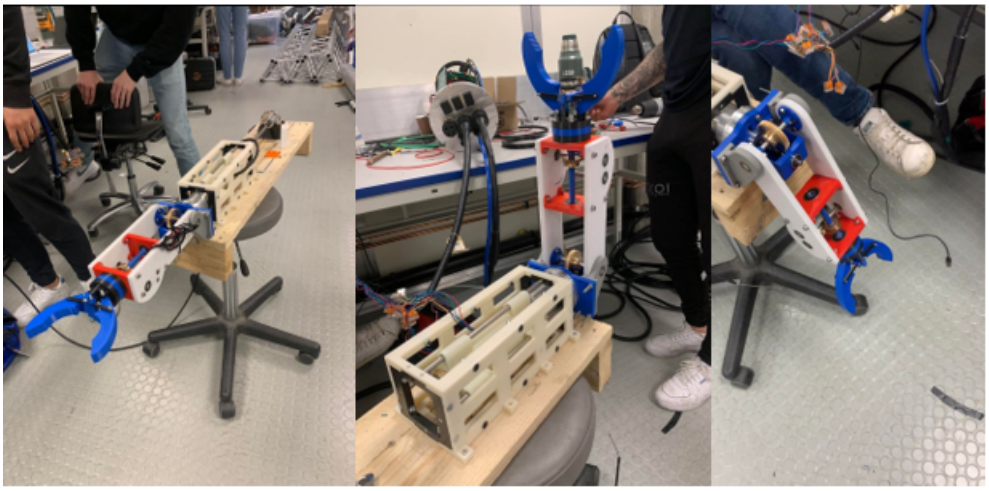

Figure 5.11: From left to right: Manipulator in leveled, upwards, and downwards position

When the testing was complete, the manipulator was placed on the ROV and prepared for water testing. The total weight of the manipulator was 6.2kg, and combined with the weight of the rest of the ROV the total weight was within the limit stated in the target specifications.

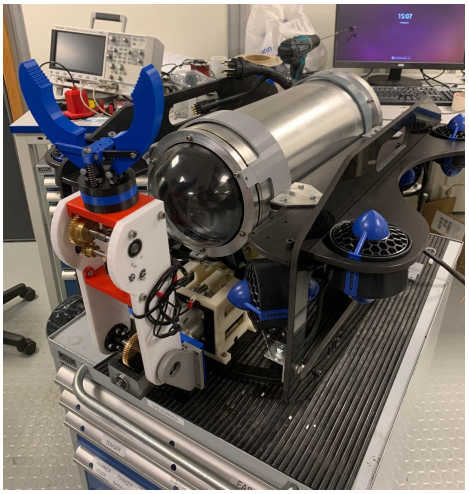

Figure 5.12: Manipulator placed on the ROV

5.2.3 Testing in water

The motor housings were tested prior to fully submerging the manipulator in water. It was crucial for the motor housings to be completely waterproof in order for the motors to function and not be damaged. Two of the motor housings were reused and had already undergone water and pressure testing. Nevertheless, it was decided to re-test them as the new motor housing had to be tested anyway. Since the new housing was inspired by the design of the old ones and was of the same material and similar dimensions, only a water test was considered sufficient. Before submersion, grease was refilled to further ensure the housings being waterproof. The motor housings were then submerged in water for a duration of three hours. The lids of the motor housings were detached and the inside was inspected using paper towels to check for any sign of leakage or failure. Fortunately, no signs of leakage or failure were observed, consequently confirming that the housings were waterproof. See Figure 5.13.

Figure 5.13: Waterproof test of motor housings

Through water testing, the functionality was tested in a subsea environment. Furthermore, many of the target specifications assigned the unit "Subj." were tested and verified. This included its maneuverability, weight distribution with regards to the ROV weight balance, and material properties concerning the ability to withstand chlorinated water.

One of the key business goals in the mission statement was that the manipulator would be ready for water testing by April 11th. This was later on discovered to be ambitious and therefore postponed. Due to manufacturing delays of manipulator parts and leakages in the electronics enclosure, the test was postponed until May 3rd. The ROV was stable in

the water and the target of weight distribution regarding both the manipulator itself and the ROV was successful. The tilt, rotation, and the telescope function worked properly and it was able to pick up and handle different objects made for the MATE qualification video. The manipulator was also easy to maneuver from topside, and combined with it being functional under water, fulfilled the target of submerged maneuverability. After the first water testing, the manipulator was cleaned with fresh water and showed no signs of damage or failure, and the target of withstanding chlorinated water and required time submerged, was achieved. See Figure 5.14 for water testing of the ROV and manipulator.

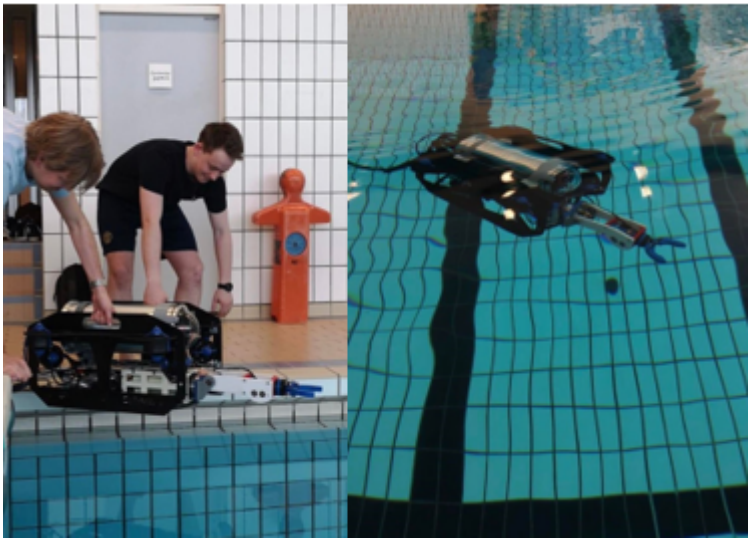

Figure 5.14: Water testing of ROV and manipulator

5.3 Product and Process Improvements

The manipulator developed and produced throughout this project contained several aspects that can serve as a foundation and be further developed and improved in future UiS Subsea projects. The combination of a telescope function, tilt, and rotational end-effector has not been a part of the previous manipulators. Last year, the manipulator had a telescope function, but no tilt, and the year before the manipulator had the tilt function but not the telescope function. This year both concepts were merged into one. The main purpose of the telescope function this year was first and foremost functionality as the telescope function from last year was dysfunctional and did not work. The group managed to come up with a design that secured stability and functionality, but the range at which it could move can be further improved. It was only able to move around 8cm,

which is not optimal and further improvement can serve UiS Subsea greatly in future competitions.

One of the most experimental and new aspects of the manipulator was the motor housing being a part of the manipulator arm. The result was a more rigid manipulator compared to the use of belts and pulleys used previously in both 2021 and 2015. The disadvantage and main problem that can be further improved in future projects is the impact shock loads had on the gear mesh between the worm and the worm gear. A more powerful motor could improve the performance significantly and allowed for more gearing to further increase the torque, given the necessary power supply is available. Given more time, the ability to change the end-effector geometry could be implemented. Having the upper half of the fingers containing the important geometry interchangeable, could be a major benefit for competition purposes. By implementing this concept in way that allowed for quick assembly and disassembly, the fingers can be swapped according to different tasks.

The process of developing, designing and producing the manipulator could be improved, even though it was planned thoroughly during the first weeks. The use of a GANTT chart served the group well and gave a good and clear overview of deadlines and weekly goals. Nevertheless, the limited experience within the team regarding product development in practice, proved to be a challenge for some aspects of the process. One of the main issues during the project was the delivery time of ordered components like gears and shafts. The delivery time for the gears was much longer than anticipated which delayed the testing greatly. In the future, long lead items should be identified and ordered as soon as possible in order to avoid this problem. In addition, even though the manufacturing of the shafts and motor housing was done for free at the UiS workshop, the delivery time was long due to high activity. The production of the motor housing took approximately a month from the day the technical drawings were delivered. In future manipulator projects, a recommendation is to contact manufacturing companies and outsource this kind of work if the budget allows it.

In order to visualize and categorize the potential causes of a problem, a fishbone diagram can be utilized. The fishbone diagram serves as a method to diagnose the problem rather than focusing on the symptoms. It gives a clear visualization of the problem and the causes that could potentially lead to a dysfunctional manipulator. The fishbone diagram shown below gives an insight into this years problems and causes, and might serve as a

tool for future manipulator projects for UiS Subsea.

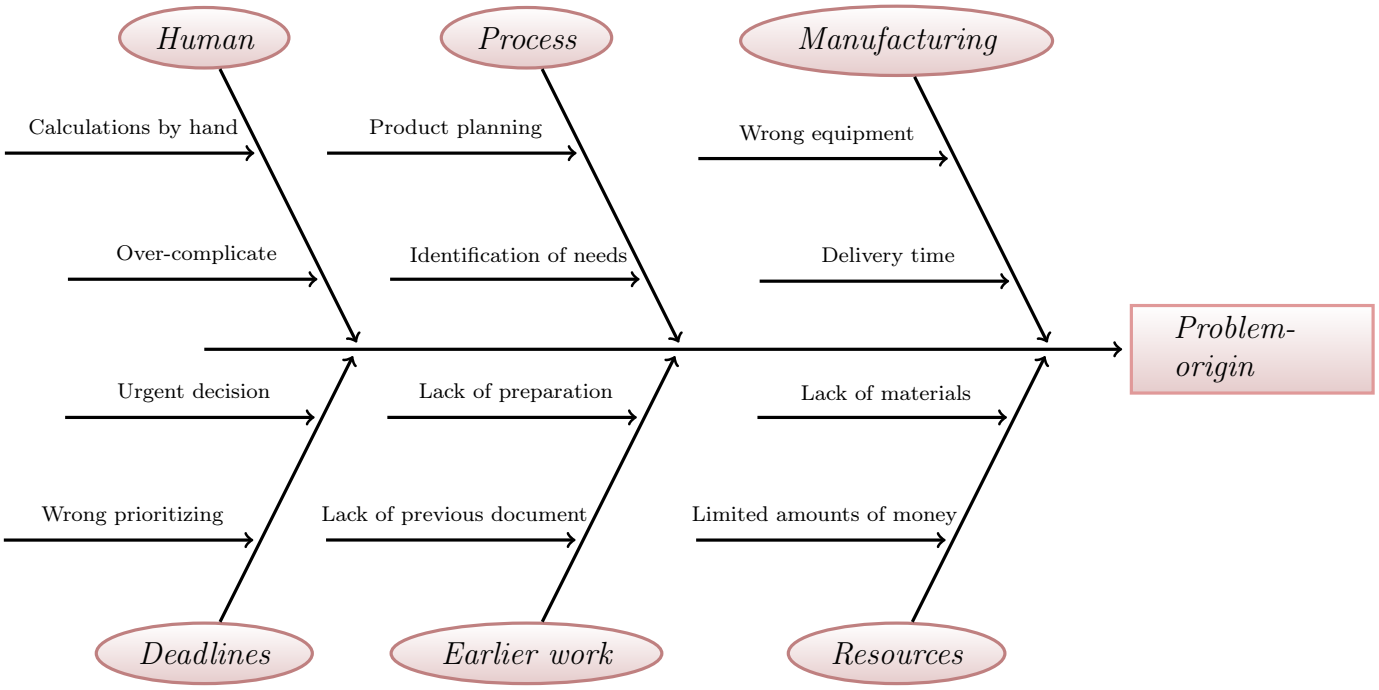

Figure 5.15: Fishbone diagram

Chapter 6

Conclusion

The aim of this thesis was to develop and design a fully functional ROV manipulator capable of completing all the tasks necessary in the MATE ROV Competition. The product development process was utilized, starting from initial planning and concept development to final detailed design. Through calculations and extensive testing the design was evaluated to ensure performance and functionality. A key aspect of the project was the implementation of a circular economy approach, which proved to have a significant impact on the project's success. Components were reused which contributed to overcome the financial and time limitations, while also promoting sustainability in engineering practices. The outcome of the project was a fully functional manipulator able to perform all the necessary MATE tasks, which contributed to a successful qualification for the 2023 MATE ROV Competition.

During the product development process, customer needs and target specifications for the manipulator were established based on MATE requirements and the ambitions of UiS Subsea. This facilitated the generation and selection of concepts, and also provided a clear direction for the design. The systematic approach to concept selection through screening matrices established the strengths and weaknesses of the concepts and helped the team locate the most promising concepts. The detailed design phase was challenging and time consuming due to limited experience and the high amount of components involved, which all had to be compatible. However, it resulted in a design that met the target specifications of degrees of freedom, load capacity, and functionality. The thoroughness of the detailed design phase also minimized the need for prototyping and allowed for efficient assembly

and modular testing.

The outcome of the process was a manipulator accomplishing most target specifications within the ideal values. All the targets regarding dimensions, weight, functionality and ease of assembly, were fulfilled. The lift capacity was a target that did not achieve its ideal value, but was still within the marginal limit. The targets assigned the unit "Subj." were evaluated and verified through successful water testing and MATE qualification. The target regarding environmental impact was addressed through the circular economy approach.

While the manipulator was functional and well-suited for the MATE competition, there were room for further improvement and optimization. Given more time, enhancements could be made to the pitch function to improve its lift capacity. Making the fingers of the end-effector interchangeable could also have been a beneficial improvement. Additionally, further reducing the weight of the manipulator by removing excess material would improve its environmental impact and cost. In the future, the range of movement of the telescope feature can be further improved. Improvements can be made to the process considering timing, prioritizing and better communication.

Participating in the 2023 UiS Subsea project has been an invaluable experience. The learning curve has been steep, and the team has been through long nights of frustrations, but also moments of great joy. Overall, the project has provided both personal and professional growth. Hopefully, this thesis will serve as a foundation for future UiS Subsea manipulator projects, where the design can be adopted or further developed to achieve even greater results.

Bibliography

[1] R. Jehangir, *What is an underwater rov?*, https://bluerobotics.com/learn/what-is-an-rov, 2022. (visited on 02/08/2023).

[2] N. T. Centre, "Remotely operated vehicle (rov) services", 2003. (visited on 02/12/2023).

[3] *Bluerov2*, https://bluerobotics.com/store/rov/bluerov2/, 2023. (visited on 03/01/2023).

[4] R. Solutions, *Underwater rovs*, https://rovtechsolutions.com/products/underwater-rovs/, 2019. (visited on 03/10/2023).

[5] OCEANEERING, *Rov systems*, https://www.oceaneering.com/rov-services/rov-systems/, 2023. (visited on 03/20/2023).

[6] SCANMUDRING. "Equipment scanmudring - excavators". (2023), [Online]. Available: %5Curl%7Bhttps://scanmudring.no/equipment/#excavators%7D (visited on 02/12/2023).

[7] AUVAC, *Bpauv configuration*, https://auvac.org/34-2/, 2023. (visited on 03/11/2023).

[8] KYSTDESIGN, *Surveyor rov*, https://kystdesign.no/rovs/surveyor/, 2023. (visited on 03/08/2023).

[9] G. O. B. array, *Float technology*, https://www.go-bgc.org/floats, 2023. (visited on 02/04/2023).

[10] Ecomagazine, *Robotic floats provide new look at ocean health and global carbon cycle*, https://www.ecomagazine.com/news/research/robotic-floats-provide-new-look-at-ocean-health-and-global-carbon-cycle, 2023. (visited on 04/08/2023).

[11] N. S. Foundation, *About the mate center*, https://www.marinetech.org/about/, 2012. (visited on 02/08/2023).

[12] M. I. for Innovation, *About mate ii*, https://mateii.org/about-mate-ii/, 2023. (visited on 03/02/2023).

[13] M. I. for Innovation, $2023_e xplorer_m anual_f inal_{11}7_2023_w ithcover$, https://files.materovcompetition.org 2023. (visited on 03/02/2023).

[14] M. I. for Innovation, *Mate floats!*, https://materovcompetition.org/content/mate-floats, 2023. (visited on 03/12/2023).

[15] M. P. Groover, *Fundamentals of Modern Manufacturing, Materials, Processes, and Systems*, 4th ed. John Wiley Sons, INC., 2010.

[16] J. S. M. S. Fjermdal, "Design and control of rov manipultors", University of Stavanger, Tech. Rep., 2021.

[17] *What are the different types of industrial robots and their applications?*, https://processsolutions.com/are-the-different-types-of-industrial-robots-and-their-applications/, 2018. (visited on 01/20/2023).

[18] R. N. Jazar, *Theory of Applied Robotics: Kinematics, Dynamics, and Control*, 2nd ed. Springer, 2010.

[19] F. M. M. Ben-Ari, *Kinematics of a Robotic Manipulator*, 1st ed. Springer, 2018.

[20] M. A.-S. M. Farman, "Design of a three degrees of freedom robotic arm", Khalifa University of Science Technology, Tech. Rep., 2018.

[21] J. K. N. R. G. Budynas, *Shigley's Mechanical Engineering Design*, 9th ed. McGraw-Hill, 2011.

[22] H. G. Lemu, "Dimensjonering av maskinelementer", University of Stavanger, Tech. Rep., 2020.

[23] MonroeEngineering, *"whats's the difference between bolts and screws?"*, https://monroeengineering.com/blog/bolts-vs-screws-whats-the-difference/, 2017. (visited on 03/23/2023).

[24] MITcalc, *Theory - fundamentals*, https://www.mitcalc.com/doc/springs/help/en/springs.htm, 2023. (visited on 02/11/2023).

[25] EngineeringLearn, *3 types of fits*, https://engineeringlearn.com/3-types-of-fits-clearance-fit-interference-fit-transition-fit-complete-guide/, 2023. (visited on 03/25/2023).

[26] BaartGroup, *How to determine bearing shaft and housing fit*, https://baartgroup.com/how-to-determine-bearing-shaft-and-housing-fit/, 2023. (visited on 02/20/2023).

[27] M. K. Saini, *Difference between stepper motor and dc motor*, https://www.tutorialspoint.com/difference-between-stepper-motor-and-dc-motor. (visited on 02/08/2023).

[28] M. Power, *Brushless vs brushed dc motors: When and why to choose one over the other*, https://www.monolithicpower.com/en/brushless-vs-brushed-dc-motors, 2018. (visited on 04/20/2023).

[29] LearnMech, *Stepper motor construction*, https://learnmech.com/what-is-stepper-motor-types-application-advantages/, 2018. (visited on 02/11/2023).

[30] Hubs, *What is 3d printing*, https://www.hubs.com/guides/3d-printing/, 2023. (visited on 02/05/2023).

[31] Prusa. "Original prusa i3 mk3s+". (2023), [Online]. Available: https://www.prusa3d.com/category/original-prusa-i3-mk3s/ (visited on 03/19/2023).

[32] Ultimaker. "Ultimaker s5". (2023), [Online]. Available: https://3dnet.no/products/ultimaker-s5 (visited on 03/25/2023).

[33] M. C. Karl T. Ulrich Steven D. Eppinger, *Product design and development*, 7th ed. McGraw - Hill Eductaion, 2Penn Plaza, New York, NY10121, 2020.

[34] Innova. "Schilling robotics titan 4 manipulator". (2023), [Online]. Available: https://www.innova.no/e/products/rov-equipment/schilling-robotics-titan-4-manipulator/ (visited on 03/22/2023).

[35] S. Tech. "Sub tech atom rov manipulator". (2023), [Online]. Available: https://www.subsea-tech.com/ (visited on 03/08/2023).

[36] S. D. E. Karl T. Ulrich, *Product design and development*, 6th ed. McGraw - Hill Eductaion, 2Penn Plaza, New York, NY10121, 2020.

[37] E. Parliament, *Circular economy: Definition, importance and benefits*, https://www.europarl.europa.eu/news/en/headlines/economy/20151201STO05603/circular-economy-definition-importance-and-benefits, 2023. (visited on 03/02/2023).

[38] StepperOnline, *Nema 17 bipolar 1.8deg 65ncm (92oz.in) 2.1a 3.36v 42x42x60mm 4 wires*, https://www.omc-stepperonline.com/nema-17-bipolar-1-8deg-65ncm-92oz-in-2-1a-3-36v-42x42x60mm-4-wires-17hs24-2104s, 2023. (visited on 04/01/2023).

[39] K. Gears. "Suw0.8-r1". (2023), [Online]. Available: https://khkgears2.net/catalog5/SUW0.8-R1 (visited on 03/08/2023).

[40] K. Gears. "Bg0.8-60r1". (2023), [Online]. Available: https://khkgears2.net/catalog5/BG0.8-60R1 (visited on 03/08/2023).

[41] SKF, *Skf bearing select*, https://www.skf.com/group/support/engineering-tools/bearing-select, 2023. (visited on 03/12/2023).

[42] K. Gears, *Suw0.5-r1*, https://khkgears2.net/catalog5/SUW0.5-R1, 2023. (visited on 03/03/2023).

[43] K. Gears, *Bg0.5-60r1*, https://khkgears2.net/catalog5/BG0.5-60R1, 2023. (visited on 03/03/2023).

[44] K. Gears, *Bss1-40a*, https://khkgears2.net/catalog2/BSS1-40A, 2023. (visited on 03/03/2023).

[45] K. Gears, *Bss1-18b*, https://khkgears2.net/catalog2/BSS1-18B, 2023. (visited on 03/03/2023).

[46] "Aluminum, al". (2023), [Online]. Available: https://www.matweb.com/search/datasheet.aspx?bassnum=AMEAL00 (visited on 03/14/2023).

[47] Ultimaker. "Ultimaker cpe technical data sheet". (2022), [Online]. Available: https://makerbot.my.salesforce.com/sfc/p/#j0000000HOnW/a/5b000004Tvwj/dXpbTiHlbQejB7l7OhC40z4FkiF3VuNJM1k7xgeHhJE (visited on 03/20/2023).

[48] Ultimaker. "Ultimaker pla technical data sheet". (2022), [Online]. Available: https://makerbot.my.salesforce.com/sfc/p/#j0000000HOnW/a/5b000004UiRV/lt4XCkl0KOSLfPMcyG06mKKbES33WnYiFrMsG8bFGhw (visited on 03/20/2023).

[49] "Grade 304 stainless steel". (2023), [Online]. Available: https://www.azom.com/article.aspx?ArticleID=2867 (visited on 03/04/2023).

[50] Ultimaker. "Ultimaker abs technical data sheet". (2022), [Online]. Available: https://makerbot.my.salesforce.com/sfc/p/#j0000000HOnW/a/5b000004UWOb/mqEDmbBEqiM6dfNicGFkHQEgcV9T8W762bqwplt4bxo (visited on 03/20/2023).

Appendix A: Technical Drawings

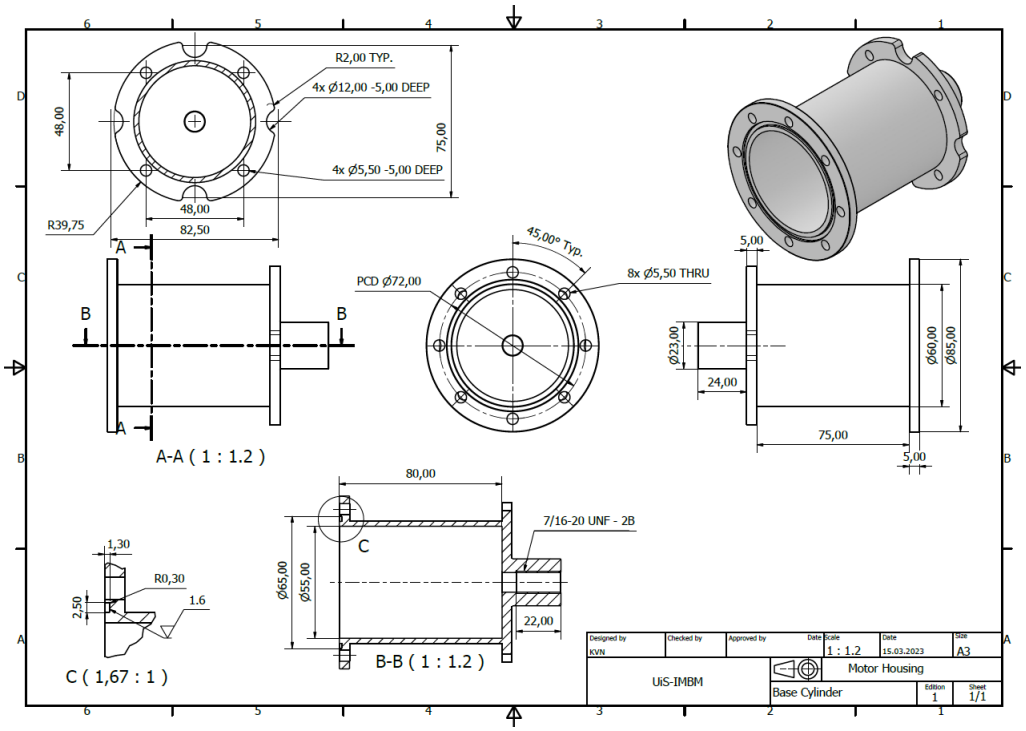

Figure 1: Technical drawing of Base Cylinder

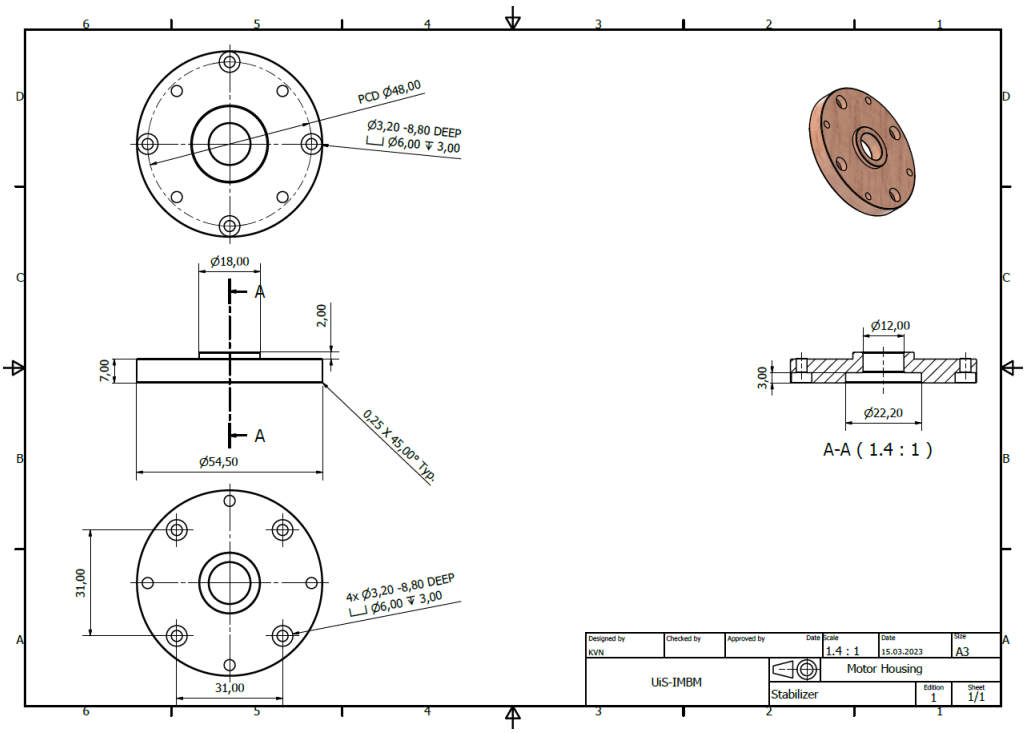

Figure 2: Technical drawing of Stabilizer

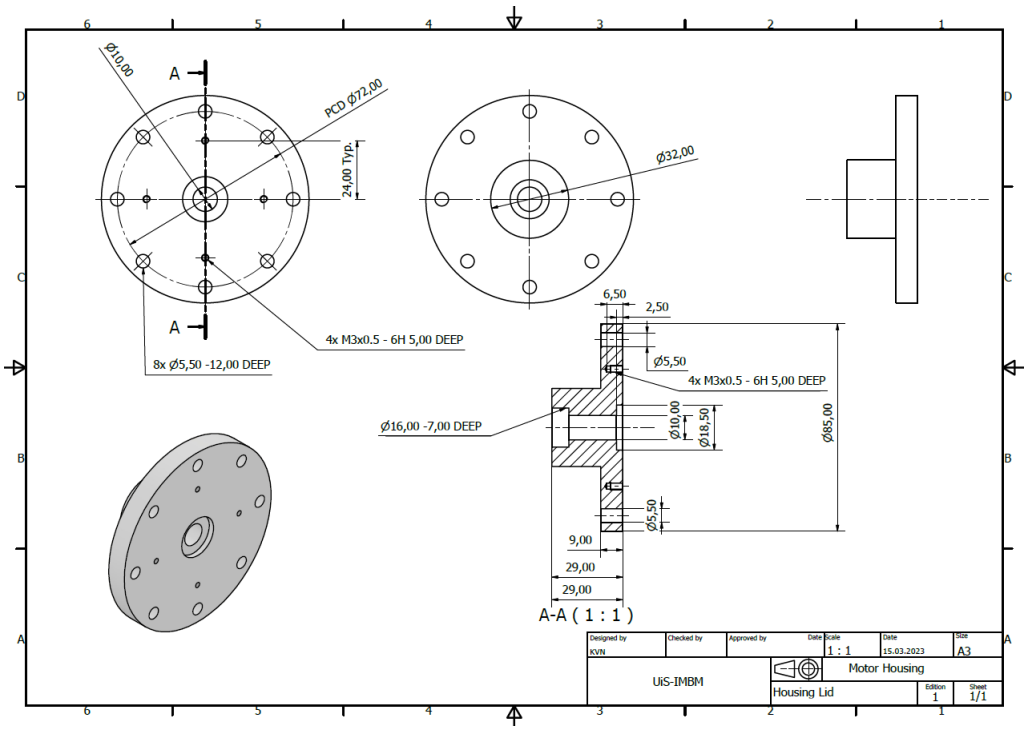

Figure 3: Technical drawing of Housing Lid

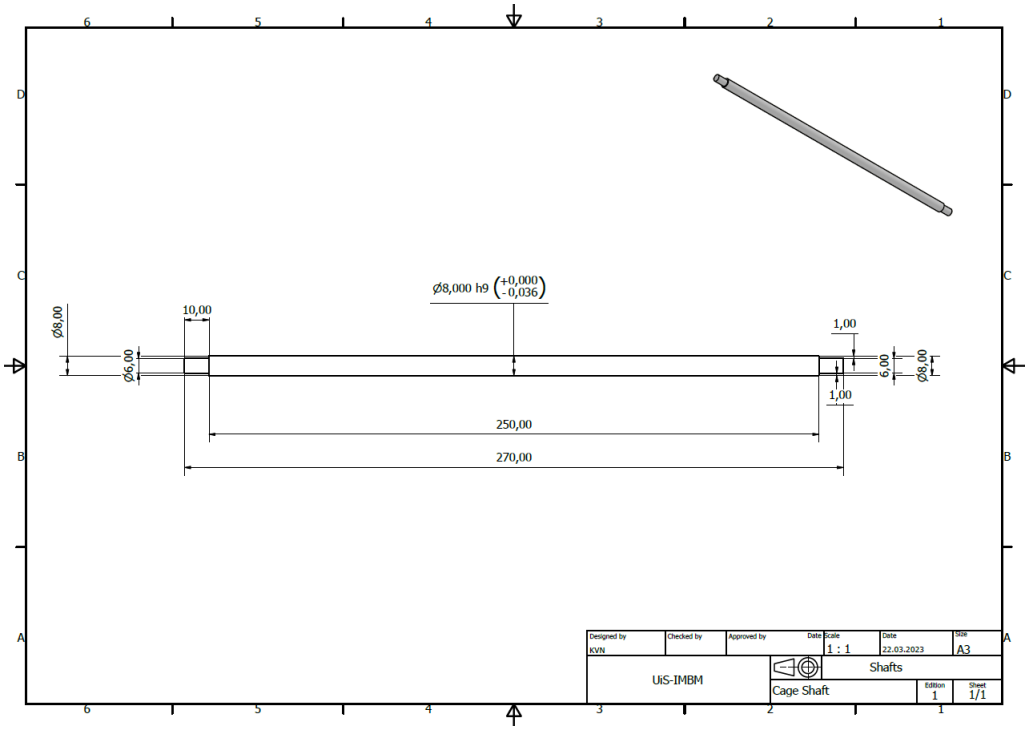

Figure 4: Technical drawing of Cage Shaft

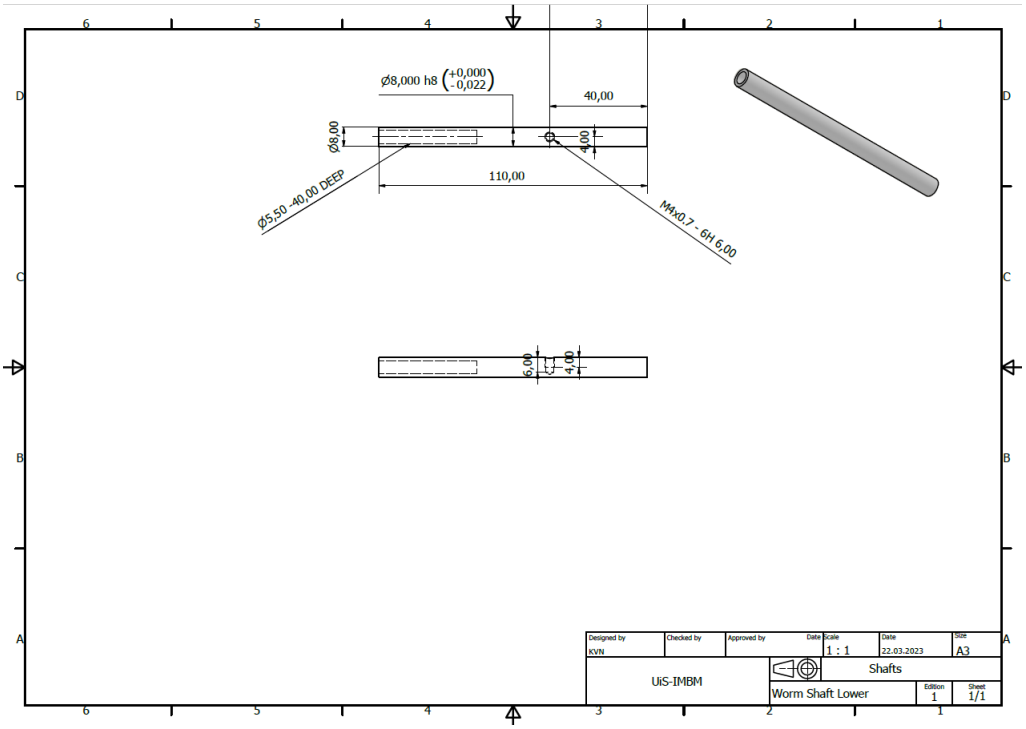

Figure 5: Technical drawing of Worm Shaft Lower

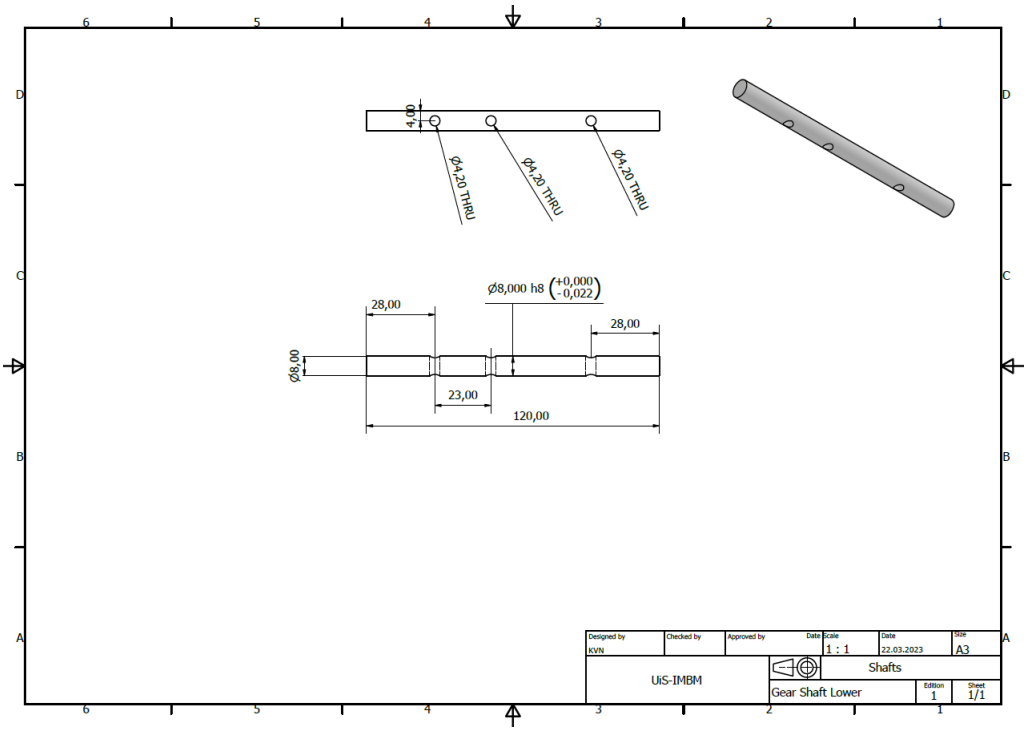

Figure 6: Technical drawing of Gear Shaft Lower

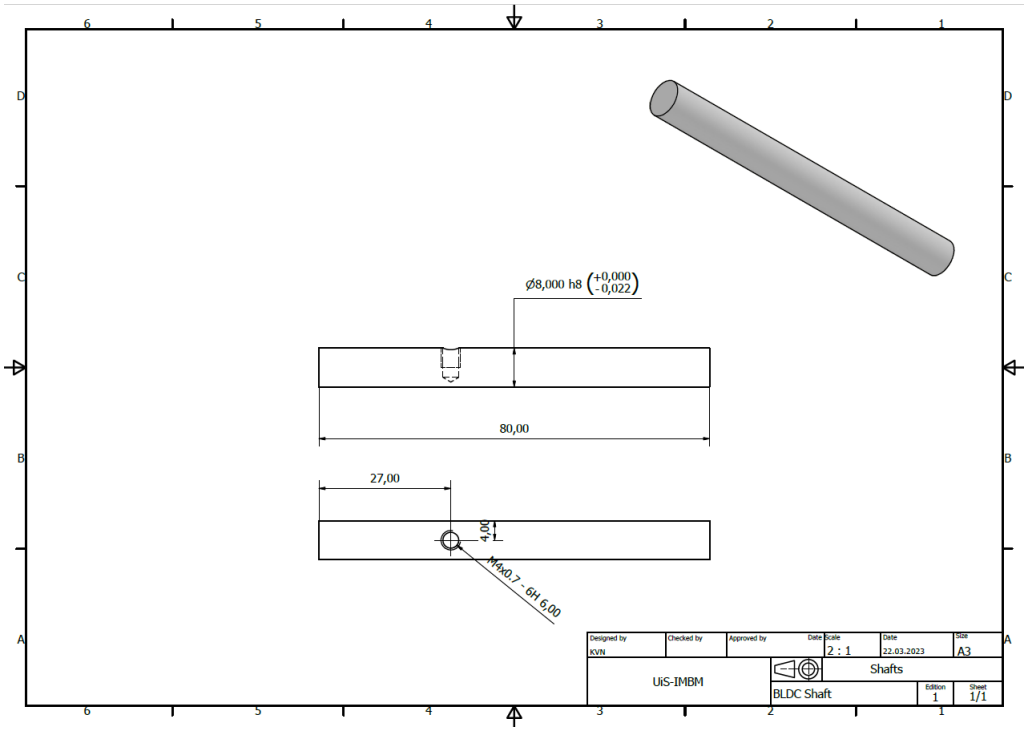

Figure 7: Technical drawing of BLDC Shaft

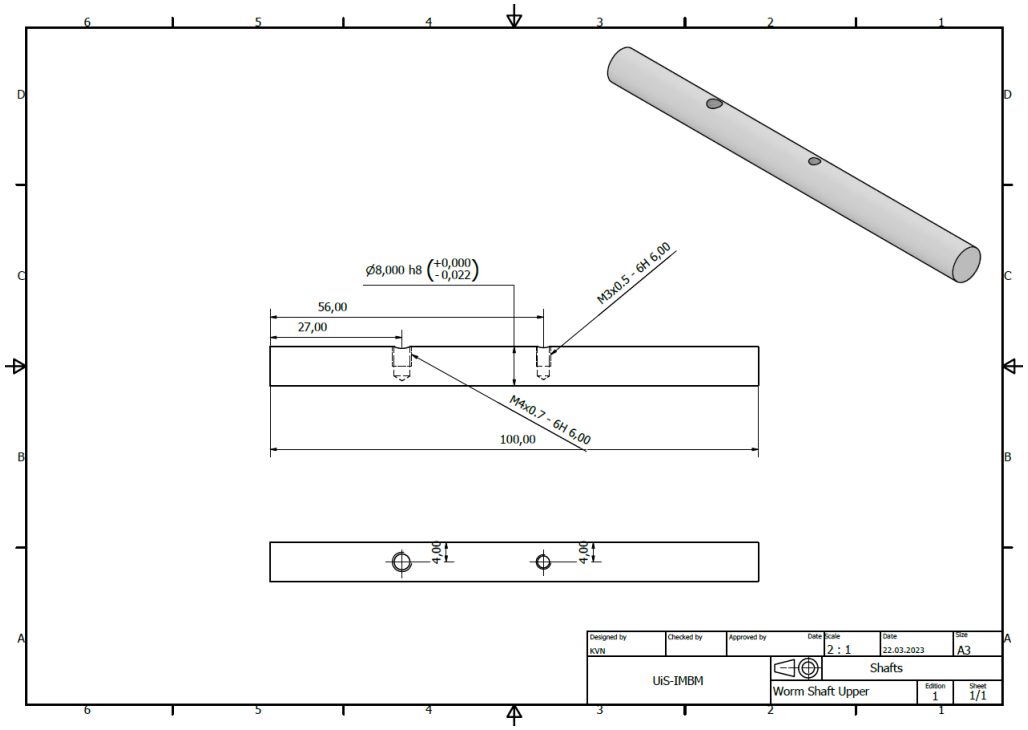

Figure 8: Technical drawing of Worm Shaft Upper

Appendix B: Additional Theory

Important calculations to be performed if the use of press fits is relevant are as follows:

The tangential shear stress is,

$$\tau_t = \frac{M_z}{2\pi {r_n}^2 h} \tag{1}$$

where M_z is the torsional torque, h is the depth of hole, and r_n is the radius of hole.

The axial stress is given by

$$\tau_z = \frac{F_z}{2\pi r_n h} \tag{2}$$

where F_z is the axial force.

Furthermore, the magnitude of the two shear stress components is given as follows,

$$\tau = \sqrt{{\tau_t}^2 + {\tau_z}^2} \tag{3}$$

When an interference fit is present between a hole and shaft, contact pressure is also generated between the two components. This contact pressure can be calculated using the following equation.

$$p = \frac{\delta}{2(\alpha_n + \alpha_a)} \tag{4}$$

where α_n and α_a is the hole coefficient of influence and shaft coefficient of influence, respectively.

$$\alpha_n = \frac{1}{E} \frac{r_{ni}^2}{r_{no}^2 - r_{ni}^2} r_{ni} \left(1 - v + (1 + v) \frac{r_{no}^2}{r_{ni}^2} \right) \tag{5}$$

where v is the Poisson's ratio (r_{ni} is the inner radius of the hole, and r_{no} is the outer radius of the hole).

$$\alpha_a = \frac{1}{E}\frac{r_{ao}^2}{r_{ao}^2 - r_{ai}^2} r_{ao}\left(1 - v + (1+v)\frac{r_{ai}^2}{r_{ao}^2}\right) \tag{6}$$

where r_{ao} is the outer diameter of the shaft and r_{ai} is the inner diameter.

The diametrical interference between the shaft outside diameter and the hub inside diameter is given by the following equation,

$$\delta = d_{shaft} - d_{hub} \tag{7}$$

From equation 5, 6, and 7 we can derive the equation for the contact pressure between the hole and shaft.

$$p = \frac{\delta}{2(\alpha_n + \alpha_a)} \tag{8}$$

As we assume the shaft to be solid, $r_{ai} = 0$, equation 6 then reduces to,

$$\alpha_a = \frac{1}{E} r_{ao}(1 - v) \tag{9}$$

The ensure that the fit is proper, and that there is no danger of slip at the face of interference, the following no slip condition is considered,

$$\tau \leq p\mu \tag{10}$$

where μ is the coefficient of friction.